HELSINGIN YLIOPISTO
HELSINGFORS UNIVERSITET
UNIVERSITY OF HELSINKI

The Composition and Evolution of Fluids in Quartz Veins in Tonalites of the Kuittila Prospect, Hattu Schist Belt, Ilomantsi, Eastern Finland

Jukka Multanen

M.Sc. Thesis

May 2019

Department of Geosciences and Geography

University of Helsinki

Tiedekunta/Osasto Fakultet/Sektion – Faculty Faculty of Science	**Laitos/Institution– Department** Department of Geosciences and Geography

Tekijä/Författare – Author

Jukka Taneli Multanen

Työn nimi / Arbetets titel – Title

The Composition and Evolution of Fluids in Quartz Veins in Tonalites of the Kuittila Prospect, Hattu Schist belt, Ilomantsi, Eastern Finland

Oppiaine /Läroämne – Subject

Geology

Työn laji/Arbetets art – Level	**Aika/Datum – Month and year**	**Sivumäärä/ Sidoantal – Number of pages**
Master's Thesis	05/2019	98

Tiivistelmä/Referat – Abstract

The Archean Hattu schist belt in Ilomantsi, eastern Finland, hosts several orogenic gold deposits and prospects, including the Pampalo gold mine. This study focuses on the quartz veins hosted by the Kuittila tonalite intrusion, which is a gold mineralized intrusion of the same age as the gold deposits in the surrounding metasediments. The aim of this study is to assess the relevance of magmatic-hydrothermal fluid contributions in the formation of orogenic gold deposits. Fluids of selected quartz veins located within Kuittila tonalite intrusion are studied to potentially get an answer to whether the Kuittila tonalite act simply as a trap for the gold precipitation, or if it can be considered as one of the potential sources for the gold. The analyzing methods comprise mineralogical and petrographic studies done with polarization and reflected microscope and electron microprobe (EPMA) along with fluid inclusion studies including microthermometry studies, Raman laser spectroscopy and laser-ablation-inductively coupled-mass spectrometry (LA-ICP-MS) analyses of selected fluid inclusions in different type of quartz veins.

Seven different type of fluid inclusions were identified from selected quartz veins representing interpreted four different stages of quartz vein generation. Based on the petrography, the earliest fluids are aqueous-hydrocarbon bearing fluids, which are then followed by moderate salinity aqueous and aqueous-carbonic fluids, which are then accompanied by high salinity aqueous inclusions. Low salinity aqueous fluids are postdating the main mineralization stages.

Fluids migrated through Kuittila tonalite contain features that are characteristic for fluids from both magmatic and metamorphic origin. The highly variable elemental compositions as well as the variable salinities and in particular molar Cl/Br ratios of different fluid types indicate that several pulses of fluids have migrated through the Kuittila tonalite with potentially variable origin of the fluids. The notably low molar Cl/Br ratios in all of the analysed fluid inclusion assemblages suggest that the contribution of metamorphic fluids have been significant even in the earliest fluids.

The fact that in this study no gold were observed in the fluids with typical characteristics for magmatic fluids, and on contrary, those with gold signal shared more of the characteristics of metamorphic fluids would suggest that the magmatic fluids are not necessarily involved in the formation of the orogenic gold deposits in the Hattu schist belt and are not therefore mandatory in the formation of orogenic type gold deposits. It seems rather likely that the metamorphic fluids delivered potentially from country metavolcanites and metasediments are the sources for the gold and are precipitated in already formed fractures in the Kuittila zone.

Avainsanat – Nyckelord – Keywords

fluid inclusion, fluid evolution, composition, geochemistry, microthermometry, LA-ICP-MS, Tonalite, quartz, vein, EPMA, Kuittila, Hattu schist belt, Ilomantsi, orogenic gold deposit

Säilytyspaikka – Förvaringställe – Where deposited

University of Helsinki, Kumpula Science Library

Muita tietoja – Övriga uppgifter – Additional information

Tiedekunta/Osasto Fakultet/Sektion – Faculty

Matemaattis-luonnontieteellinen tiedekunta

Laitos/Institution– Department

Geotieteiden ja maantieteen laitos

Tekijä/Författare – Author

Jukka Taneli Multanen

Työn nimi / Arbetets titel – Title

The Composition and Evolution of Fluids in Quartz Veins in Tonalites of the Kuittila Prospect, Hattu Schist belt, Ilomantsi, Eastern Finland

Oppiaine /Läroämne – Subject

Geologia

Työn laji/Arbetets art – Level	**Aika/Datum – Month and year**	**Sivumäärä/ Sidoantal – Number of pages**
Pro Gradu	05/2019	98

Tiivistelmä/Referat – Abstract

Myöhäisarkeeisella Hatun liuskejaksolla Ilomantsissa on useita orogeenisia kultaesiintymiä, joista tunnetuin on Pampalon esiintymä. Tässä tutkimuksessa keskitytään Kuittilan tonaliitin kvartsijuoniin. Kuittilan tonaliitti valittiin tutkimuskohteeksi, sillä se on mineralisoitunut intruusio, joka on samanikäinen kuin sitä ympäröivät kultamineralisoituneet metasedimentit. Tutkimuksen tavoite on saada vastauksia vieläkin väitellylle kysymykselle magmaattis-hydrotermisten fluidien merkityksestä orogeenisten kultamalmien synnyssä. Valituista kvartsijuonista otettuja näytteitä tutkimalla on tarkotus saada selvyyttä siihen, että voidaanko Kuittilan plutonia pitää yhtenä mahdollisena lähteenä kullalle vai onko kullan lähteenä muualta kulkeutuneet metamorfiset kultapitoiset fluidit, jotka ovat saostaneet kullan Kuittilan tonaliittiin aiemmin syntyneisiin rakoihin. Analyysimenetelmät koostuvat mineralogisista ja petrologisista tutkimuksista polarisoivalla ja heijastavalla mikroskoopilla ja elektronimikroprobilla (EPMA), sekä fluidisulkeumatutkimuksista mikrotermometrillä, Raman-spektrosopialla ja laserablaatio-icp-massaspektrometrillä (LA-ICP-MS).

Seitsemän erilaista fluidityyppiä tunnistettiin näytteistä, jotka edustivat neljää eri vaiheen kvartsijuonta. Petrografian perusteella tunnistettiin ensimmäisiksi fluideiksi vesi-hiilivety -pitoiset fluidit, joita on seurannut keskisuolaiset vesipitoiset ja vesi-hiilipitoiset fluidit. Tämän jälkeen ovat tulleet korkeasuolaiset vesipitoiset fluidit. Myöhäiset matalasuolaiset vesipitoiset fluidit ovat tulleet päämineralisaation jälkeen.

Analysoiduissa eri tyypin fluideissa on havaittavissa piirteitä molemmista magmaattisesta sekä metamorfisesta lähteestä. Fluidien vaihteleva geokemia, eritoten molariiset Cl/Br -suhteet sekä vaihtelevat suolapitoisuudet viittaavat useisiin pulsseihin fluideja, jotka ovat todennäköisesti tulleet eri lähteistä. Huomattavan alhaiset Cl/Br suhteet kaikissa analysoiduissa fluideissa viittaavat siihen, että metamorfisten fluidien vaikutus on ollut suurta jopa aivan ensimmäisissä havaituissa fluidityypeissä.

Fluideista, joilla oli tyypillinen magmaattis-hydroterminen koostumus ei löytynyt kultaa, ja toisaalta niistä, jotka osoittivat enemmän merkkejä metamorfisten fluidien vaikutuksesta, löytyi kultapitoisuuksia. Tämä viittaa siihen, että magmaattis-hydrotermiset fluidit eivät todennäköisesti ole osallisena orogeenisten kultamalmien synnyssä Hatun liuskejaksolla. Näyttää todennäköisemmältä, että kultapitoisten fluidien lähteenä ovat sivukivet; metavulkaniitit ja karbonaatti-pitoiset metasedimentit, josta kultapitoiset fluidit ovat kulkeutuneet ja sitten saostuneet aikaisemmin Kuittilan tonaliittiin muodostuneisiin rakoihin.

OPTAvainsanat – Nyckelord – Keywords

fluidisulkeuma, fluidievoluutio, koostumus, geokemia, mikrotermometri, LA-ICP-MS, tonaliitti, kvartsi, juoni, EPMA, Kuittila, Hatun liuskejakso, Ilomantsi, orogeeninen kultaesiintymä

Säilytyspaikka – Förvaringställe – Where deposited

Helsingin yliopisto, Kumpulan kampuskirjasto

Muita tietoja – Övriga uppgifter – Additional information

TABLE OF CONTENTS

1. INTRODUCTION

Orogenic gold deposits are the dominant gold deposit type in Finland. According to Eilu (2015), orogenic type gold mineralization occurs in nearly all Finnish greenschist- to amphibolite-facies supracrustal belts, such as the study area Hattu schist belt, which is located in Ilomantsi, eastern Finland. Over 90 percent of the known gold deposits in Finland are orogenic in genesis (Eilu 2015).

The late Archean Hattu schist belt is a host for several gold deposits, out of which the most well-known is the Pampalo deposit, which is being mined by Endomines Oy. In addition, several other prospects and deposits have commercial potential, including the Kuittila deposit. In 2017, the total size of the Pampalo gold deposit was announced to be 255 513 ton with the gold grade of 2.6 g/t (Endomines 2018) and the supposed announced mineral reserves 776 738 ton with the average gold grade of 2.8 g/t. In comparison, supposed gold reserves of the Kuittila deposit are 275 000 ton with grades of 2.6 g/t (Endomines 2018).

The Pampalo deposit is naturally the most studied deposit within the Hattu schist belt area. However, other deposits are also generally well-studied in several publications and Master's theses (e.g. Molnár et al. 2016a, Hicks 2015, Poutiainen and Partamies 2003a, Poutiainen and Partamies 2003b, Sorjonen-Ward 1993). While fluid inclusions in the quartz veins within Kuittila tonalite have been studied briefly in a publication by Bornhorst and Wilkin (1993), a study that would seize deeper into the nature and geochemistry of the fluids in the Kuittila tonalite and the associated quartz veins and their evolution is still lacking.

Genesis of the orogenic gold deposits remains controversial, as some models are favouring metamorphic fluids as the major source for the gold without any necessary contribution of magmatic-hydrothermal fluids, whereas other models support the relevance of magmatic-hydrothermal imput. A recent study of the auriferous fluids of Pampalo mine (Fusswinkel et al. 2017) shows that no significant contributions of magmatic fluids are necessarily needed to form an economically important orogenic gold deposit in Archean greenschist belts. This study will seize deeper on the question of the contribution of magmatic and metamorphic fluids in orogenic gold settings by studying the fluids of selected quartz veins located within the Kuittila tonalite intrusion itself to potentially get an answer to whether the Kuittila tonalite acted simply as a trap for the gold precipitation or can be considered as a potential source for the gold. The Kuittila tonalite was selected for this study since it represents a well preserved and generally not deformed gold mineralized intrusion of the same age as the gold deposits in the surrounding metasediments.

The analyzing methods used in this study comprise mineralogical and petrographic studies done with polarization and reflected microscope and electron microprobe (EPMA) along with fluid inclusion studies including microthermometric studies, Raman laser spectroscopy and laser ablation-inductively coupled plasma-mass spectrometry (LA-ICP-MS) analyses of selected fluid inclusions in different type of quartz veins.

1.1. Sources and transportation mechanisms of hydrothermal fluids

The processes related to fluid forming and evolving events in the Earth's crust are complicated, as many different types of fluids are involved in hydrothermal ore-forming processes (Robb 2005). The depth of formation effects on which type of fluids play a role in the evolution of the fluid (Phillips 1993). At shallow crustal depths the origin of ore-forming hydrothermal fluids is in open systems of meteoric, seawater and basinal fluid settings, (Robb 2005) where geothermal activity, basinal dewatering and circulation of seawater through rocks have great impact in the evolution of these shallow fluids (Phillips 1993). At greater depths, the magmatic fluids formed by melting and affected by metamorphic devolatilization play a key role in hydrothermal cycle.

Magmatic fluids originate from the magma as it cools and crystallizes at various levels in the crust (Robb 2005). The temperatures of these fluids are ~600 °C (Robb 2005). During the crystallization process the dissolved volatiles in the magmas are released into the country rocks (Yardley and Bodnar 2014). At the early stages of crystallization the vapors released are generally CO_2-rich due to the low solubility of CO_2 compared to H_2O. Volatiles that have undergone extensive differentiation or reach shallow crustal levels tend to be H_2O dominated, since the more insoluble gases like CO_2 and N_2 have already bubbled away (Robb 2005). Magmatic-hydrothermal fluids can then be affected by other fluids in various degrees and also by devolatilization due to thermal activity between the fluid and the country rocks.

Metamorphic fluids are formed by devolatilization of metamorphic rocks during prograde metamorphism or by contact metamorphic devolatilization caused by emplacement of plutons in high-grade metamorphic terranes (Cartwright and Oliver 2000). The country metasediments contain a good amount of water in their minerals, which might then be released in mineral dehydration during the metamorphic cycle (Yardley and Bodnar 2014; Cartwright and Oliver 2000). For example metamorphic shales and graywackes contain approximately 4 wt. % of H_2O (Cartwright and Oliver 2000).

Fluid flow is typically triggered by thermal and pressure gradients in the Earth's crust that occur during deformation (Robb 2005). At shallow crustal levels, pervasive fluid flow is often set off by gravity-driven hydraulic head formed by uplifted topography (Robb 2005). In oceanic crust, fluids are believed to flow in response to thermal gradients formed because of the high heat flow that characterizes the mid-ocean ridges (Robb 2005). At deeper levels in the crust, where the fluid volume contained in the rocks are reduced, fluid migration can only occur along channelways represented by structural discontinuities formed during deformation. Therefore most of the fluid movements that occur at deeper crustal levels are located within faults that may become locally mineralized (Robb 2005).

1.2. Characteristics of orogenic gold deposits

1.2.1. Origin of orogenic gold deposits

Orogenic gold deposits are complex geological settings hosted by highly variable rock types (Goldfarb and Groves 2015). They are epigenetic deposits formed in orogenic belts by syn- to late-orogenic fluids (Eilu 2015). Mineralization generally occurs in accreted terranes and back-arc settings (Fig. 1) (Goldfarb and Groves 2015).

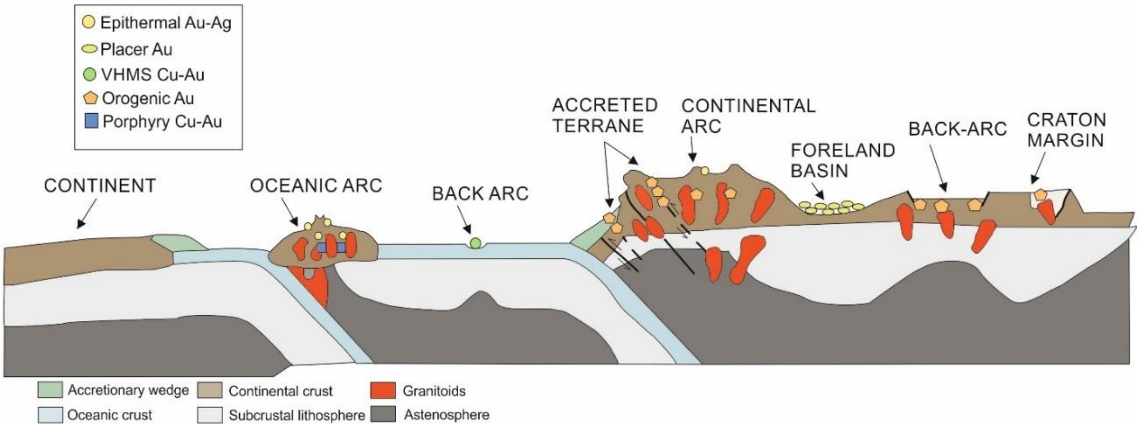

Figure 1*. Schematic image presenting different tectonic settings related to gold-rich epigenetic deposits. The mesothermal orogenic gold ores are emplaced during compressional to transpressional regimes. (Modified after Groves et al. 1998 and Goldfarb and Groves 2015.)*

Orogenic gold deposits can form in depths from 3 km to 20 km, reflecting pressures of 1–5 kbar (Fig. 2) (Eilu 2015; Goldfarb and Groves 2015). At these depths the active fluids will be mostly magmatic and metamorphic (Yardley and Cleverley 2013; Phillips 1993), as it is impropable for meteoric water to reach the deeper crustal levels where orogenic gold deposits generally form (Goldfarb and Groves 2015).

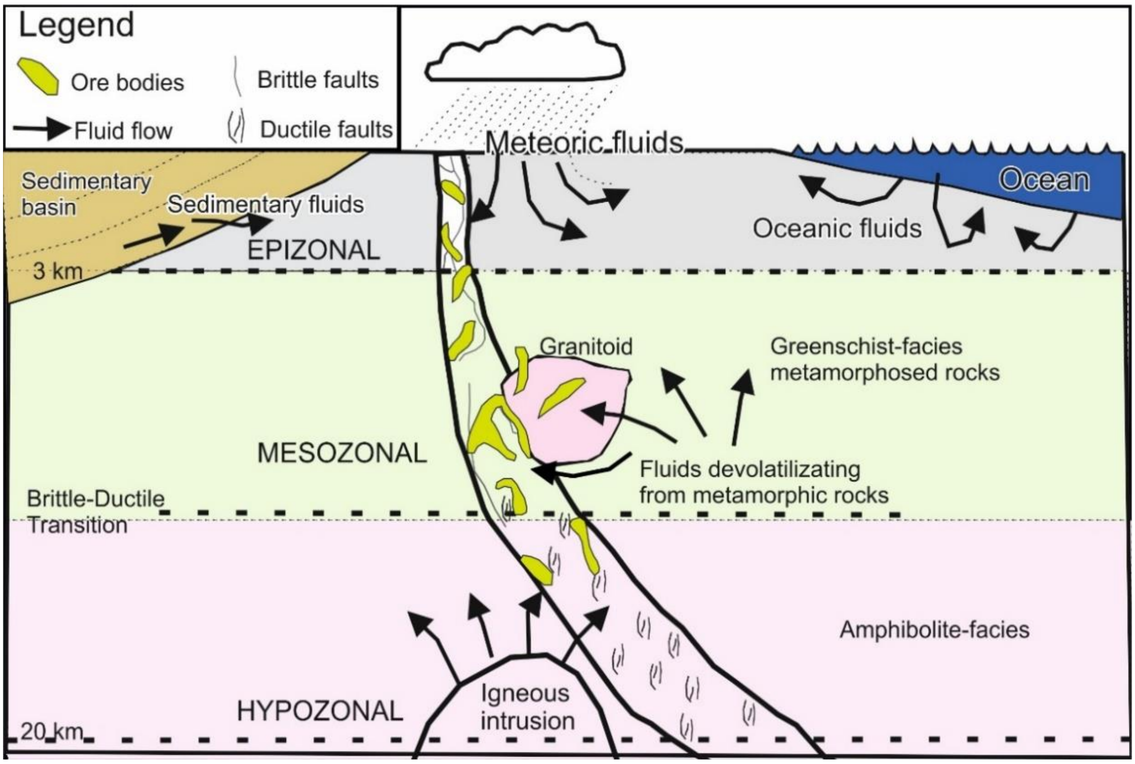

Figure 2*. Schematic image showing the model for orogenic gold deposit and potential different origins of fluids. Note that the relationship between shallow fluids sources and fault system related to orogenic gold deposits are completely schematic (Modified after Robb (2005) and Goldfarb and Groves 2015).*

Although the characteristics of ore forming fluids between different gold deposits are generally quite similar, the ultimate source of fluids involved in the forming of orogenic gold deposits is still being debated. According to Tomkins (2013), the plausible sources for gold are either metamorphic fluids, from which fluids are evolved as temperatures increase, or felsic to intermediate magmas, which release fluids as they crystallize. One of the controversial issues remaining is whether the magmatic model is critical to evolve a giant orogenic gold deposit (Goldfarb and Groves 2015). The contribution of magmatic-hydrothermal fluids in such settings has been suggested mainly based on the emplacement of granitic intrusions with the gold deposits in some cases and stable and radiogenic isotope data (Goldfarb and Groves 2015). However, the timing of gold mineralization relative to the emplacement of granitic intrusions is uncertain in many cases (Goldfarb et al. 2008). Furthermore, some deposits have no granitoid plutons at all in their host terrane (Goldfarb and Groves 2015). The stable and radiogenic isotope data is also equivocal and commonly inconsistent with a magmatic fluid and metal source (Goldfarb and Groves 2015). According to Eilu (2015), most of the stable and radiogenic isotope data from gold and associated trace elements in metamorphosed belts point toward progressive metamorphic dehydration, mostly at midcrustal levels, as being the main process releasing the fluids and metals, with no detectable contributions from local rocks. This data would also exclude the meteoric and magmatic fluids delivered from local granitoids or the mantle as significant metal sources.

The formation of orogenic gold deposits is considered to be associated with the growth of a new continental crust (Goldfarb et al. 2001). Greenstone belts usually contain syngenetic sulphide minerals disseminated in the metamorphosed crust. The sulfur will be partly released into the hydrothermal fluids via prograde desulfidization reactions during crustal heating. The sulfur-bearing hydrothermal fluids that migrate through the fractures of crustal rocks are capable of transporting a significant amount of leachable gold along the flow path, which will be deposited in secondary and tertiary fault systems, adjacent to the main fault at shallower crustal levels of the uplifting orogeny. If temperatures exceed about 700 °C in and below fluid source areas, both fluids and metals will migrate upward simultaneously (Goldfarb et al. 2001).

It is also questioned, whether there is one single deep source for gold or is it a result of temporal evolution of the fluids (Goldfarb and Groves 2015). According to Goldfarb and Groves (2015), the consistent characteristics of the fluid inclusions in typical orogenic gold deposits from Neoarchean to Phanerozoic, which will be discussed further in the next chapter, are likely characteristics of a single main-fluid source with limited fluid evolution. Phillips and Powell (2010) have calculated that already 2 ppb of gold, which is the average value in mafic igneous rocks, provide a sufficient amount of gold to the hydrothermal fluid to form a giant ore system. This indicates that a favourable protolith is not necessarily needed to form an orogenic gold deposit, as both mafic igneous rocks and sedimentary rocks are theoretically capable of sourcing fluids and most metals for this model (Goldfarb and Groves 2015). A broad contact metamorphic event driven by magma emplacement can also lead to significant devolatilization and orogenic gold formation (Goldfarb and Groves 2015).

Nevertheless, despite the ongoing debate of the ultimate source of the gold mineralizing fluids, orogenic gold deposits are commonly deposited in quartz veins by changes in pressure during seismic events and adjacent to veins by reaction between the fluids and the wall rocks (Eilu 2015). Gold is transported in fluids mainly as bi-sulphide complexes and it is deposited in the temperatures between 250 to 400 °C (Eilu 2015). The activators for gold deposition are in rapid changes of temperatures, changes in sulphur activity and changes in oxygen activity (Phillips and Powel 1993). Reduction of sulphur is readily achieved as the fluid reacts with Fe-rich host rocks causing formation of pyrite or pyrrhotite (Phillips and Powel 1993). These fluid-rock interactions and wall-rock sulphidation are considered as the most important precipitation mechanism for gold deposits (Mikucki 1998). However, with decreasing depth, phase separation and fluid mixing become more significant processes for the precipitation mechanism (Mikucki 1998). Changes in oxygen activity are achieved by interaction with carbonaceous metasediments (Phillips and Powel 1993). Boiling, or effervescence, along with fluid-mixing are also considered as one of the major causes of ore deposition, as it makes possible to acquire the rapid supersaturation of hydrothermal fluids in a restricted rock volume (Wilkinson 2001).

1.2.2. Properties of mineralizing fluids in orogenic gold deposits

Despite of the highly variable and complex setting and uncertainty of the fluid origin for orogenic gold deposits, the composition of the ore-forming fluids in orogenic gold deposit settings are generally well-known and they share common features. Many authors characterize them as low to moderate salinity (3–7 wt. % NaCl equivalent), near-neutral pH of ~5.5 and CO_2-H_2O-NaCl(±CH_4/N_2/H_2S)-bearing fluids (Eilu 2015; Goldfarb & Groves 2015; Yardley and Cleverley 2013; Ridley and Diamond 2000; Kesler 2005; Robb 2005). H_2O, CO_2 and CH_4 are the most abundant and significant components (Robb 2005). The CO_2 content of these aqueous-carbonic fluids are typically 5–20 mol %, although unmixing during extreme pressure fluctuation can lead to entrapment of much more CO_2-rich fluid inclusions in some cases (Goldfarb & Groves 2015). Temperatures of these ore-forming fluids are below 200 °C, according to Phillips (1993).

A common feature for all different orogenic gold deposits is the high abundances of gold related to sulphides (Yardley and Cleverley 2013; Phillips 1993). This is because the ore fluids are generally of low salinity and gas-rich, so their capacity to transport gold is enhanced by the relatively high levels of H_2S, whereas their ability to transport base metals is limited by the low concentration of chloride (Yardley and Cleverley 2013). Common estimates of H_2S concentration in ore forming fluids are 0.01–0.036 mol % (Goldfarb & Groves 2015). The geochemistry of ore forming fluids in orogenic gold deposit settings are characterized by elevated concentrations of As, B, Ba, Bi, Hg, Na, Rb. Sb, Te, W, with hydrothermal addition of K, S, CO_2, H_2O, Si and Au and low base-metal concentrations (Fusswinkel 2017; Goldfarb & Groves 2015; Phillips and Powell 1993).

1.3. The principles of fluid inclusion studies

Fluid inclusion studies serve as a window into the past. Fluid inclusions record the properties of crustal fluids during the time of their trapping. Studying fluids is valuable as fluids are responsible for a number of different geological processes, including ore formation and modification (Robb 2005). At a room temperature, fluid inclusions typically appear as a small, ~10–100 µm or smaller bubble with various shapes, and they often consist of two distinct phases: liquid and vapour. In cases of aqueous-carbonic inclusions, the appearance is generally 3-phase at room temperatures, consisting of liquid water, liquid CO_2 and gaseous CO_2 phase. Fluid inclusions may also contain solid daughter minerals, which will form when the inclusions become oversaturated during cooling (Kerkhof and Hein 2001). The usual appearance of 2-phase and 3-phase fluid inclusions with the possible daughter minerals that are observed in a laboratory, is the result of cooling to surface temperatures of the fluids that were homogenous at the time of trapping (Roedder 1974).

Microthermometry is an important aspect in fluid inclusions studies, as it allows one to determine the temperatures of phase changes in single fluid inclusions by heating and cooling them while observing the changes. However, to be able to logically interpret fluid inclusion microthermometric data, the inclusions must be prior grouped as petrographically associated groups of inclusions, fluid inclusion assemblages (FIA) (Goldstein and Reynolds 1994). Without carefully recognizing fluid inclusions as FIAs, the microthermometry data would be equivocal and linking the results to petrographic context would be impossible. In cases of hydrothermal quartz veins this can be challenging task, since they often appear cloudy due to the millions of fluid inclusions in the same thick section.

The usual classification of the fluid inclusion assemblages is as primary, pseudosecondary or secondary. Primary inclusions are trapped during the growth of a mineral and therefore record the conditions that existed during the time of crystal growth (Goldstein and Reynolds 1994; Kerkhof and Hein 2001). These are easiest to recognize in growth zones of the host mineral. In some publications, inclusions occurring isolated are assumed to be direct proof of the inclusions being primary (Goldstein and Reynolds 1994). However, this simply is not enough proof of the primary nature of the fluid, as in some situations inclusions may appear to be isolated when viewed on a plane depending on the intersection and might therefore, in fact, be part of a small trail of secondary inclusions. Pseudosecondary inclusions become entrapped in microcracks before the crystal growth is complete, and like primary inclusions they document the prevailing conditions during the crystal growth (Goldstein and Reynolds 1994). Secondary inclusions form by cracking of the host mineral after it has finished growing and they are most easily recognized as trails of inclusions entrapped in fractures which are cutting through the entire crystal. In recrystallized quartz veins the secondary inclusions turn up as trails that are cutting through several different crystals. The classification between these has however often proven to be problematic in hydrothermal veins with several phases of fluid flow and reactivation (Wilkinson 2001). This was also the case in the quartz veins within the Kuittila tonalite, especially since they have gone through multiple phases of deformation. Kerkhof and Hein (2001) state that in cases of deformed or anhedral crystals or in massive rocks, dividing between primary or secondary inclusions may be misleading and should rather be thought of as “early” or “late” inclusions. Although primary fluid inclusions are usually of most interest, in some cases studying secondary inclusions may be more relevant, since they could be related to later hydrofracturing events that have brought large volumes of gold and other elements into the host vein (Goldfarb and Groves 2015). Relationships of relative ages between different FIAs may be determined from inclusion trails cross-cutting each other.

For fluid inclusion to reliably capture the prevailing pressure-temperature conditions that occurred during the entrapping of certain fluids, it is required that the fluid inclusion is a diathermic, isochoric and isoplethic system. For this to be the case in reality, it is required that three following Roedder’s rules apply for a single inclusion: 1) The inclusion traps a single, homogenous phase, 2) Nothing is added to, or removed from the inclusion after trapping, 3) The inclusion volume remains constant following trapping (Bodnar 2003a). Any inclusions which show signs of re-equilibration, necking or immiscibility should be approached with caution, since they are potentially at disagreement with the Roedder’s rules and may therefore cause variability in the data within a single FIA (Goldstein and Reynolds 1994). There are many aspects that can cause re-equilibration of the fluid inclusions, for example during the burial or uplift of the rock to the surface, or it can also occur during the sample preparation and data collection in the laboratory (Bodnar 2003b) Also, in surface outcrops it could simply occur by the long-time exposure to sun or freezing conditions. Re-equilibration can also be overlooked if the inclusions completely equilibrate in new P-T conditions, leading to FIAs with consistent phase ratios as well as microthermometric results (Bodnar 2003b).

For inclusions that pass the criteria of being a diathermic, isochoric and isoplethic system, phase changes observed in microthermometry will reveal the temperatures at which minerals form, the thermal history a rock has experienced, and the composition of the fluids (Goldstein and Reynolds 1994). Knowing the final melting temperature of ice enables calculations of the salinity of aqueous fluid inclusions. The minimum temperature for the fluid entrapment can be acquired from the temperature at which the inclusion homogenizes into a single phase. If either pressure or temperature of the setting during the time of entrapment is known e.g. based on mineral geobarometry or geothermometry, the true entrapment temperature can be obtained from isochores plotted on a temperature-pressure diagram by specific density.

1.4. Geochemical tracers of fluids from different origins

Analyzing the geochemistry of hydrothermal fluids allows the obtaining of hints of the fluid origin. Some elements are particularly favoured in fluids of magmatic origin, whereas some propose more of the metamorphic contribution in the fluid evolution. For example, halogens tend to behave stably during fluid-rock interaction and therefore they are excellent tracers for fluid sources (Rittenhouse 1967; Worden 1996). Since the average crustal abundance of Cl is low, ~50 ppm (Phillips and Powell 1993), the molar Cl/Br ratios of magmatic fluids tend to be higher than in metamorphic ones. The potential tracers of fluid origin are discussed in further detail in chapters 1.4.1. Tracers of magmatic fluids and 1.4.2. Tracers of metamorphic fluids. In Table 1 below, is a compilation of the geochemistry of representative fluids of metamorphic and magmatic origin. The geochemistry in all measurements is obtained from fluid inclusions.

***Table 1**. Geochemistry of fluid inclusions representing typical metamorphic and magmatic samples. For clarity reasons, concentrations between 1000–9999 ppm are rounded to nearest hundred, and concentrations ≥10000 ppm to nearest thousand.*

Fluid type	**Metamorphic fluids**							**Magmatic fluids**						
Area	Pyrenees	Pyrenees	Central Alps	Columbia	Columbia	Modum	Irish Variscan	Mole	Mole	Cornwall	Cornwall	Capitan	Industrialnoe	Industrialnoe
Location	La Glere	Pic de Port Vieux	Thusis	Cincho	Chivor			Yankee	Gol 1		East Vitifier			
Temp	300	300	320±20	320	320	220	260	528	420	400	500	570	800	800
Element concentrations (ppm)														
Na	56000	42000	15000	95000	68000	17000	17000	73000	65000	26000	70000	174000		
K	7700	1600	390	19000	8800	1000	1500	35000	63000	5800	13000	69000	44000	36000
Li	810	456	28	1300	2500	13	326	1500	530	336	392			
Mg	692	919	6	5400	1400	27	446			664	182	297		
Ca	50000	28000	430	17000	17000	5500	19000			4300	29000	37000	4600	6900
Sr	2000	1200	27	228	1500	83	841		69		504	1361		120
Ba	450	1000	3	303	1500	31	130			164	148	767		
Fe	1300	1500		11000	4600	53	178	40000	93000	3800	5900	14000	46200	27400
Mn	647	176	2	1000	1000	26	291	14000	12000	1200	3500	17000	7000	5800
Zn	191	75		199	950	3	64	3200	2800	190	686	2100	3400	3200
Pb		3	0.1	60	315		118	2600	1700		190	680	4400	1300
Cu	107		17			1	89	600	200	547	35		310	76
B	84	100	680			24	193	2400		1900	967	192		
F											899	3157		
Cl	180000	130000	10000	224000	183000	36000	67000	210000	210000	39000	172000	402000	319000	127000
Br	4400	1000	70	40	43	221	169			51	329	122	250	339
As			43	370	48						98			45
Reference	(1), (2)	(1), (2)	(3)	(4)	(4)	(5)	(6)	(7)	(7)	(8)	(8)	(9)	(10)	(10)

References: (1) Banks et al. (1991) , (2) McCaig et al. (2000), (3) Miron et al. (2013), (4) Banks et al. (2000), (5) Munz et al. (1995), (6) Meere and Banks (1997), (7) Heinrich et al. (1992), (8) Smith et al. (1996), (9) Campbell et al. (1995), (10) Kamenetsky et al. (2002).

1.4.1. Tracers of magmatic fluids

High metal concentrations are present in high-salinity magmatic fluids, making magmas with high Cl/H_2O ratios important sources of ore fluids (Yardley 2005). Studies of porphyry Cu and Mo systems have shown that the early generation of fluids are generally high-salinity with high temperatures and they show evidence of liquid-vapor phase separation and/or boiling (Roedder 1984).

The magmatic-hydrothermal fluids contain significant amounts of sodium, potassium and calcium, which is proven by the usual presence of daughter minerals halite (NaCl) and sylvite (KCl) (Robb 2005). The concentrations of these dominant cations can be as high as 35 wt. % for Na and 18 wt. % for K (Bodnar et al. 2014). Iron is also one of the most significant cations of magmatic fluids and individual analyses of fluid inclusions or fluid inclusion assemblages from porphyry copper deposits show that the Fe concentration can reach up to 33 wt. % in magmatic fluids (Bodnar et al. 2014). In Table 1, the high iron concentrations can be seen systematically in the magmatic fluids. The Mole granite contains almost 10 wt. % of Fe, whereas in metamorphic fluids the iron concentrations are generally way less than 5000 ppm. One exception is the Columbia Cincho sample where measured iron is over 10000 ppm, which is unusually high for a metamorphic fluid. The analyses of samples from Columbia are however clearly different from the other metamorphic fluid analyses, e.g. remarkably high Li, K, Zn and Pb for metamorphic fluids.

Magmatic-hydrothermal fluids are also characterized by high base metal concentrations, such as Cu, Pb and Zn (Robb 2005). As can be seen in Table 1, the base metals Cu-Zn-Pb are clearly favoured in magmatic fluids and potentially act as a good tracer of magmatic source. Cu concentrations in different magmatic fluid settings vary from 35 ppm to 600 ppm, and are remarkably more abundant than in metamorphic fluids. Fluid inclusion analyses of magmatic fluids from granites show that high Fe, Zn and Pb values are quite constant, Zn and Pb being up to 1 wt. % and Fe up to 17 wt. % (Yardley and Bodnar 2014). Cu contents are more varying, ranging from below the limit of detection up to 900 ppm in some analyses.

Chlorine concentrations vary notably between the different magmatic-hydrothermal fluid types, ranging from only 3.9 wt. % in the Cornwall sample up to over 40 wt. % in the

Capitan sample. Bromine is consistently low in all the analyses, especially compared to the most Br-enriched samples of metamorphic fluids from the Pyrenees. Despite the highly variable Cl concentrations, the molar Cl/Br ratios of magmatic fluids in Table 1 ranges from lowest of 844 in Industrialnoe to the highest of 7400 in Capitan sample, which are much higher than measured in metamorphic fluids. Generally the molar Cl/Br ratios of magmatic fluids range from 500 up to about 1600 (Fusswinkel et al. 2017). Exceptionally high molar Cl values are interpreted to reflect crustal contamination.

1.4.2. Tracers of metamorphic fluids

Because of the low average chlorine concentration in the crust, metamorphic fluids are generally low salinity (Phillips and Powell 1993). However, this is not a clear marker for metamorphic fluids, since low-salinity fluids also come from meteoric fluids in geothermal systems and in some cases magmatic fluids (Phillips and Powell 1993).

Besides of the remarkably lower base-metal concentrations in metamorphic fluids compared to magmatic ones, the metamorphic fluids tend to have much higher strontium contents compared to those of igneous-origin (Yardley and Bodnar 2014). In an analysis from La Glere, Pyrenees, the Sr concentration reaches as high as 2000 ppm, and in most analyses of metamorphic fluids, elevated concentrations are observed (Table 1). On the contrary, in magmatic fluids the Sr content is low (69–504 ppm) or even below detection limit in some samples. One exception is the sample from Capitan, where Sr content reaches to levels of typical metamorphic fluids (1400 ppm). Moreover, metamorphic fluids related to gold deposits are characterized by reduced sulphur and enrichment in As, Hg, Sb, Ba and Rb (Phillips and Powell 1993).

Another distinct feature that has been considered as a marker for metamorphic origin of the fluids are low Cl/Br ratios. The study of Pampalo shows molar Cl/Br ratios as low as 9–20 in some of the fluid types (Fusswinkel et al. 2017). In samples representing metamorphic fluids from Pyrenees, the Cl/Br-ratios are 93 and 282, which are also significantly lower compared to those of magmatic fluids. Similar low molar Cl/Br-ratio of 330 is also measured in foliation-parallel veins from Thusis, Central Alps (Table 1).

According to Fusswinkel et al. (2017), the low Cl/Br ratios in Pampalo can be best explained by fluid-rock reactions with Br-rich organic matter in shelf sediments.

2. GEOLOGICAL SETTING

The Ilomantsi greenstone belt in Eastern Finland belongs to the Archean 2.5 Ga domain in the Fennoscandian shield area (Fig. 3). The Archean shield area is present in the northern and eastern parts of Finland and it is a host for several greenschist belts, which are known to be of high economical potential, hosting several commercially important gold and base/precious metal deposits. These Archean domains in Finland are post-dated by 1.93–1.80 Ga Svecofennian Paleoproterozoic rocks, with only a small part of the Finnish bedrock being younger than 1.80 Ga (Vaasjoki et al. 2005). All gold-mineralized environments in Finland, except the possible Archean epithermal deposits and the recent placers, can be related to supercontinent evolution of the region between 2.75–1.77 Ga (Eilu 2015).

2.1. The geology of the Hattu schist belt

The Hattu schist belt is part of the Ilomantsi greenstone belt which consist of late Archean supracrustal units and intrusive rocks (Sorjonen-Ward 1993). The Hattu schist belt hosts several small and some larger orogenic gold deposits, such as the most significant discovery, the Pampalo deposit. The gold deposits in the Hattu schist belt occur roughly along N-S, NE-SW and NW-SE oriented shear zones that cut across the supracrustal metasedimentary and metavolcanic rocks (2.79–2.75 Ga) as well as younger to possible syntectonic plutonic intrusions and dikes (2.75–2.72 Ga) (Fig. 3) (Sorjonen-Ward 1993). Further, younger 2.70 Ga unmineralized leucogranite intrusions intrude the schist belt (Sorjonen-Ward 1993).

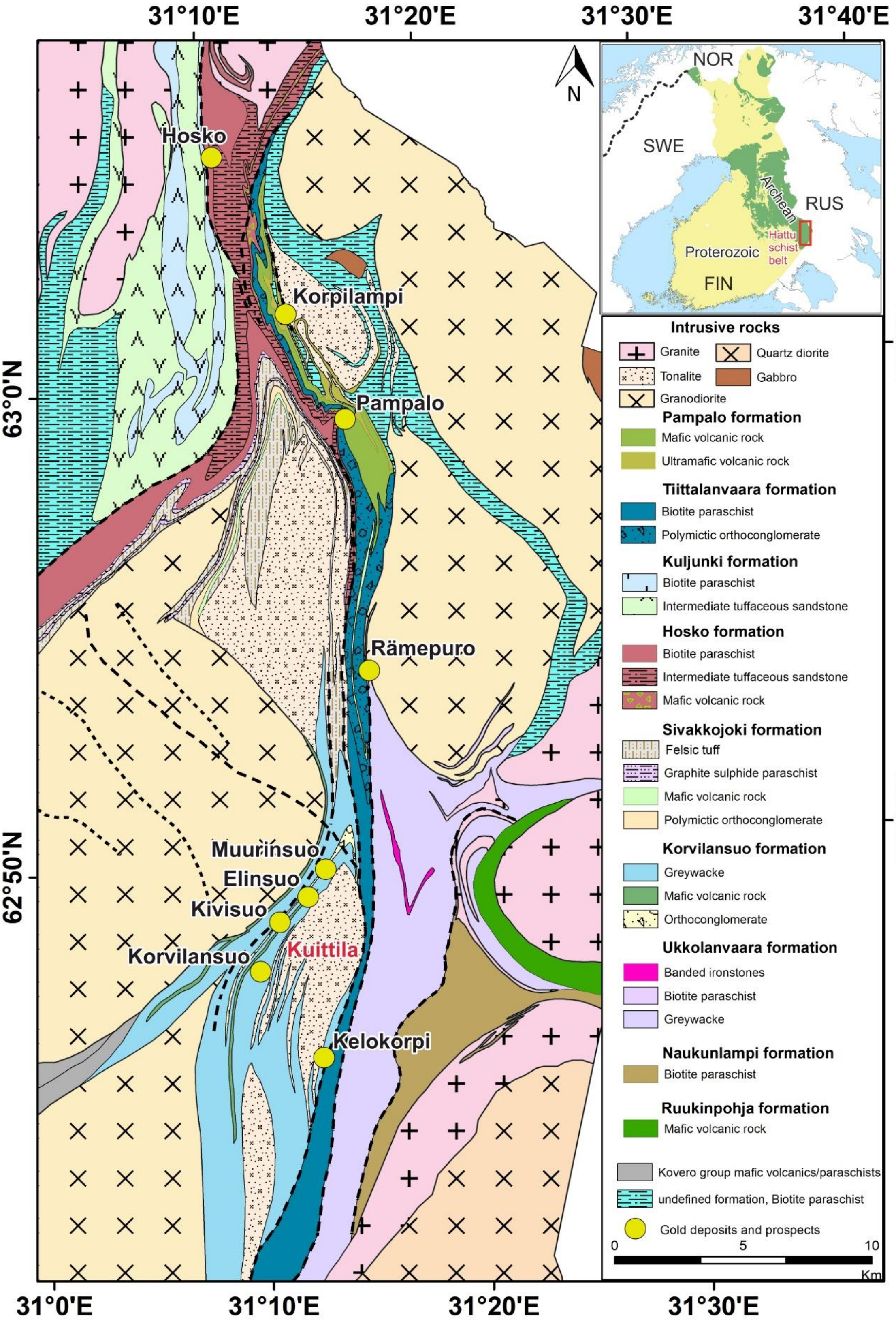

Figure 3. *Geology of the Hattu schist belt, also showing the most significant gold deposits and prospects within the Hattu schist belt. Supracrustal units are classified in stratigraphic order from the youngest to oldest after Sorjonen-Ward (1993), Pampalo being the youngest unit. The main shear zones are shown as dotted lines. Geological map and amended legend from GTK's bedrock of Finland 200k.*

Common feature for the gold occurrences within the Hattu schist belt are elevated values of Au-Te-Bi-Ag, Mo-W-CO_2 and Cu-S assemblages (Molnár et al. 2016b; Sorjonen-Ward et al. 2015). The molybdenum-tungsten mineralization is in some cases associated with the gold mineralization in the tonalitic intrusions, although elevated Mo-W signals also occur separately from the gold mineralization (Sorjonen-Ward et al. 2015). The involvement of syn-orogenic magmatic fluids with the mineralization have been suggested based on the abundance of scheelite, molybdenite and tourmaline along with several bismuth- and tellurium-bearing minerals within and proximal to the mineralization of granitoids (Sorjonen-Ward et al. 2015). However, paragenetic and structural evidence of the mineralized veins within the Kuittila tonalite indicate that auriferous shear zones and veins were superimposed on an earlier set of veins (Sorjonen-Ward et al. 2015).

Alteration characteristics related to the gold mineralization in different prospects are reasonably similar in the whole schist belt, which includes hydration, carbonation and potassic alteration, all known to be typical features for Archean lode gold deposits. Noticeable albite-carbonate alteration, however, have only been identified in the Pampalo deposit, whereas in other gold prospects it is not as pervasive as in a typical Archean orogenic gold deposit (Sorjonen-Ward et al. 2015). Alteration of the mineralized metasediments is controlled by addition of chlorite, muscovite and tourmaline (Sorjonen-Ward et al. 2015). Multiphase alteration events are likely, as the early sericite-microcline alteration assemblages have been deformed and foliated prior to vein hosted gold mineralization and associated alteration (Sorjonen-Ward et al. 2015). The peak metamorphism occurred at lower amphibolite facies at pressures of 3–5 kbar and temperatures of 500–600 °C at around 2.70 Ga and it post-dates the hydrothermal alteration and ore formation (Molnár et al. 2016b).

Gold mineralization occurs in almost all different rock types within the Hattu schist belt, indicating that fluid-rock interactions and mineralization are controlled by the mechanical and compositional differences within and between different rock units (Sorjonen-Ward et al. 2015). Since the gold deposition occurred at considerable depth, boiling or mixing of the fluids with ground waters are not likely (Nurmi 1993). Most of the gold occurs as fine grained (<15 µm) and are typically found as intergrowths with tellurides and native bismuth in grain boundaries of silicates, sulphides and carbonate (Kojonen et al. 1993). The overall abundance of sulphides is low within the Hattu schist belt compared to other typical Archean lode gold deposits (Kojonen et al. 1993). Because of the lack of correlation of Au and S and absent of association with Fe-rich lithologies, sulphidization is not considered as the main deposition mechanism (Nurmi 1993). Mineralization occurred at around 400–500 °C for arsenopyrite and associated gold, whereas the main crystallization of telluride-bismuth-gold assemblages has took place at around 250–350 °C (Kojonen et al. 1993).

Some of the studies indicate that the mineralization of the gold within the Hattu schist belt has happened in multiple stages. According to Poutiainen and Partamies (2003b), the gold mineralization at Rämepuro prospect happened in two phases. Firstly, the early fluids precipitated quartz, sulphide minerals and gold in fractures. The later fluids circulated through newly formed fractures and probably also reopened older veins, also causing quartz and gold precipitation and minor mobilization of the previous sulphides. In Pampalo, according to Molnár et al. (2016a), the emplacement of feldspar porphyry triggered the hydrothermal processes, which resulted albite-tourmaline-mica (biotite/muscovite) alteration and formation of a stockwork hosted disseminated mineralization of gold with variable grades. Later high-strain deformation and associated fluid flow generated intense biotite-pyrite-carbonate alteration and the major concentrations of gold in the shear zones. The study by Fusswinkel et al. (2017), however, suggests that the gold mineralization in Pampalo occurred without any necessary imput of magmatic-hydrothermal fluids.

2.1.1. Earlier fluid inclusion studies from different gold prospects within the Hattu schist belt

Plentiful of fluid inclusion studies have been done of several different gold prospects within the Hattu schist belt. In a study of the Hosko prospect (Fig. 3) done by Poutiainen and Partamies (2003a), three different fluid generations were identified: 1) H_2O-CO_2-CH_4-halite, which are the earliest stage fluids related to sulfide mineralization, 2) H_2O-CO_2-CH_4 fluids related to gold mineralization and 3) late H_2O fluids postdating mineralization. The homogenization temperatures range from 205 °C to 338 °C for the earliest fluid related to the sulphide mineralization stage and from 217 °C to 396 °C in the later fluid type related to the main gold mineralization stage. Isochores acquired from the data of the fluid inclusions related to the gold minetalization stage, together with alteration and ore assemblages yield temperatures of 300–350 °C and pressures of 2–3.5 kbars. Salinities are generally low, as the final ice melting temperatures are ranging from -5.7 to -0.7 in the earliest fluid, and are a bit higher in fluid related to the postmineralization (-9 to -3).

The Rämöpuro prospect (Fig. 3) has as well been studied by Poutiainen and Partamies (2003b). According to the authors, the results are indicating that the oldest, H_2O-CH_4 fluids, are related to Late Archean (2.7 Ga) regional metamorphism. Fluids related to Paleoproterozoic Svecofennian overthrusting (1.9 Ga) show increase in pressure and temperature. The latest fluids related to Svecofennian (1.9-1.8 Ga) metamorphism and gold mineralization consists of H_2O-CO_2 fluids. Salinities of the earlier fluids related to peak metamorphism are similar to those related to sulfide mineralization in Hosko. The salinities of the fluids related to gold mineralization are higher, ranging from 8 to 12 wt. % NaCl equivalent. The melting temperatures of solid CO_2 range from -57.7 °C to -56.8 °C, which indicates that some amount of different compounds than CO_2 are present in the fluids. The homogenization temperatures are quite similar to those in Hosko, although a bit lower. Aqueous fluids in Rämepuro studied by Bornhorst and Wilkin (1993) yield homogenization temperatures of similar range (214 °C to 310 °C), and the salinities from 1.8 to 11.7 wt. % NaCl equivalent.

Fluids of the Korvilansuo prospect (Fig. 3) have been briefly studied in a master's thesis done by Hicks (2015). In this study, a similar CH_4-rich fluid type was observed as the likely earliest fluid type. The other fluid types observed consist of H_2O-NaCl and H_2O-CO_2 assemblages, with measured total homogenization temperatures of average 109 °C and 323 °C, respectively.

Selected quartz veins hosted by Kuittila tonalite have been studied by Bornhorst and Wilkin (1993). The studied vein types were termed early molybdenite-scheelite quartz vein, auriferous main stage quartz vein and late stage barren vein. Fluid inclusion studies showed that quartz from all vein types contains inclusions characterized by two phases of H_2O-rich liquid and vapor, with no distinct CO_2 vapor phase. The authors classified the inclusions into three different types, of which all had average 5:1 liquid to vapor ratio. Type 1 inclusions are classified as being relatively isolated and occurring as small clusters located near grain boundaries and lacking fracture control, which according to the authors could indicate that they may be primary inclusions. Type 3 inclusions are located along healed fracture zones indicating they are secondary in origin. Type 2 inclusions could not be classified neither as primary nor secondary, since they did not occur along fractures nor were they clearly isolated. The measured median homogenization temperatures for aqueous inclusions in early quartz veins are 232 °C, which according to the authors are considered to be the best estimate for quartz-scheelite-molybdenite and main gold stage mineralization. However, without any pressure correlations done, this is only proving a minimum temperature estimate. For primary inclusions in main gold stage quartz the medium temperature is 243 °C. Medium homogenization temperature measured from late-stage quartz is 164 °C. The median salinities for quartz-scheelite-molybdenite and main stage Au mineralization are 8.5 wt. % NaCl equivalent. In comparison, the median salinity of late-stage hydrothermal fluids are ~2 wt. % NaCl equivalent.

In a study of ore-forming related fluids from Pampalo mine by Molnár et al. (2016a), it is suggested that primary fluid inclusions in quartz have been re-equilibrated and therefore the microthermometry data cannot be used for characterization of the ore-forming processes. These primary re-equilibrated fluid inclusions yield total homogenization temperatures of average 377 °C and salinity of 9.5 wt. % NaCl equivalent. The secondary inclusions which are fracture hosted gives average homogenization temperatures of 150 °C and salinity of 3.8 wt. % NaCl equivalent. Similar homogenization temperatures have been measured in a study by Fusswinkel et al. (2017), where the reported homogenization temperatures for auriferous fluids in the early boudin neck quartz are 160 ± 5 °C, and 150 ± 5 °C for the barren fluids in the late extensional quartz veins. Salinities of these fluids are 5.0 to 8.0 wt. % NaCl equivalent and 4.2 to 5.5 wt. % NaCl equivalent, respectively. The study by Fusswinkel et al. (2017) provides trace elemental geochemical data of the auriferous fluids from the Pampalo deposit. The fluid inclusion elemental data is interpreted to be representative of typical orogenic gold fluids, e.g. low-moderate salinity, presence of CO_2, CH_4 or N_2, high S contents, enrichment in B, As, Sb and W, and low base-metal (Pb-Zn) concentrations. Based on the mass balance calculations using metal concentrations and Cl/Br ratios, the Au-forming fluid type at Pampalo is not compatible with any significant magmatic-hydrothermal fluid contribution indicating that all the fluid types at Pampalo are metamorphic in origin. The reported molar Cl/Br ratios are as low as 9, making the fluids one of the most Br-enriched crustal fluids ever reported.

In summary, a similarity of many of the fluids is the CH_4-rich nature of the early fluids. Salinities of the fluids in auriferous veins are more or less similar, showing generally low to moderate salinities (~5–12 wt. % NaCl equivalent). The total homogenization temperatures show variance, ranging from ~150 up to almost 400. The characteristics of different fluid types observed in earlier fluid inclusions studies within the different prospects in the Hattu schist belt are combined in Table 2 below.

***Table 2**. Summary of characteristics of different fluid types studied in different prospects and deposits within the Hattu schist belt.*

Deposit	Type*	Vein type	Stage	Fluid type	TmCO2	TmCla	TmH2O	Th Tot	Salinity	Reference
Hosko	1	Au-quartz-tourmaline	II Sulfide mineralization	H_2O-CO_2-CH_4-halite	-63 to -59		-5.7 to -0.7	205 to 338		(1)
Hosko	2	Au-quartz-tourmaline	III Gold mineralization	H_2O-CO_2-CH_4	-63 to -59			217 to 396		(1)
Hosko	3	Au-quartz-tourmaline	IV Postmineralization	H_2O			-9 to -3			(1)
Rämepuro	1	Au-quartz-tourmaline-sulphide	I Peak metamorphism	H_2O-CH_4			-5.8 to -2.6	225 to 355	4 to 9	(2)
Rämepuro	2	Au-quartz-tourmaline-sulphide	III Gold mineralization	H_2O-CO_2	-57.7 to 56.8		-8.2 to 5.4	155 to 312	8 to 12	(2)
Korvilansuo	1	Quartz-tourmaline		CH_4+-N_2+-H_2O/CO_2				no changes		(3)
Korvilansuo	2	Quartz-tourmaline		H_2O-NaCl				109	~27.7	(3)
Korvilansuo	3	Quartz-tourmaline		H_2O+-CO_2				323	low salinity	(3)
Pampalo	A	Quartz	Early boudin neck vein, likely gold ore fluid	Aqueous			-5.0 to -3.0	160+-5	5 to 8	(4)
Pampalo	B	Quartz	Early boudin neck vein	Aqueous			-10.9 to -6.4		9.9 to 15	(4)
Pampalo	C-I	Quartz	Micro-scale tension gash hosted	Aqueous-carbonic	-57.3 to -56.6	6.8+-0.3			4.6 to 5.3	(4)
Pampalo	C-II	Quartz	Feather vein hosted	Aqueous-carbonic						(4)
Pampalo	D	Quartz	Tension gash quartz	Aqueous			-3.2 to -2.2		3.7 to 5.2	(4)
Pampalo	E	Quartz	Late extensional quartz veins	Aqueous			-3.3 to -2.5	150+-5	4.2 to 5.5	(4)
Pampalo		Quartz	Southern orebody	Aqueous, primary			-8.7 to -2.9	299 to 440	4.8 to 12.5	(5)
Pampalo		Quartz	Southern orebody	Aqueous, secondary			-2.5 to -2	135 to 160	3.4 to 4.2	(5)
Pampalo		Quartz	Central orebody	Aqueous, secondary			-9.2 to -1.5	203 to 230	2.6 to 13.1	(5)
Pampalo		Quartz	Central orebody	Aqueous, secondary			-14.4 to -1.5	134 to 180	2.6 to 18.1	(5)
Pampalo		Quartz	Central orebody	Aqueous, secondary			-10 to -4.7	74 to 105	7.4 to 13.9	(5)
Pampalo	1			H_2O				168 to 227	4.9 to 6.9	(6)
Pampalo	2			H_2O				146 to 260	n/a	(6)
Pampalo	3			H_2O				234 to 245	5.8	(6)
Rämepuro	1			H_2O				221 to 298	9.7 to 11.5	(6)
Rämepuro	2			H_2O				214 to 310	5.9 to 11.7	(6)
Rämepuro	3			H_2O				240 to 256	1.8 to 1.9	(6)
Kivisuo	1			H_2O				220 to 326	10.7	(6)
Kivisuo	2			H_2O				209 to 346	6.5 to 12.8	(6)
Kivisuo	3			H_2O				210 to 332	7.2. to 8.2	(6)
Kuittila	1	Quartz-scheelite-molybdenite	Early veins	H_2O				195 to 246	4.3 to 8.9	(6)
Kuittila	1	quartz (Au)	Main gold stage	H_2O				237 to 251	6.9	(6)
Kuittila	1	barren quartz	Late veins	H_2O				134 to 180	1.5 to 3.5	(6)
Kuittila	2	barren quartz	Late veins	H_2O				117 to 195	n/a	(6)
Kuittila	3	barren quartz	Late veins	H_2O				178 to 191	0.8 to 2.0	(6)

References: (1) Poutiainen and Partamies (2003a), (2) Poutiainen and Partamies (2003b), (3) Hicks 2015, (4) Fusswinkel et al. (2017), (5) Molnár et al. (2016a), (6) Bornhorst and Wilkin (1993). *Type refer to fluid type reported in the certain study, therefore they are not comparable between different studies.

2.2. The geology of Kuittila tonalite

The Kuittila tonalite is a small, approximately 12 km^2, lenticular pluton and one of the many intrusive units formed approximately at the same time during active regional deformation within the Hattu schist belt (Fig. 4) (Sorjonen-Ward 1993). It is typically medium-grained and equigranular, although locally foliated. Subhedral plagioclase occurs as randomly oriented, whereas fine grained biotite appear as oriented aggregates. Hornblende is absent and K-feldspar is uncommon (Sorjonen-Ward et al. 2015).

Composition of the central part of the tonalite is trondhjemitic, which possibly represents a separate intrusive phase (O'Brien et al. 1993). At the western part, the Kuittila pluton dips at about 60° to the west beneath the schist belt. At the northern parts similar dips are present in the country rocks (Sorjonen-Ward 1993). Further to the south the dips of the country rocks steepen to vertical attitude, where tonalitic dikes and country rocks form alternating layers. This suggests that these acted likely as the feeder channel for the magma (Sorjonen-Ward 1993). This is in an agreement with the assumption of the probable source for the magma being metasomatized subcontinental lithosphere mantle, which has been enriched by fluids from subducting oceanic crust and possibly sediments as has been proposed by Heilimo et al. (2010).

The gold mineralization of Kuittila deposit is entirely hosted by the tonalite itself and the sericite schist enclaves in the southern part of the intrusion (Molnár et al. 2016b). Gold is deposited in a network of veins that are enriched in Mo, W and CO_2 (Eilu 2015). Concentrations of up to 0.5 wt. % molybdenite, 1–2 wt. % pyrite and an average of 4 g/t Au have been measured in a small exploration trench, where mineralization occur along with distinct foliation (Stein et al. 1998). In the proximity of Korvilansuo-Kivisuo gold prospect, at the western part of the Kuittila pluton, the Mo-W mineralization is confined to a set of quartz and tourmaline veins. The structures of the veins and the microscopic textures of ore samples show that the main mineralization process was filling of fractures and fissures of less altered host rocks (Kojonen et al. 1993).

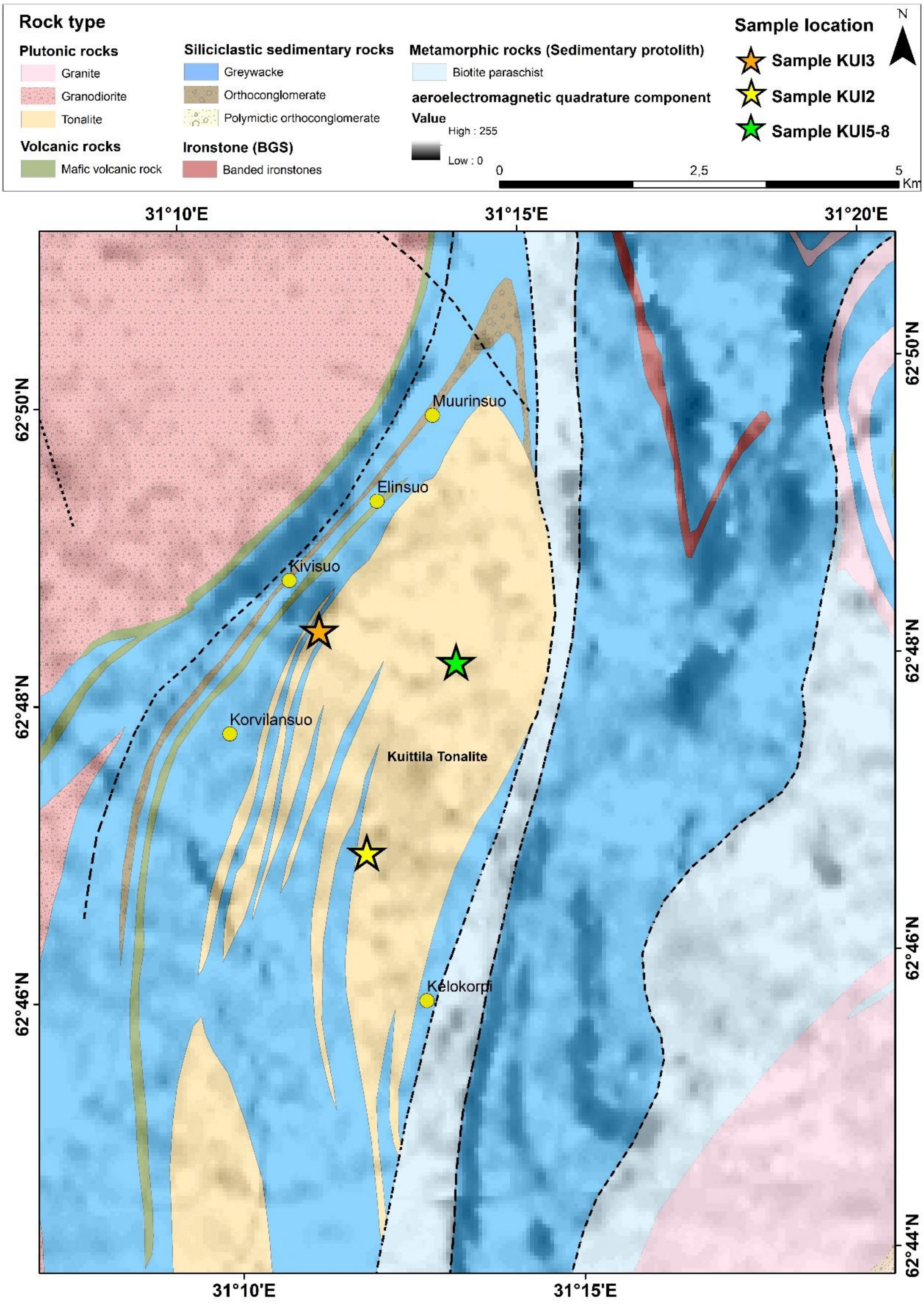

Figure 4. *Detailed geology of the Kuittila tonalite also showing the sample locations and other gold prospects within the area. Lithological map used is Geological Survey of Finland's digitalized 200k bedrock map. Anomalies seen on the aeroelecromagnetic map (aeroelectromagnetic_low_altitude_survey_quadrature_component_map_of_finland_kkj3_grayscale.ecw) are caused by electromagnetically active metasediments.*

The geochemistry of the Kuittila tonalite is characterized by significant average enrichments of Mn and Mg and depletion of Na. In addition, K and loss of ignition (LOI) commonly show significant increases. Si, Ti, Al, Fe, Ca and P show average enrichments in some mineralized zones, and immobility in others (Rasilainen 1996). Barium and strontium contents are relatively high (Ba 977 ppm, Sr 781 ppm) (O'Brien et al. 1993). According to Heilimo et al. (2010), the high Ba-Sr signature was formed by an effective accumulation process in the source, possibly including two metasomatic events. The average K/Rb ratio in Kuittila is 195 in mineralized samples and 200 in the least altered ones (Rasilainen 1996), which is a bit less than the bulk crustal values of K/Rb of 285.

The prevailing metasomatism within the Kuittila pluton has caused chloritization, sericitication, alteration of ilmenite to rutile, and replacement of plagioclase by K-feldspar (Kojonen et al. 1993). The potassium metasomatism, hydration and carbonatization are more intense in the Kuittila tonalite than in the other rock types within the Hattu schist belt (Rasilainen 1996). Sericite and muscovite are also commonly replacing plagioclase (Stein et al. 1998), which is thought to be related to the Au mineralization, as the most highly mineralized zones are intensively sericitized and deformed (Sorjonen-Ward et al. 2015; Nurmi et al. 1993).

The measured mean Re-Os ages of molybdenite and pyrite yield ages of 2778±8 Ma (Stein et al. 1998). As the weighted mean U-Pb ages for the hosting Kuittila tonalite are 2753±5 Ma, it suggest that formation of Mo-W±Au mineralization took place coevally with the emplacement and crystallization of the host rock.

2.2.1. Quartz vein generations within the Kuittila tonalite

According to Sorjonen-Ward (1993), four different vein systems have been recognized in the outcrops within the Kuittila prospect. The earliest type of these veins is a scheelite- and molybdenite-bearing quartz vein. These early veins consist of two potentially coeval sets of veins which are oriented between 080°-110° and 130°-150°. Recrystallization is visible at the vein margins, which indicate that they predate the main north-trending foliation of the host tonalite (Sorjonen-Ward 1993). Younger barren milky quartz veins are crosscutting the early Mo-W-bearing veins along with narrow brittle-ductile shear zones. Quartz-tourmaline veinlets are cutting the milky quartz veins, proving they are younger than not just the milky quartz veins, but also younger than the early scheelite-molybdenite-bearing veins. The auriferous quartz veins truncate the early Mo-W veins, but their relationship to the barren milky quartz veins is unknown. They are characterized by ductile deformation and pervasive hydrothermal alteration.

According to Molnár et al. (2016b) the mineralization happened in three stages, which are the early molybdenum-tungsten (-gold) stage, gold-sulphide-telluride stage and gold-telluride sulphide stage. The inferred temperature of hydrothermal processes of the different stages are ~450 °C, 450-300 °C, <300 °C, respectively. Traces of native gold have started to mineralize in already the earliest stage, which is followed by the large quantities of native gold and Au-Ag-tellurides and Au-Sb-Te phases. The type of mineralization for the early stage is presumed as magmatic-hydrothermal, whereas for the later stages it is presumed to be shear-zone hosted hydrothermal.

3. SAMPLES AND METHODS

3.1. Materials and sample preparation

All of the samples used in this study were collected by Tobias Fusswinkel. Sample selection was done on the selected quartz veins located within the Kuittila tonalite intrusion itself and the samples were selected so that they would represent all aforementioned different types of quartz veins recognized by Sorjonen-Ward (1993).

Samples KUI2 and KUI3 represent the supposed auriferous quartz veins, which are called Type 4 quartz veins in this study. The sample KUI2 has been collected from an outcrop in a forest area located close to the Kuittila farm area. Sample KUI3 is collected from an outcrop on the eastern side of forest road, located approximately 600 meters east of Hatuntie. The remaining samples have been collected from a quarry located approximately 3 km north from the Kuittila village. See Fig. 4 for the location of the selected samples.

In total, thick sections for further studies were made from 8 samples and the sample picking was done so that the quartz veins used are as clear as possible for the best appearance of the fluid inclusions. Since the main focus of this study is in the fluid inclusions, standard doubly polished 200 µm thick sections were prepared of each sample. In total, eight representative doubly polished fluid inclusion thick sections were studied microscopically. Out of all the samples, 5 samples were selected for further studies. Prior to performing microthermometric and LA-ICP-MS studies, the thick sections were cut into smaller chips (~2x2 cm) that were small enough to fit in the sample holder of the microthermometry instrument and LA-ICP-MS sample chamber. Chips were detached from the glass section by gentle diamond blade sawing down to the glass and then they were put into acetone for one night. After that the chips were loose enough to be simply picked up with tweezers. A summary of the sample material can be found in Table 3.

Table 3. Samples used in this study presented in age sequence from oldest vein type (V_1) to youngest (V_4). $^{(a)}$ Number of chips prepared from the thick section. $^{(b)}$ Microthermometric, EPMA, Raman, LA-ICP-MS analyses.

Sample	Chips$^{(a)}$	Vein type	Analysed$^{(b)}$	Description
KUI7	6	Type 1 (V_1)	Yes	Early Mo-W quartz vein, massive
KUI7a	none	Type 1 (V_1)	No	Early Mo-W quartz vein, massive
KUI7b	none	Type 1 (V_1)	No	Early Mo-W quartz vein, massive
KUI8	2	Type 1 (V_1)	Yes	Massive quartz, contain host rock tonalite as well
KUI5	6	Type 2 (V_2)	Yes	Barren milky quartz vein, "cloudy" appearance
KUI6	3	Type 3 (V_3)	Yes	Tourmaline-carbonate quartz vein
KUI2	none	Type 4 (V_4)	No	Auriferous quartz vein, recrystallized quartz
KUI3	6	Type 4 (V_4)	Yes	Auriferous quartz vein, recrystallized quartz

3.2. Analytical methods

3.2.1. Transmitted and reflected light microscopy

All of the thick sections were first photographed with a Leica DM2005P polarizing microscope to get high resolution overview images used for mapping of the different fluid inclusion assemblages. The thick sections were then thoroughly studied optically with both transmitted and reflected light to recognize the most common gangue and ore minerals. Following that, with the help of the obtained high resolution images, the samples were mapped carefully by systematically marking all the different identified fluid inclusion assemblages (FIA). The basic petrographic studies were done for all of the samples, out of which five samples were selected for further analyses. In those samples that were excluded (*KUI2, KUI7a and KUI7b*), the fluid inclusions were mainly too small and therefore not suitable for further microthermometry or LA-ICP-MS studies.

3.2.2. Electron-probe microanalysis (EPMA)

After the petrographic studies were done with the transmitted and reflected light microscopy, the samples were studied using the electron microprobe (EPMA) to get a better understanding of the mineralogy and also of the microstructures of the samples. This was essential, since nearly all of the ore minerals in the samples occur as very fine grained and therefore identification with optical microscopy turned out to be impossible in many occasions. The EPMA studies were done at the University of Helsinki with JEOL JXA-8600 Superprobe electron microprobe equipped with SAMx hardware and XMAs/IDFix/Diss5 analytical and imaging software package. Samples KUI3, KUI5, KUI6, KUI7 and KUI8 were studied semi-quantitatively using SEM-BSE imaging together with an energy dispersive spectrometer (EDS) analysing method. Before the analyses, conductive layer of carbon coating were applied to all samples.

3.2.3. Microthermometry

Microthermometry studies were done at the University of Helsinki. The instrument used to observe phase transitions in fluid inclusions was a Linkam THMSG-600 heating-freezing stage that has been mounted on a Leica DM2005P microscope. The observed phase changes were final ice melting temperature (T_mIce), melting temperature of solid carbonaceous-phase (T_mCar), clathrate melting temperature (T_mCla), partial homogenization of carbonaceous-phase (T_hCar) and total homogenization temperature (T_hTot). Cooling was performed with liquid nitrogen. Calibration was performed daily prior observing the phase changes with synthetic fluid inclusions by Syn-Flinc (VA, USA). Calibration standards used were H_2O-CO_2, H_2O-NaCl and pure H_2O fluid inclusions.

Bulk compositions of fluid inclusions were calculated with the BULK and Q2 software tools belonging to the FLUIDS computer software package (Bakker 2003). BULK was used for aqueous and Q2 for aqueous-carbonic fluids. For aqueous inclusions, the salinity as equivalent weight percent of NaCl was calculated from the final ice melting temperatures. Salinity of aqueous-carbonic inclusions were calculated based on the clathrate dissolution temperatures.

3.2.4. Raman Spectroscopy

Raman spectroscopy is a non-destructive method, which allows analysis of the gaseous and solid phases within a single fluid inclusion (Frezzotti et al. 2012). The basic procedure behind the Raman spectroscopy is that it records the interaction of electromagnetic radiation with molecular vibrations as a shift in the vibration from an incident source (Hurai et al. 2015). Qualitative identification of different gaseous species and solids were done based on the specific vibration each solution yields based on the values given in publication by Frezzotti et al. (2012). The analyses were done with a 100x magnification objective, and the measured spectra was 550–4200 cm^2, to cover all the potential compounds. The Raman spectroscopy measurements were done at the University of Helsinki with Dilor Labram II micro-Raman spectrometer. Calibration was done with a silicon standard before starting the analyses.

The obtained Raman spectra were fitted using a Python script provided by Anselm Loges. Since Raman was only used to qualitatively recognize the different gas species and potential solids in the analysed samples, specific calibration correlations were done only in cases where shifting had happened and the quartz peaks were shifted from their original position.

3.2.5. Laser ablation inductively coupled mass spectrometry (LA-ICP-MS)

LA-ICP-MS analyses were done at the University of Helsinki with an Agilent 7900s quadrupole ICP-MS that is equipped with a high-sensitivity s-lens ion lens configuration, and coupled to a Cohorent GeoLas Pro MV 193 nm excimer laser ablation system. To ensure high sensitivities and lowest possible limits of detection a fast washout small-volume 1 cm^3 ablation cell was used. Isotopes measured were ^{7}Li ^{11}B, ^{23}Na, ^{24}Mg, ^{29}Si, ^{32}S, ^{35}Cl, ^{39}K, ^{44}Ca, ^{49}Ti, ^{57}Fe, ^{63}Cu, ^{66}Zn, ^{75}As, ^{81}Br, ^{85}Rb, ^{88}Sr, ^{95}Mo, ^{107}Ag, ^{121}Sb, ^{133}Cs, ^{137}Ba, ^{182}W, ^{197}Au, ^{208}Pb and ^{209}Bi. Dwell times used were 5 ms for most elements, exceptions were 10 ms for ^{23}Na, ^{32}S and ^{95}Mo. 20 ms dwell times were used for ^{35}Cl, ^{81}Br and ^{107}Ag. ^{197}Au were analysed with 60 ms dwell time. Accuracy of the LA-ICP-MS instrument was ensured by daily calibration prior to analysis to maximize the signal-to-background ratios and to allow optimal ablation, transport and plasma conditions by keeping the U/Th as close to 100 % as possible. Also, to ensure low oxide production values, ThO/Th was kept below 0.4 %. Daily accuracies for both parameters were within the preferred values given by Spandler et al. (2011). External standardization was done using NIST610 synthetic glass standard for all elements except halogens, for which Sca17 standard, representing composition of natural scapolite was used. Internal standardization was done using Na concentrations calculated from microthermometry data. Summary of the LA-ICP-MS parameters are shown in Table 4 below.

Table 4. Summary of the settings used in LA-ICP-MS analyses.

Laser	Cohorent MICROLAS: GeoLas Pro MV2
Carrier gas flow (He)	1.13 l/min
Wavelengt	193 nm
Ablation chamber	Small volume aluminium cell (1 cm3)
Energy density on sample J/cm2	10-17 J/cm2
Crater size	16-160
ICP-MS	Agilent Technologies 7900 ICP-MS
Plasma gas flow (Ar)	15 l/min
Nebulizer flow (He)	0.85 l/min
RF Power (W)	1500

Drilling procedures were started with careful predrilling with small apertures with crater sizes of 16 and 24 µm. Then, depending of the depth of the target inclusion according aperture and crater sizes was selected.

Data-reduction for the acquired LA-ICP-MS data was done with SILLS 1.2.0 add-on in MATLAB. SILLS allows calculating the LODs (Limit of detection) with 95 % accuracy (Guillong et al. 2008). Restrictions regarding the selection of fluid inclusions and reliability of the measurements are discussed in further details in chapter 4.5.1. Reliability of the LA-ICP-MS data.

4. RESULTS

4.1. Mineralogy of the samples

4.1.1. Optical microscopy

The most abundant gangue minerals in the selected quartz veins and the host rock tonalite are carbonates, biotite, chlorite and K-feldspar, and they occur as fine to medium grained, although some are present as larger aggregates consisting of several different minerals. Ore minerals occur as mainly very fine grained and they are commonly affected by intense hydrothermal alteration, making recognition of some of those altered minerals reasonably hard. For that reason, and also to obtain more detailed view of the microstructures in the veins, one sample of each vein system was prepared for further electron microprobe analysis.

4.1.1.1. Quartz veins

Most of the quartz veins studied are massive, however samples KUI2 and KUI3, which represent type 4 quartz veins, consist of intensively recrystallized quartz. Quartz in sample KUI6, representing type 3 tourmaline-carbonate-quartz vein, is also partly recrystallized. Undulose extinction caused by minor bending of the crystal lattice (Winter 2001) is common in all of the massive type of quartz veins and indicates high degree of deformation of the quartz veins (Fig. 5).

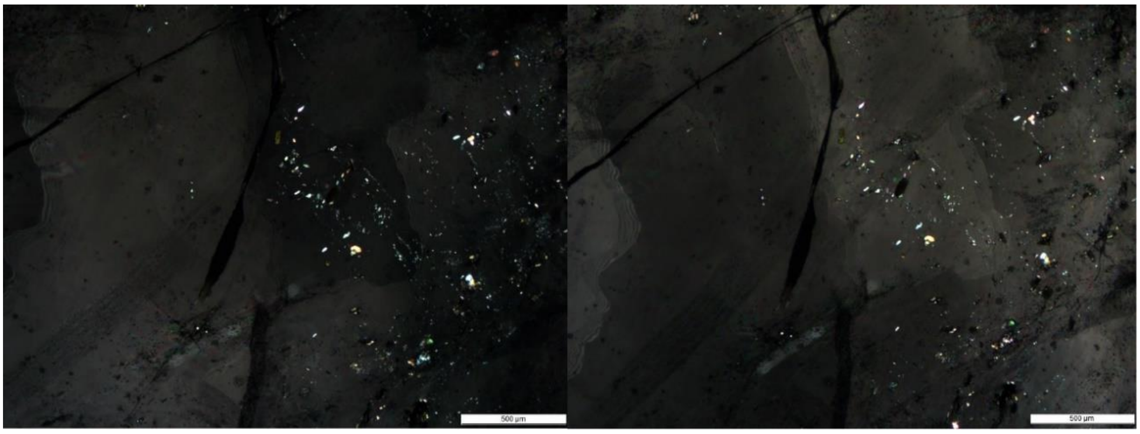

***Figure 5**. Undulose extinction in the quartz caused by high degree of deformation.*

Fine to medium grained biotite is present in most of the samples and it has been for most parts altered into chlorite. Tourmaline is only present in the tourmaline-carbonate-quartz vein (V_3), where it forms aggregates of tourmaline with different very fine grained ore minerals, which appears to be mostly more or less oxidized pyrite. Chalcopyrite is found mostly as very fine grained single grains, however in the sample KUI5, representing the vein type 2 (V_2), very coarse grained chalcopyrite occurs (Fig. 6). The margins of the chalcopyrite grain have been oxidized and partly altered into malachite and azurite. Hematite alteration is abundant in all different samples and it exists mainly on pyrites and in their grain boundaries. Some of the ore minerals present are completely hematized (Fig. 6).

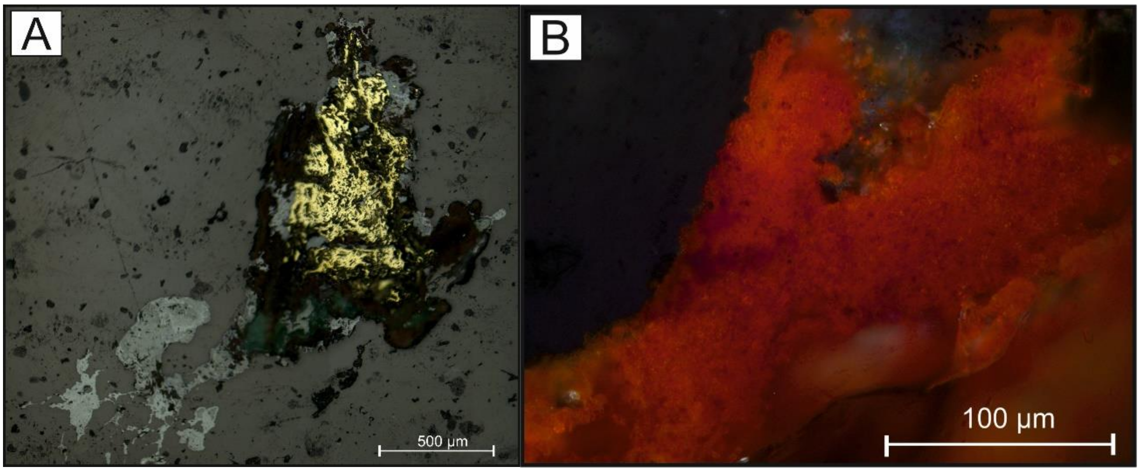

***Figure 6**. A) Chalcopyrite in KUI5 sample representing V_2. Margins of the grain have been oxidized, as green malachite can be seen. B) Intensely hematite altered Iron-carbonate complex on vein quartz.*

Pyrite is the most abundant ore mineral and like chalcopyrite it appears mostly as a very fine grained and it usually occurs along with biotite and chlorite (Fig. 7). Carbonates are abundant and in many cases they contain opaque minerals. K-feldspar is most abundant in V_3 and V_4 where it was occasionally found as fine to coarse grained with several intergrowths of different opaque minerals.

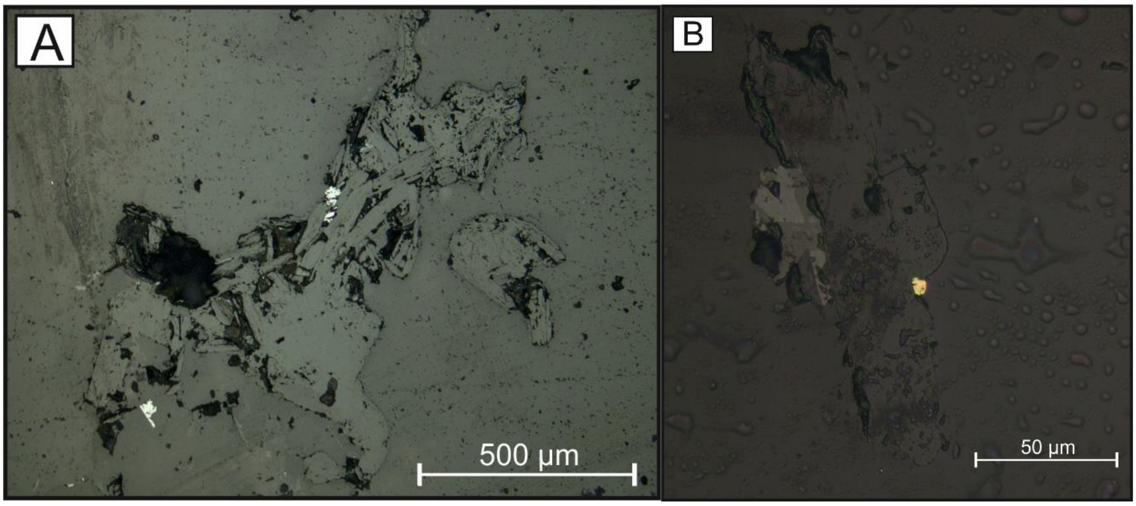

***Figure 7**. A) Very fine grained pyrite associated with biotite in sample KUI7 (V_1). Reflected light. B) Small, less than 5 microns in size chalcopyrite grain on the margin of chlorite altered biotite in KUI7 sample. Reflected light.*

4.1.1.2. Tonalite

Minerals in the tonalite are fine to medium grained and mainly altered. Biotite occurs mostly as fine grained and foliated, although some medium to even medium-coarse grained biotites were observed. Some potentially primary cluster-forming fluid inclusions could be seen in the biotite, but as they are mainly found as less than 1 µm in size and due to the dark appearance of biotite, studying of those inclusions turned out impossible. Euhedral zircons are abundant as intergrowths in the biotite (Fig. 8). Primary plagioclase is absent and it has been replaced mainly by quartz and sericite. According to Sorjonen-Ward (1993), the destruction of primary plagioclase is visible also in the geochemistry by enrichment of Mo, W, CO_2, Cu, S, Rb, K and Si and depletion of Na and Sr. Carbonate alteration is abundant and can be best seen in the boundary of the host rock tonalite and V_1 quartz vein (Fig. 8). The most common ore mineral present is pyrite, which is very fine to fine grained and mostly in anhedral form, and is usually associated with carbonate minerals and biotite (Fig. 8).

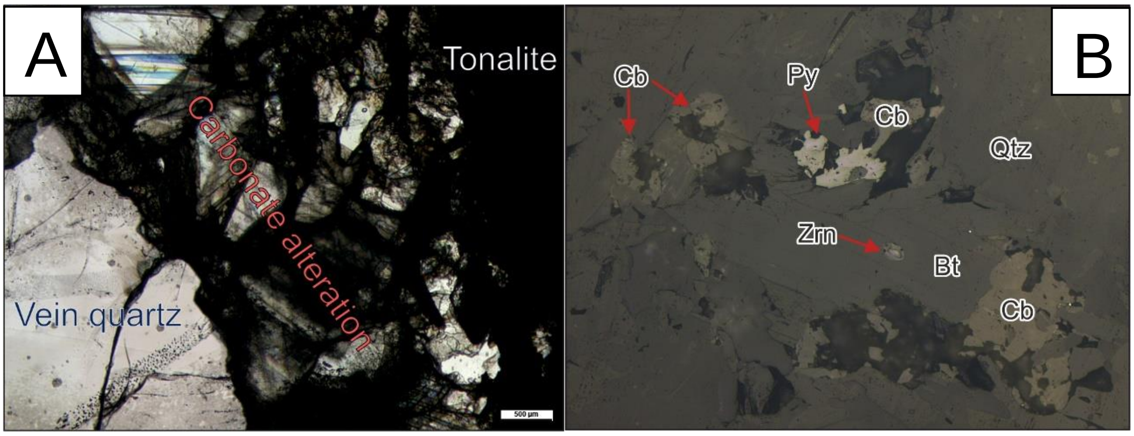

Figure 8*. A) Carbonate altered boundary between quartz vein and tonalite in plain polarized light. B) Pyrite associated with biotite and carbonates in tonalite. Reflected light.*

4.1.2. Electron-probe microanalysis (EPMA)

In total, 5 samples with at least one sample representing each different vein type were studied with EPMA. Summary of the samples selected for the EPMA analyses are shown in Table 5 below.

Table 5*. Samples selected for the microprobe analyse and their representive of different vein systems based on field observations.*

Vein type	Sample
Early Mo-W quartz vein (V_1)	KUI7
Early Mo-W quartz vein/host tonalite (V_1)	KUI8
Barren milky quartz vein (V_2)	KUI5
Tourmaline-carbonate quartz vein (V_3)	KUI6
Auriferous quartz vein (V_4)	KUI3

4.1.2.1. Type 1 quartz veins

Ore minerals present in the type 1 veins are very fine to fine grained. Ore mineralization is concentrated on grain boundaries, cavities on quartz and fractures, and the ore minerals are often associated with carbonates. Carbonates, which are mostly calcite, appear as fracture filling mineral associations and they often form aggregates with biotite, which are in most cases completely chloritized and together with apatite minerals they are often associated with REE-mineralization. Monazite is present mostly as Monazite-(Ce), however the ratios of trace elements Ce, La, Nd and Sm are varying. Additionally, REE-mineralization occur as cavity filling parisite-(Ce) (Fig. 9). Monazite is also abundant in the host rock tonalite and therefore it is most likely the source for the REE-enrichment of the fracture controlled carbonate mineralization in V_1. Fracture filled carbonates also contain high amount of Fe, Mn, Pb enrichment (Fig. 9).

Galena is abundant as 1–5 µm grains and is in many cases mineralized proximal to and in calcite filled fractures. Occasionally galena also appears separately from calcite in trails of inclusions formed on healed fractures (Fig. 9). Iron is mostly in form of iron oxides and like galena, it is also associated with carbonates in metal enrichments in fractures. Pyrite is relatively rare in this type of vein compared to the other type of veins, and it was only found as very fine grained single grains. Chalcopyrite occurs as a very fine grained, approximately 10 µm grains in cavities on the healed fractures on quartz (Fig. 10). Rutile has been mineralized in carbonate vein filling fractures and they are often ~50 µm in size and euhedral (Fig. 9).

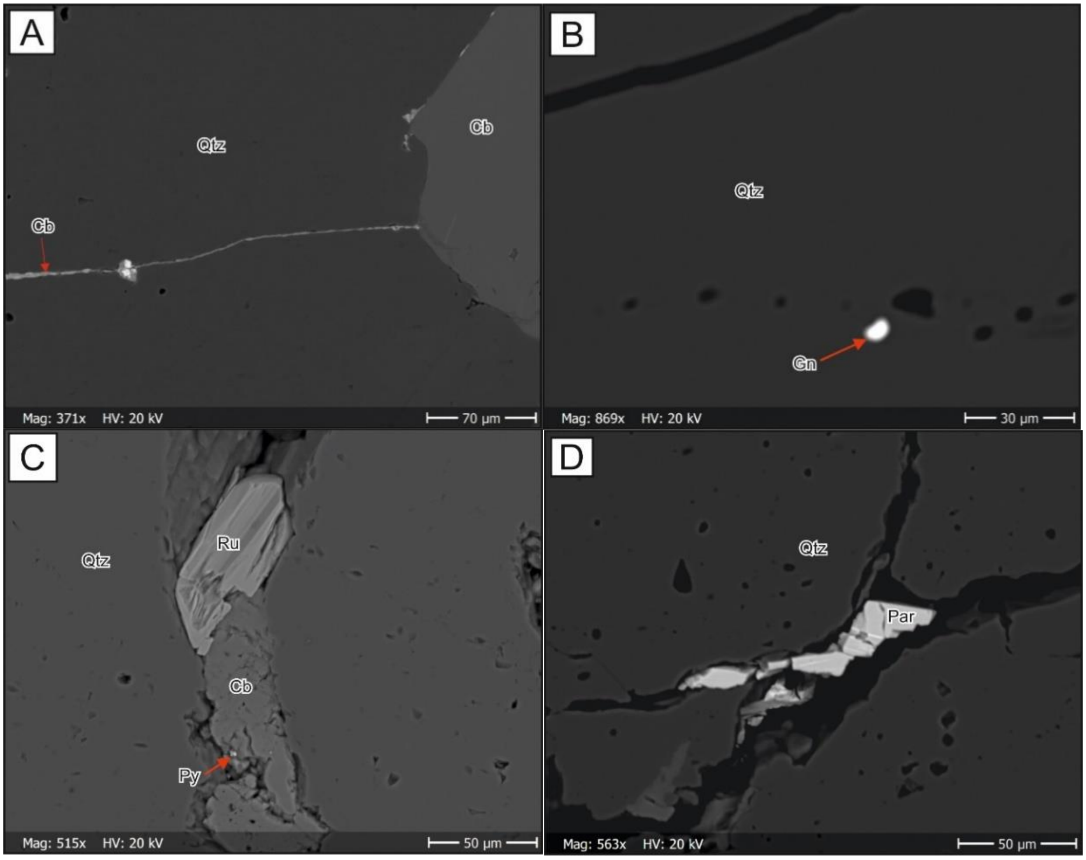

***Figure 9**. A) Fracture forming from carbonate altered boundary of host rock tonalite and vein quartz. Bright areas in the carbonate filling fracture are unidentified Mn and Pb-bearing minerals. B) Single galena grain on a healed fracture. C) Euhedral rutile in calcite vein. Also pyrite of few µm in size is visible. D) Parisite-*

(Ce) on a fracture surface in the vein quartz. Abbreviations: Cb=carbonate, Gn=galena, Par=parisite, Py=pyrite, Ru=rutile, Qtz=quartz.

As was already easily seen with polarizing microscope, the boundary between the host rock tonalite and quartz vein is thoroughly carbonatized. Many of the observed carbonates were found to be commonly REE- and Sr-enriched, where REE mineralization occur as subhedral minerals or some massive aggregates of microcrystalline minerals within the carbonate. Apatite is likewise abundant and is commonly present as euhedral crystals or as mineral associations with K-feldspar (Fig. 10).

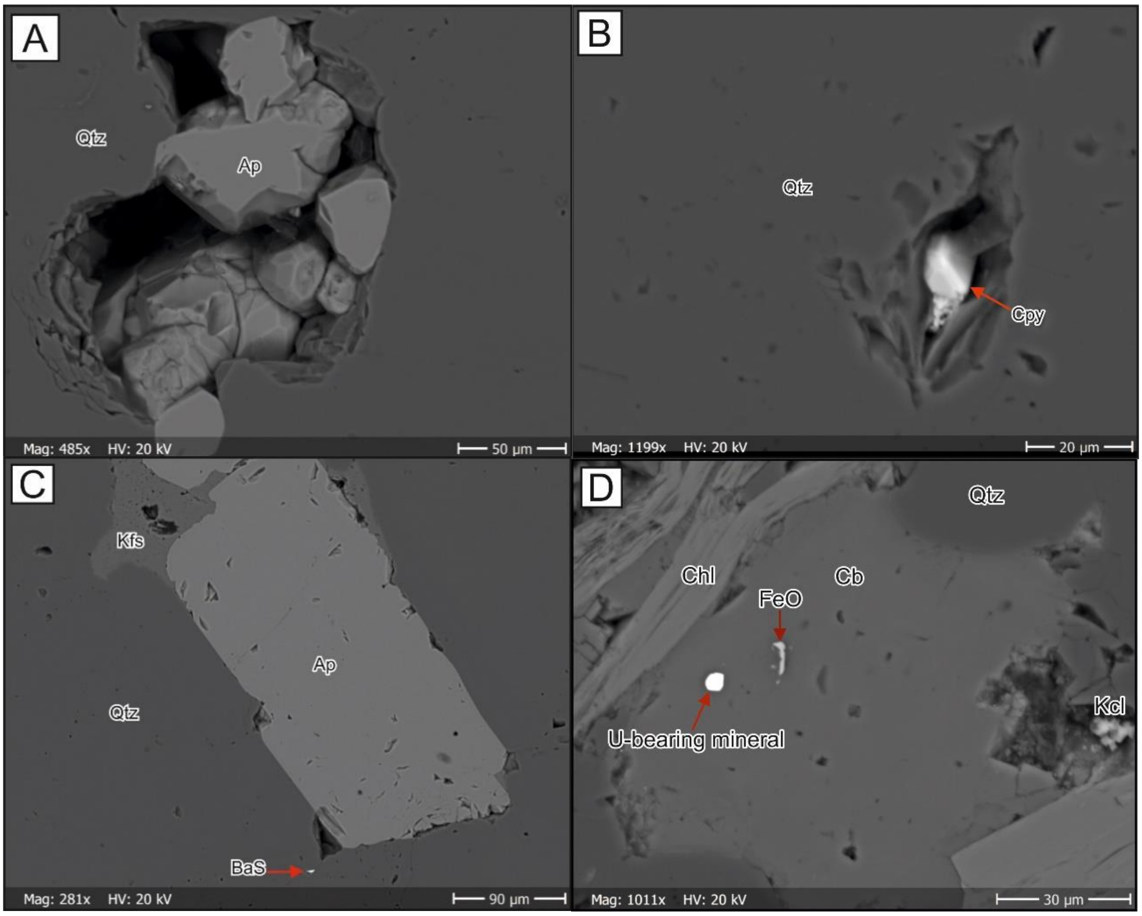

***Figure 10**. A) Apatite grains in a cavity in quartz B) Euhedral chalcopyrite grain in a cavity within the massive vein quartz. C) Apatite associated with K-feldspar. Very fine grained barite is mineralized on a healed fracture in the massive quartz. D) Iron oxides and unidentified U-bearing mineral in carbonate. Foliated hydrothermal chlorite occur along the carbonate. Note the sylvite (KCl) crystals in the cavity in quartz on the right. Abbreviations: Qtz=quartz, Ap=apatite, Cpy= chalcopyrite, Kfs=K-feldspar, BaS=barite, Chl=chlorite.*

4.1.2.2. Type 2 quartz vein

Pyrite and other ore minerals in general are not as abundant in V_2 as they are in other vein types. Exceptions are the single coarse grained chalcopyrite, and a large aggregate of microcrystalline hematite (Fig. 11). Sphalerite occurs as a very fine grained euhedral to subhedral crystals and were found in cavities formed along the healed fractures within the massive quartz (Fig. 11). Other than that, the type 2 vein is mostly quartz where inclusions formed within the healed fractures in quartz are dominating. A single native bismuth grain of approximately 1 µm in size was also observed in a fracture surface. On few occasions on the fractures in the quartz sylvite (KCl) was observed as ~5 µm euhedral crystals (Fig. 11). It is unlikely that these have been crystallized in the quartz, as they unlikely would be stable enough. Therefore they are probably formed at some point during the sample preparations. It is however possible that they are actual daughter minerals that have been transported from a broken inclusion during the sample preparation.

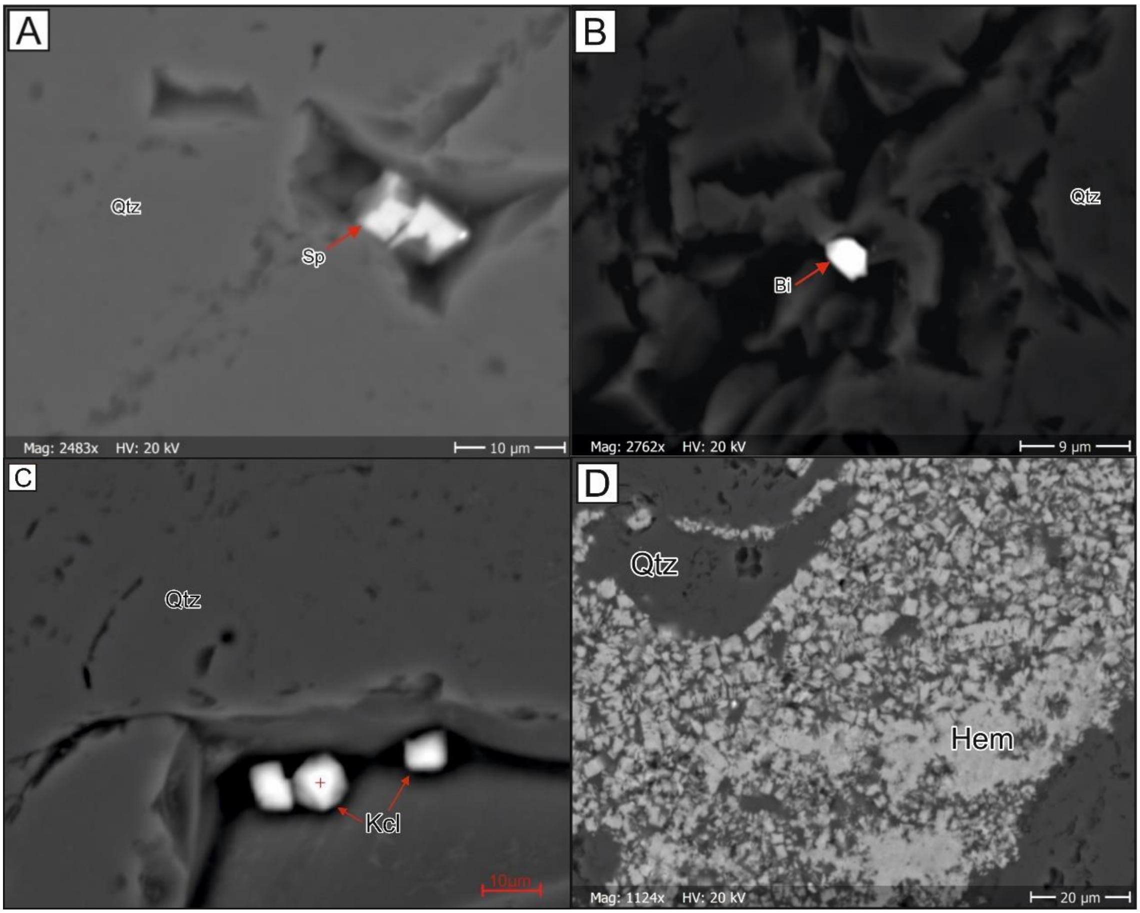

Figure 11. *A) Sphalerite in a healed fracture in massive quartz. B) VFG native bismuth in massive quartz. C) Sylvite (KCl) grains precipitated in grain boundary of recrystallized quartz. D) Hematite alteration is common. Abbreviations: Bi=native bismuth, Hem=hematite, Sp=sphalerite, Qtz=quartz.*

4.1.2.3. Type 3 carbonate-tourmaline-quartz veins

The ore mineralogy of V_3 is generally more or less similar to that of V_1. Galena occurs again as a few micron grains mostly in carbonate filled fractures in the vein quartz (Fig. 12). Carbonate in general is more pervasive in V_3 than in other vein types. Carbonate veins are commonly cutting the tourmalines, proving that the tourmaline predates carbonate (Fig. 12). Pyrite is more abundant in this vein type than in V_1, and like galena and other ore minerals, it is mainly crystallized within the fracture filling carbonates (Fig. 12).

Aside from the carbonate filling veins, ore mineralization generally occur in the grain boundaries of single tourmaline crystals. Cu-Ni-Zn-alloys without any notable detection of S or O are present in many occasions in the cracks on the grain margins of the tourmaline grains (Fig. 12). Since their sizes are very small, it is, however, possible that they are simply particles left over from sample preparation. Rutile is found as less than 10 µm grains and it is occasionally forming aggregates with more or less chloritized biotite. Apatite, which is not as common in V_3 as in V_1, occurs in between tourmaline crystals. Unidentified U-Ce-bearing mineral was observed as intergrowth in intensely seriticed plagioclase. REE mineralization, namely consisting of cerium-bearing minerals, occurs in rare occasions within the cavities in the quartz.

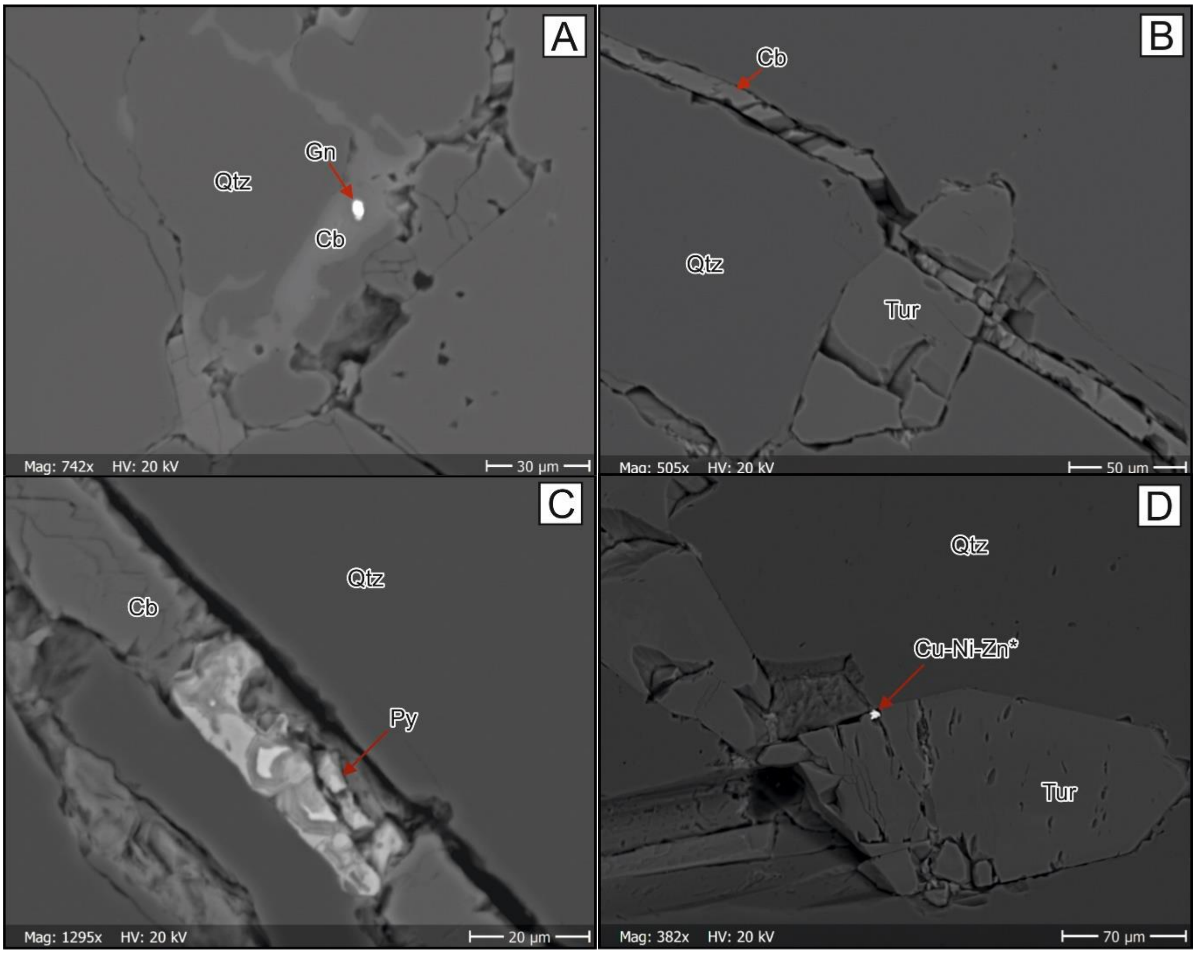

Figure 12. *A) Very fine grained galena in a fracture filled by calcite. B) Calcite vein cutting through tourmaline grain. C) Pyrite in calcite vein. D) Cu-Ni-Zn-alloy in the grain boundary of tourmaline crystal. Abbreviations: Cb=carbonate, Gn=galena, Py=pyrite, Tur=tourmaline, Qtz=quartz.*

4.1.2.4. Type 4 quartz vein

Pyrite, which is the most abundant of ore minerals, occurs as euhedral to subhedral crystals with sizes ranging from 30 µm up to 100 µm. Pyrite has generally mineralized alongside with biotite grains, some of which have almost completely chloritized. In other cases, pyrite was also found to be associated with carbonates. In a single occasion, native silver of a size of few microns was observed in the grain boundary of euhedral pyrite (Fig. 13). The core of this pyrite is healthy but the rims of it has been oxidized. Bismuth is present as very fine grained, 1-2 µm inclusions in a coarse grained K-feldspar (Fig. 13). Some of the K-feldspars are patchy albitized and contain barium enriched spots, which are visible as lighter colored areas (Fig. 13).

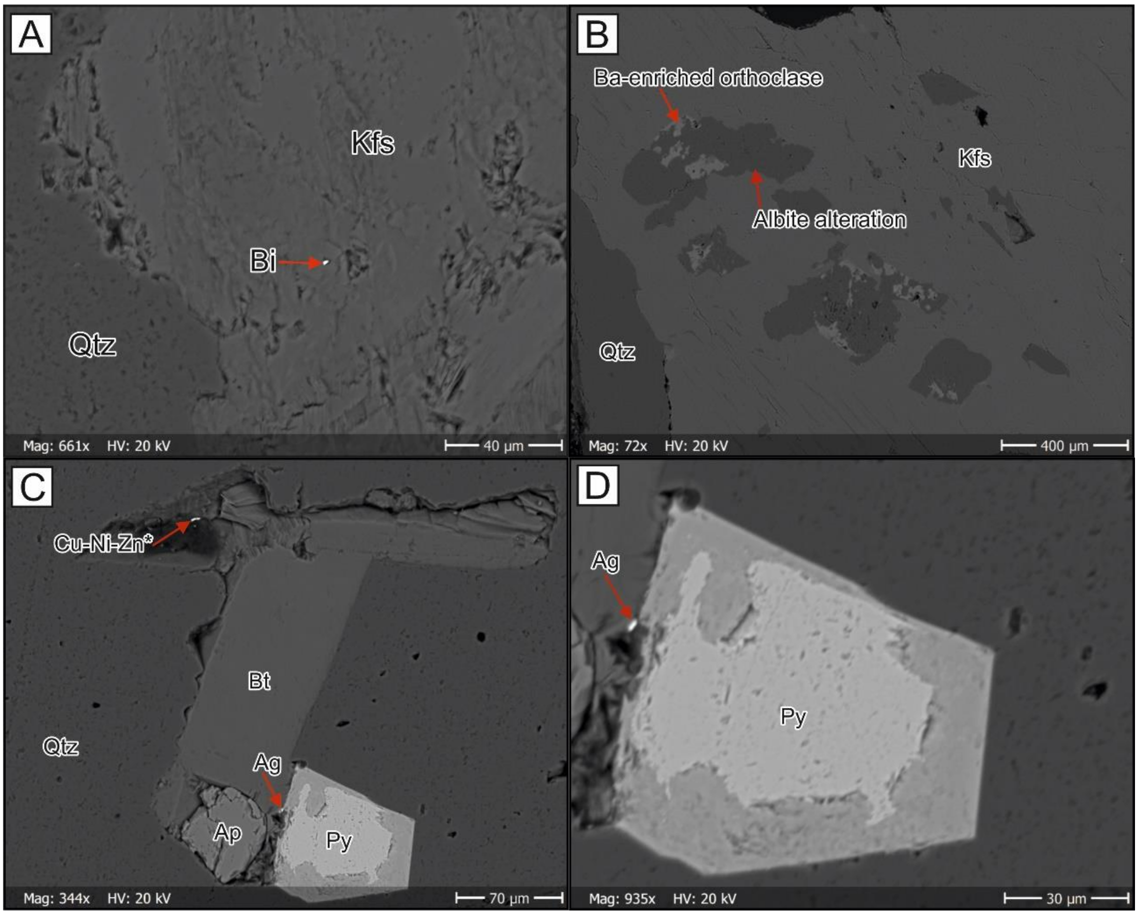

Figure 13. *A) Native bismuth in a large K-feldspar grain. B) Partly albite altered K-feldspar. C) Intergrowth of biotite, apatite and pyrite. D) Close-up image of the native Silver sitting on the edge of a partly oxidized pyrite. Abbreviations: Ap=apatite, Bt=biotite, Bi=native bismuth, Kfs=K-feldspar, Py=pyrite, Qtz=quartz.*

Like in V_1, monazite-(Ce/La) is abundant in vein type V_4 and they are mainly mineralized in the fracture surfaces (Fig. 14) and are in many cases accompanied by carbonates (Fig. 14). In some cases Monazite was also found in close associations with biotite. Monazite was also found on the grain boundaries between apatite and quartz (Fig. 14). Apatite is likewise abundant and commonly it occurs associated with biotite and carbonate. Apart from being the main fracture filling material, carbonate minerals occur as medium grained crystals. They show in many case enrichment of strontium, which can be seen as ~1 µm bright spots in BSE images. Carbonates also bear titanite and iron oxide minerals.

The characteristic for V_4 in general is the presence of As-containing minerals, which are completely lacking in the other vein types. Arsenopyrite of the size of few µm was observed on a couple of occasions in the cavities in the quartz. Also, a single mineral of tennantine-tetrahedrite solid solution was found as 3x3 µm grain (Fig. 14). The elemental ratios of this mineral show it is closer to the tennantine end-member, due to its high copper content compared to antimony. Traces of Ag were observed also in this particular mineral, suggesting that the silver is substituting the copper site.

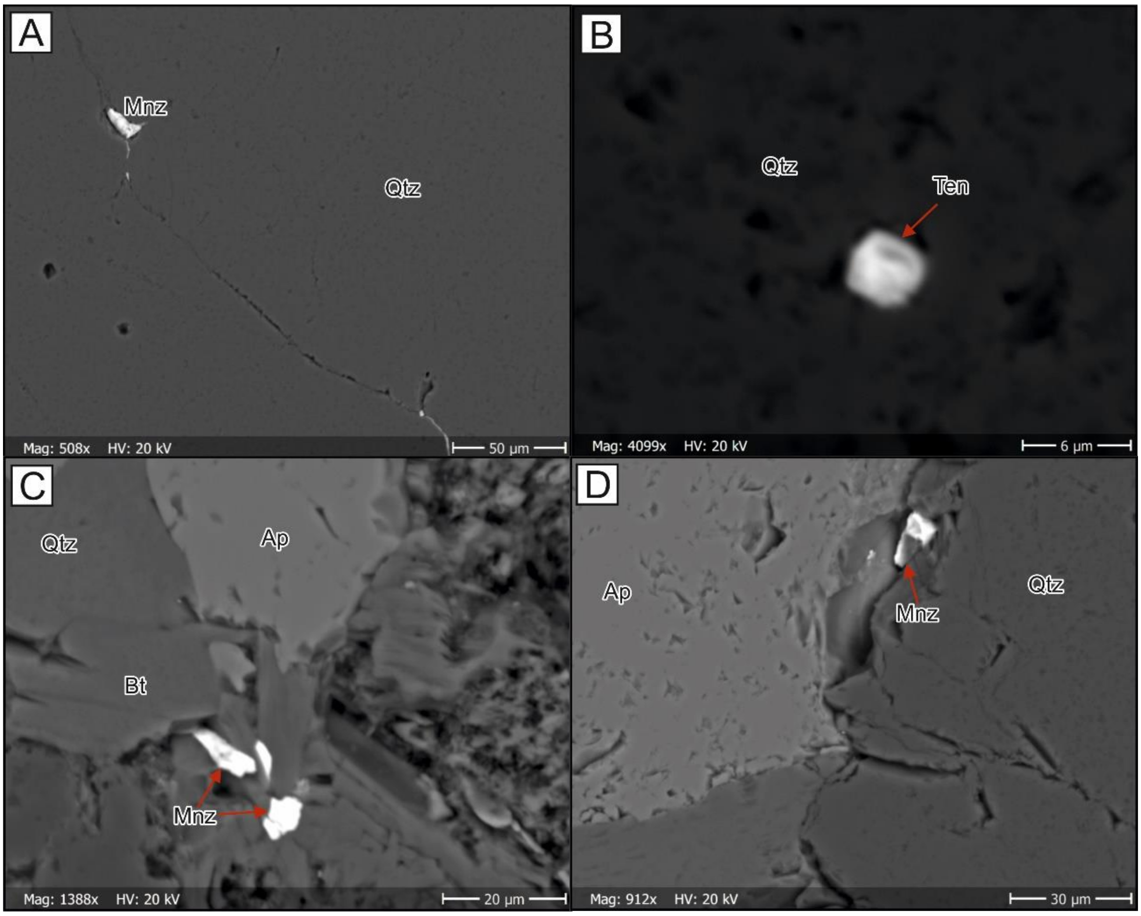

Figure 14. *A) Monazite crystallized on fracture surface. B) VFG tennantine in massive quartz. C) Monazite intergrowth in biotite. D). Monazite on a grain boundary between apatite and quartz. Abbreviations:, Ap=apatite, Bt=biotite, Mnz=monazite, Ten=tennantine, Qtz=quartz*

4.1.2.5. Tonalite

Samples representing the host rock tonalite show clear barium enrichment as inclusions in biotite and K-feldspar grains. Hydrothermal chlorite is commonly replacing biotite. Some of the chlorites contain REE-enriched spots, which are clearly observable as brighter color than in the surrounding mineral and they generally show elevated values of Ce, Th and Sm (Fig. 15). Two types of biotite were observed, which could be easily differentiated by their difference in color in BSE images (Fig. 15). The darker colored were common biotite with high Al content and low Fe and Mg concentrations. The lighter colored biotite were Mg and Fe enriched. As can be seen in (Fig. 15), the biotite appear non-foliated and generally consist of fine grained sheets which are forming larger aggregates. Zircons are common as intergrowths in the biotite. Single barites of a size of few micro meters are also present as was also observed in type 1 veins. They show also enrichment in Nd.

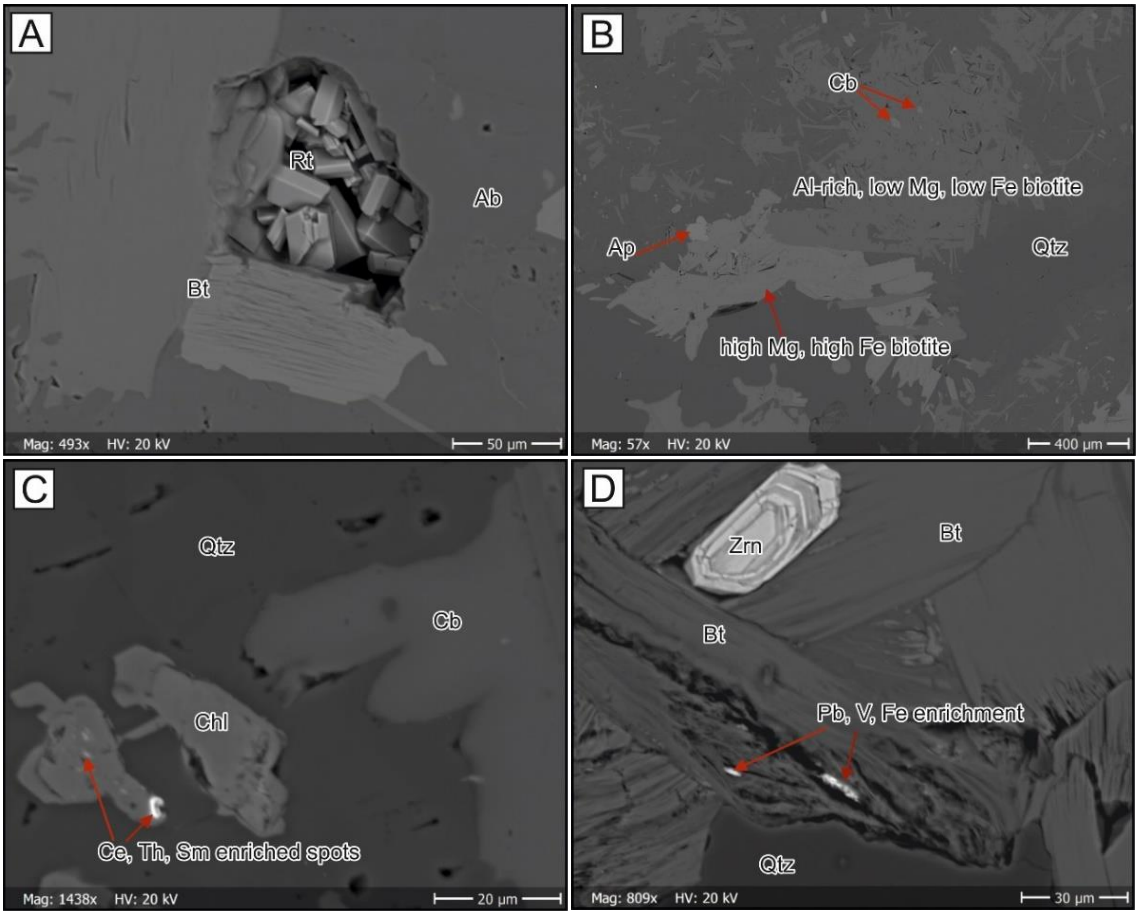

Figure 15. *A) Euhedral rutile grains mineralized in cavity formed between albite and biotite grains. B) Two types of biotite differing clearly in geochemistry. The lighter colored biotite shows enrichment in Mg and Fe, whereas the darker colored one shows enrichment in Al and depletion in Mg and Fe. C) Intergrowths of Ce, Th and Sm enriched spots in chlorite. D) Euhedral zircon intergrowth in biotite. In the lower biotite grain can be seen bright spots, which contain Pb, V and Fe enrichment. Abbreviations: Ab=albite, Ap=apatite, Bt=biotite, Cb=carbonate, Chl=chlorite, Qtz=quartz Rt=rutile,, Zrn=zircon..*

4.2. Fluid inclusion petrography

Type 1 quartz veins (V_1)

Type 1 quartz veins (V_1) are massive, and they contain all of the different kind of fluid types. Fluid inclusion assemblages appear mostly as clearly defined trails (Fig. 16), making it relatively easy to distinguish between different FIAs, which account for the fact that V_1 is the most studied sample in this study.

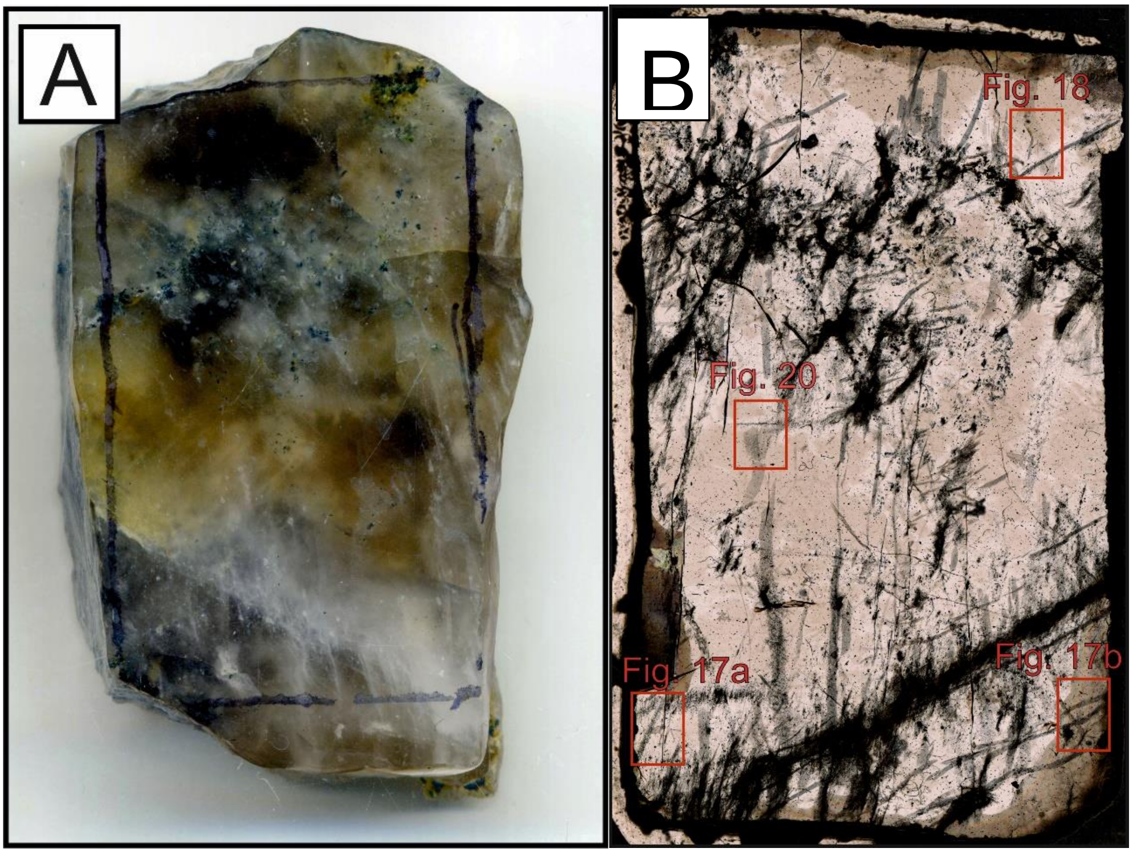

Figure 16. *A) Sample KUI7 representing the type 1 quartz vein (V_1). B) High resolution overview image of the KUI7 sample.*

The aqueous type A and B inclusions in V_1 appear as clearly defined trails. Type A inclusions are occasionally elongated clearly in the direction of the trail, although it is not definite in all trails, as can be seen in Fig. 17. They have two major orientations which are cutting each other in approximately 45 degree angle (Fig. 17). The type A and B inclusions are trapped in many cases in healed fractures, indicating the secondary nature of these fluids. The relationship between type B and C inclusions is not clear, since somewhat isolated type C inclusions may occur close to the clearly defined trails consisting of type B inclusions.

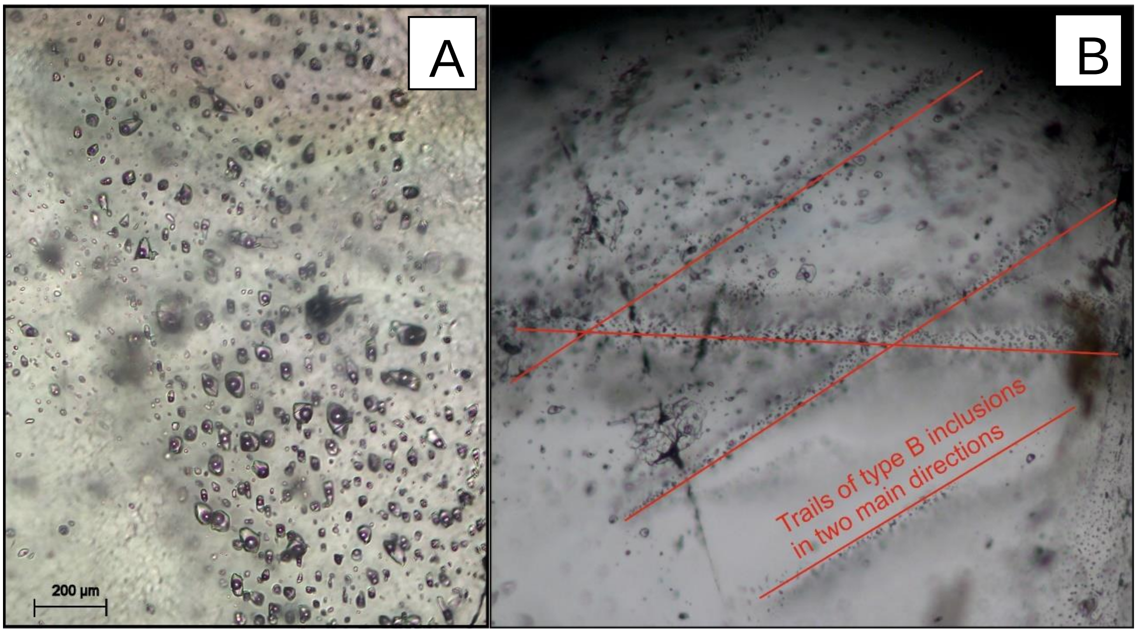

Figure 17. *A) Type A $L_{80-90}V\pm S$ aqueous inclusions. They are somewhat irregular shaped and in this particular example not clearly elongated in the direction of the trail. B) Typical appearance of aqueous type B inclusions in V_1. They are characterized by clear defined trails with two main orientations.*

Type D aqueous-carbonic inclusions occur as clearly defined trails as can be seen in Fig. 18. There is a clear crosscut sequence between type D inclusions and type B aqueous inclusions, which shows that the type D inclusions are older. Even though the relative age relationship between these fluid types can be determined, it is unknown whether the differences in trapping times are significant. The deformed textures seen in type D inclusions which cannot be seen in any other fluids type in these type 1 quartz veins would, however, suggest that these probably are significantly earlier than the other type of inclusions.

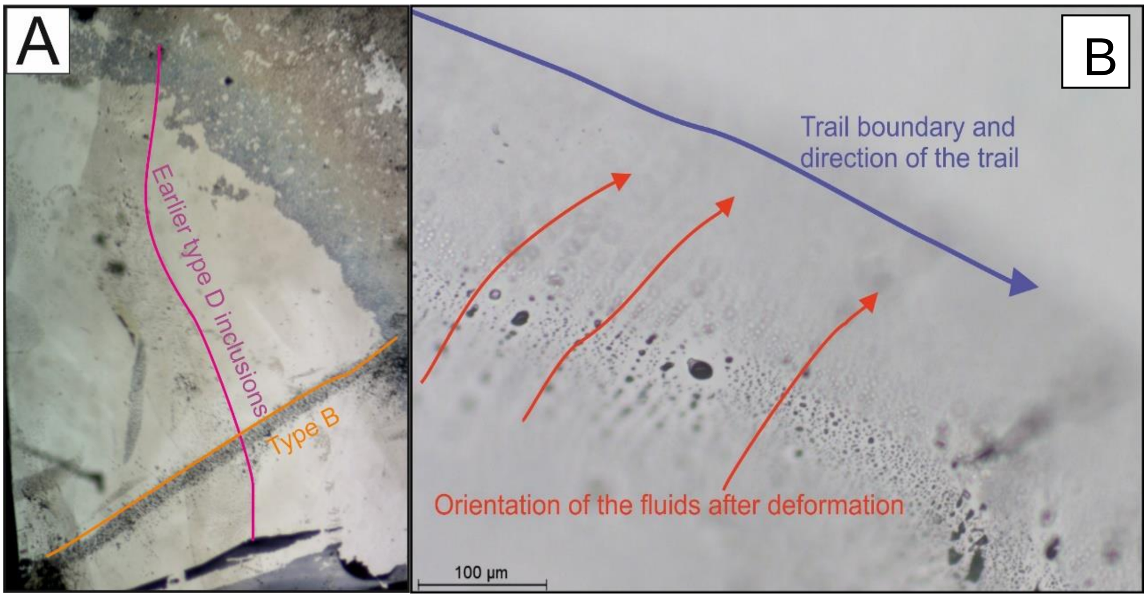

Figure 18. *A) Crosscut sequence between FIA KUI7-C4-FIA2 representing early type D fluid inclusion and FIA KUI7-C4-FIA1 representing type B aqueous inclusion. Characteristic for these trails are faint appearance with clear trail outlines. B) Close-up image of the trail of type D inclusions. They often are elongated parallel to the direction of the trail due to deformation processes. Exception is made by the larger inclusion seen in the middle of the picture, which is oriented in the direction of the trail.*

Type C aqueous-carbonic inclusions occur mainly as small trails, although in some situations they can be somewhat isolated (Fig. 19). It is however most likely that even those isolated inclusions in fact belong to unclearly defined trail of inclusions. In some of the FIAs, presence of accidental solids are abundant.

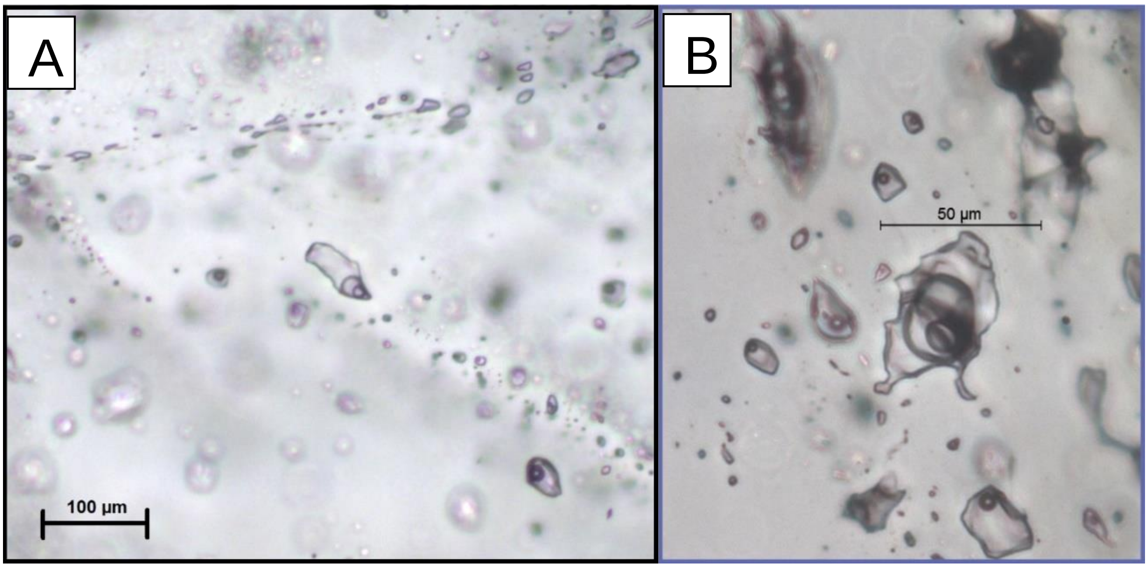

Figure 19. *A) Sort of isolated 3-phase inclusions of type C. B) Inclusion of KUI7-C1-FIA8. One of the largest aqueous-carbonic inclusions observed out of all the samples. The CO_2 vapor bubble is clearly visible in the largest inclusion in the middle of the picture.*

Signs of boiling event were observed in type B fluids, since within a single FIA there is a strict line where inclusions change from two phase liquid-vapor inclusions to vapor-rich, consisting completely of vapor-phase (Fig. 20).

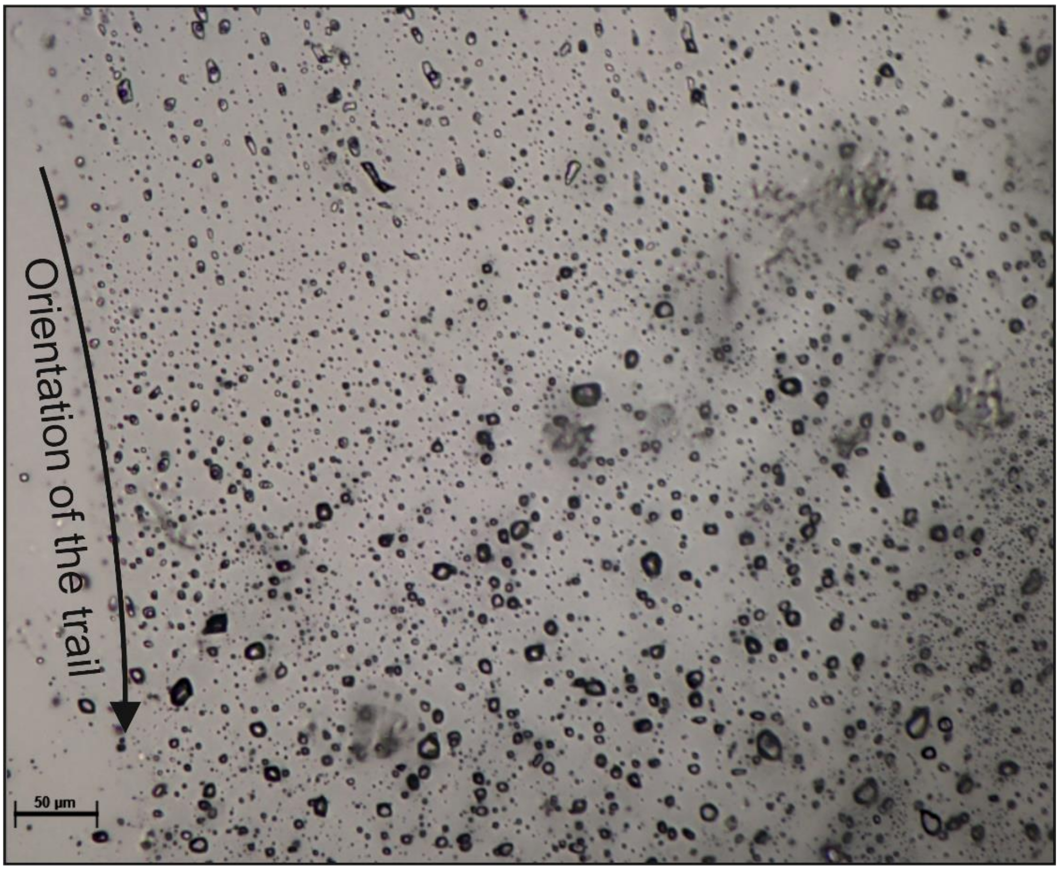

Figure 20. *Evidence of boiling system can be seen as the co-existence of two immiscible fluid phases in type B fluids. In the upper part 2-phase liquid-vapor inclusions are visible and at the bottom there are vapor-rich inclusions.*

The sample KUI8 is representing the same V_1, but in contrast to sample KUI7, it also contains the host tonalite. In this sample trails of CO_2 vapor rich inclusions are crosscutting older dominantly aqueous inclusions (Fig. 21). These type G vapor-rich carbonaceous inclusions were only observed in this sample, and it seems apparent that it is related to the carbonatization of the boundary zone between the host rock tonalite and the quartz vein.

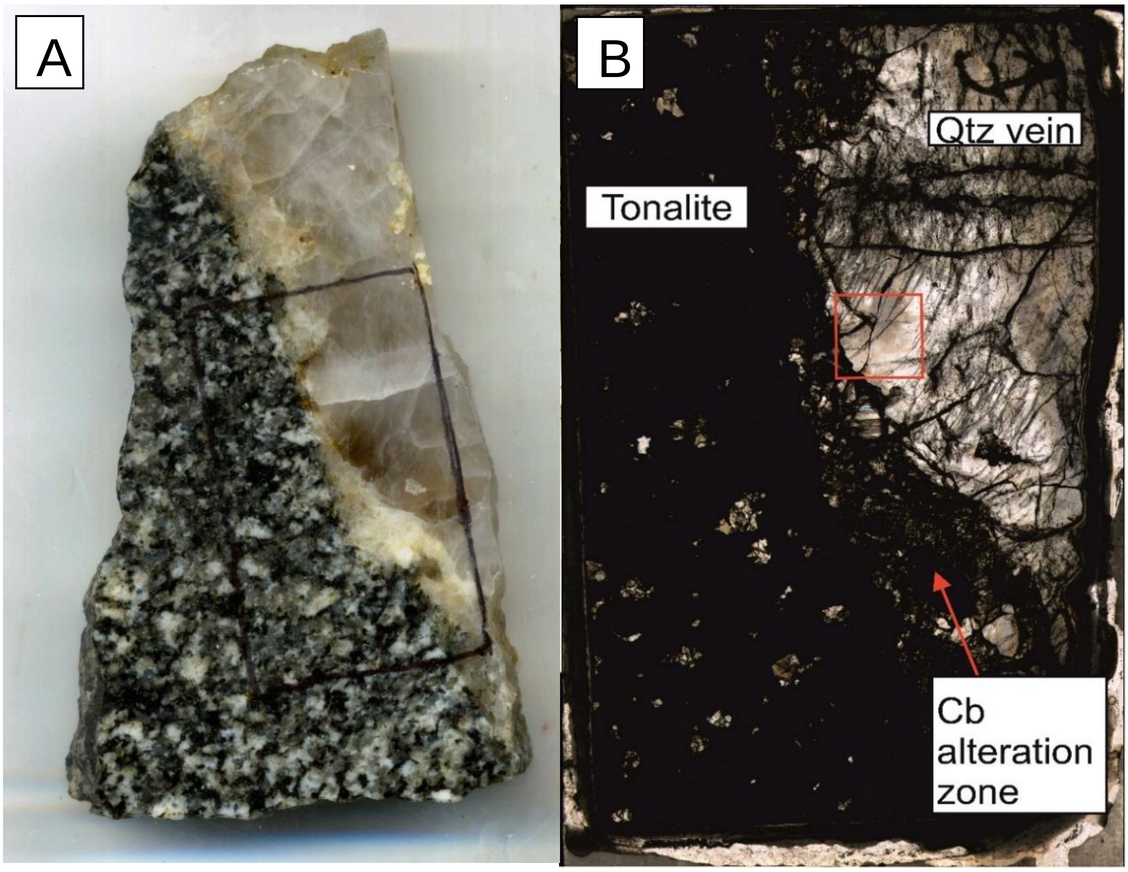

Figure 21. *A) Thick section outlines of KUI8 sample B) High-resolution overview image of KUI8 Thick section*

In Fig. 22 can be seen the close-up image of the trail consisting of type G inclusions, which is really clearly defined and the crosscut sequence is showing that the inclusions in the crosscut are elongated towards the trail direction of this type G trail, proving the later nature of this fluid type than the adjacent trail consisting of aqueous type B inclusions.

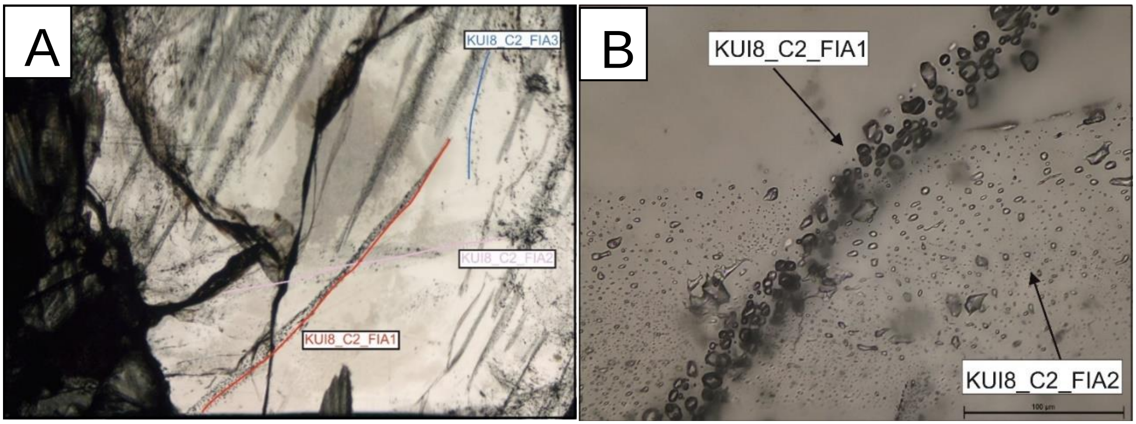

Figure 22. *C) KUI8-CHIP2 showing different FIAs studied D) Close-up image of the crosscut of KUI8_C2_FIA1 and KUI8_C2_FIA2. The dark, vapor-rich CO_2 inclusions are younger than the liquid-rich ones.*

Type 2 quartz vein (V_2)

Type 2 quartz vein (V_2) appear as milky white in the sample (Fig. 23). Similar tension gash structure as was reported in earlier study of Pampalo by Fusswinkel et al. (2017) can be seen in the overview image (Fig. 23).

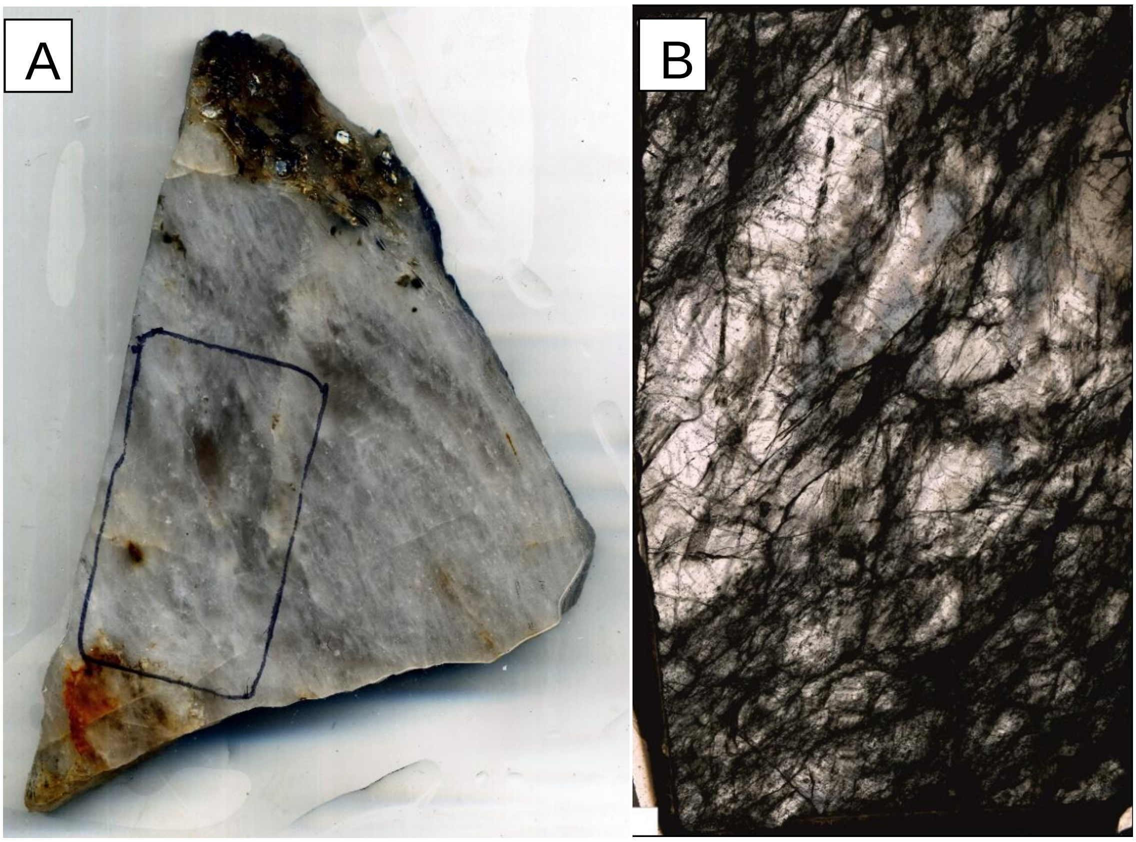

Figure 23. *A) Thick section outlines of KUI5 sample representing the type 2 quartz vein (V_2). B) KUI5 Thick section.*

The inclusions in the tension gashes are oriented parallel to the main stress direction and form continuous trails of inclusions in the same orientation (Fig. 24). Fluid inclusions observed in these tension gashes were aqueous type B inclusions, and they were crosscut by aqueous-carbonic fluids. The crosscut sequence is not clear enough to allow age determination, although it looks like the aqueous-carbonic type C inclusions are younger. These inclusions in the tension gashes were unfortunately too small and too close to the surface for further LA-ICP-MS analyses. Type C inclusions are also present as clearly defined trails with several orientations (Fig. 25), but also as petrographically unclear occurrences of wide-spread trails or possible clusters.

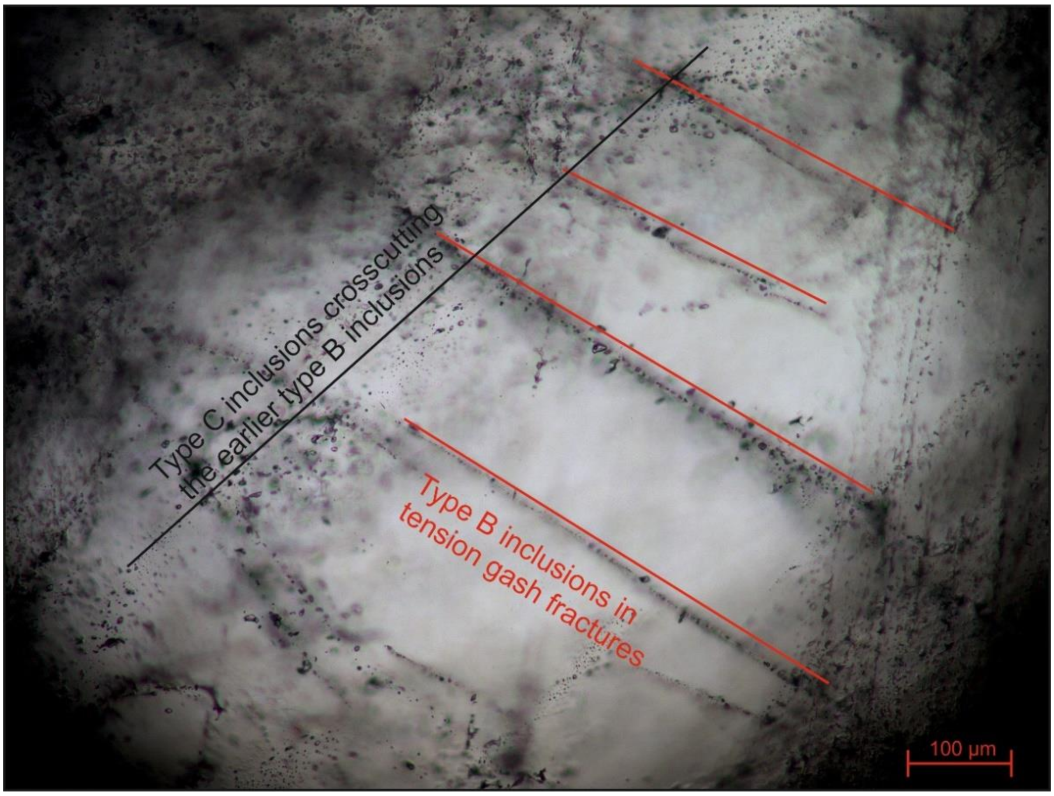

Figure 24. *Type B aqueous inclusions in possible tension gash fractures. The type B inclusions are elongated parallel to the direction of the trail. Type C aqueous-carbonic inclusions are crosscutting these earlier aqueous fluid inclusions.*

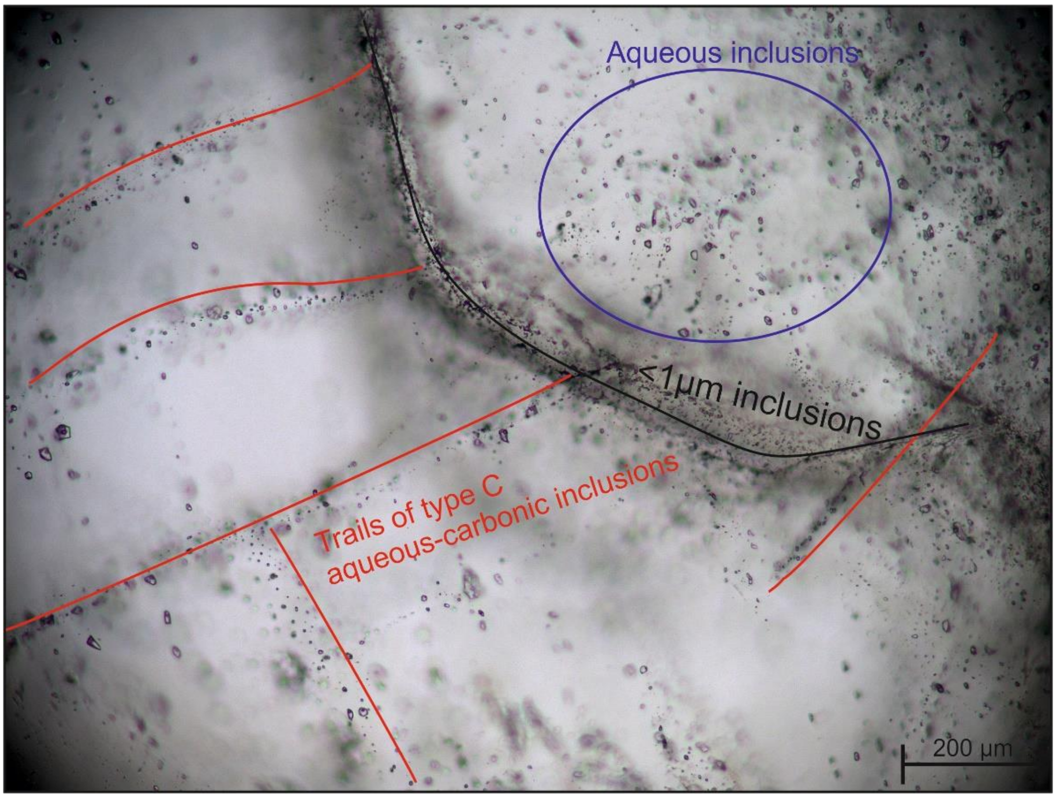

Figure 25. *Trails of type C aqueous-carbonic inclusions in* V_2.

Type 3 carbonate-tourmaline-quartz vein (V_3)

The sample and the overview image of the type 3 carbonate-tourmaline-quartz vein is shown in Fig. 26. Recrystallization of the quartz is visible especially in the lower part, although it is not as intense as in V_4.

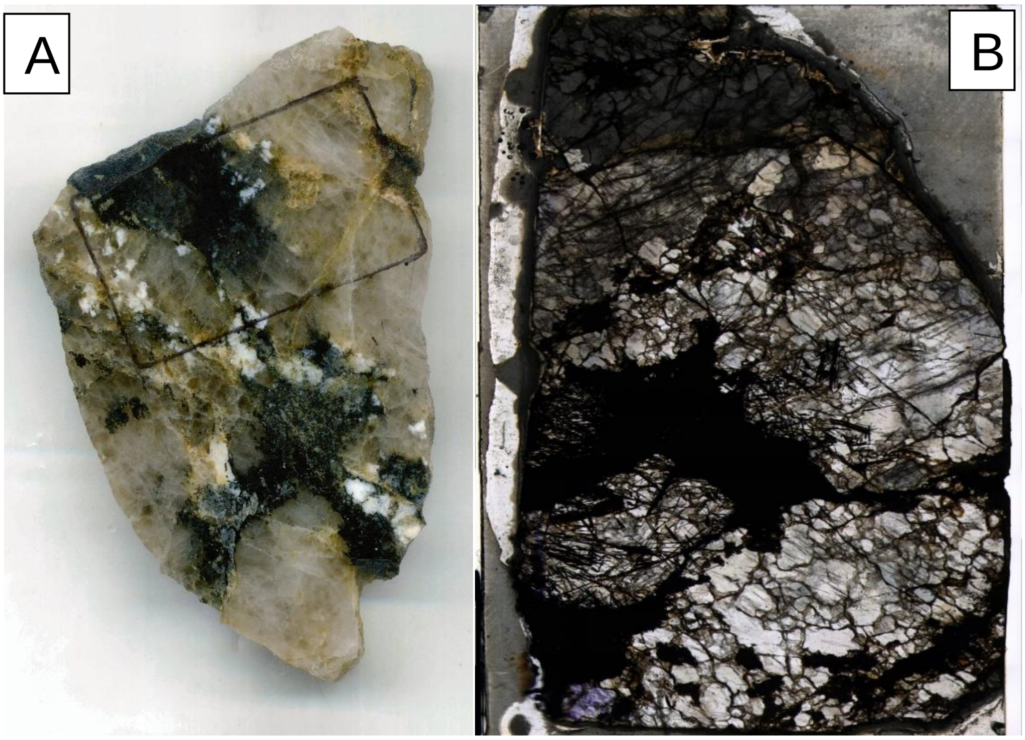

***Figure 26**. A) Thick section outlines of KUI6 sample, representing the type 3 carbonate-tourmaline-quartz vein type (V_3). B) High resolution overview image of the KUI6 thick section. The black elongated minerals are tourmalines.*

The Type D inclusions in V_3 have a deformed nature with potential signs of re-equilibration (Fig. 27). They are in some cases closely associated with tourmalines by forming distinct trails of inclusions, which are in some cases ending at tourmaline crystals (Fig. 27). This would suggest that these type of inclusions are possibly related to forming of the tourmalines.

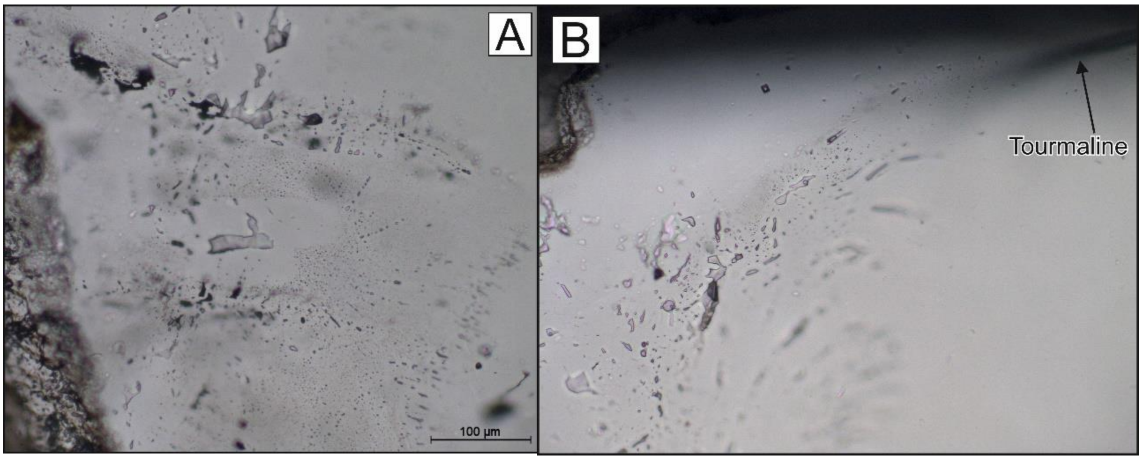

Figure 27. A) Type D inclusions with deformation and re-equilibliration textures. B) Trail of Type D inclusions that seems to be related to forming of tourmaline crystal.

Type A inclusions in V_3 occur in two main orientations, as seen in Fig. 28. They are in many cases crosscutting each other, but as they represent same type of inclusions, they are most probably trapped almost coevally and therefore the crosscutting relationships does not help in building an image of the evolution of the fluids in this type of vein. However, the type A inclusions do not show any deformation or clear re-equilibrilation textures that were observed in the assumed early type D inclusions. The sizes of individual fluid inclusions are highly variable within single FIAs (Fig. 28).

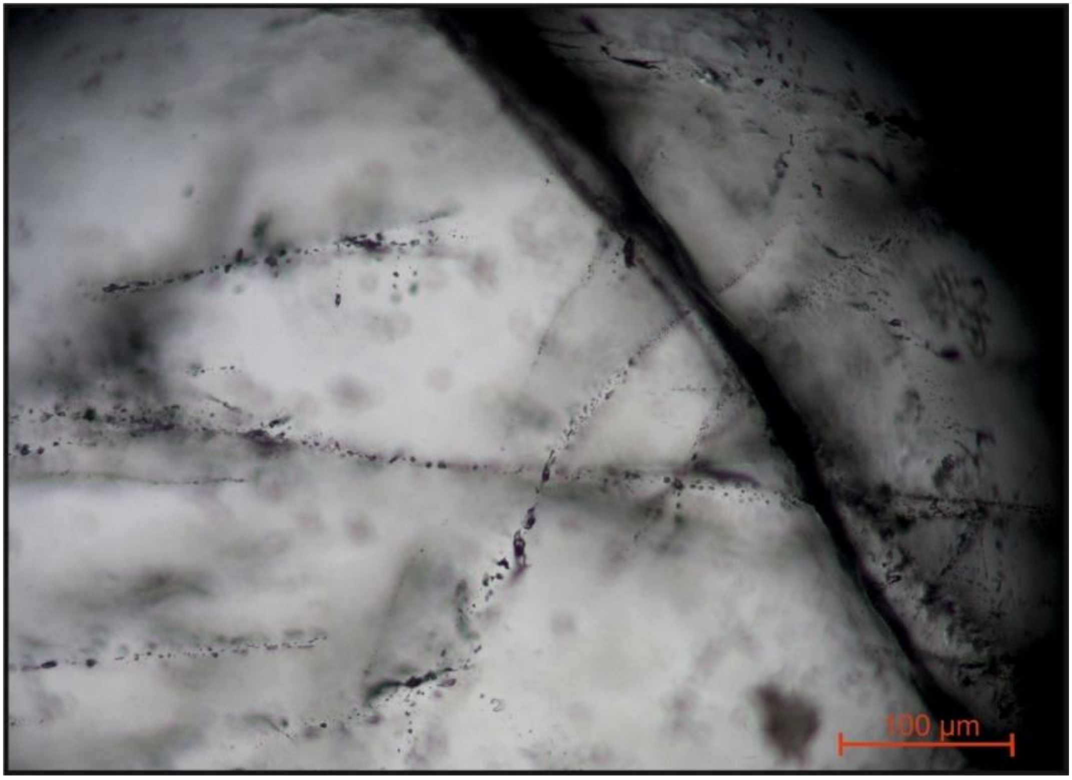

***Figure 28.** Secondary trails consisting of small high-salinity type A inclusions occurring in two main orientations.*

Type 4 quartz vein (V_4)

Recrystallization of the quartz is a characteristic for type V_4 veins. In cases with recrystallized quartz it is easy to identify fluid inclusion assemblages as secondary as they are cutting through several different quartz crystals (Fig. 29). Fluid types present in V_4 are aqueous type B, aqueous-carbonic type C and type E late aqueous fluids.

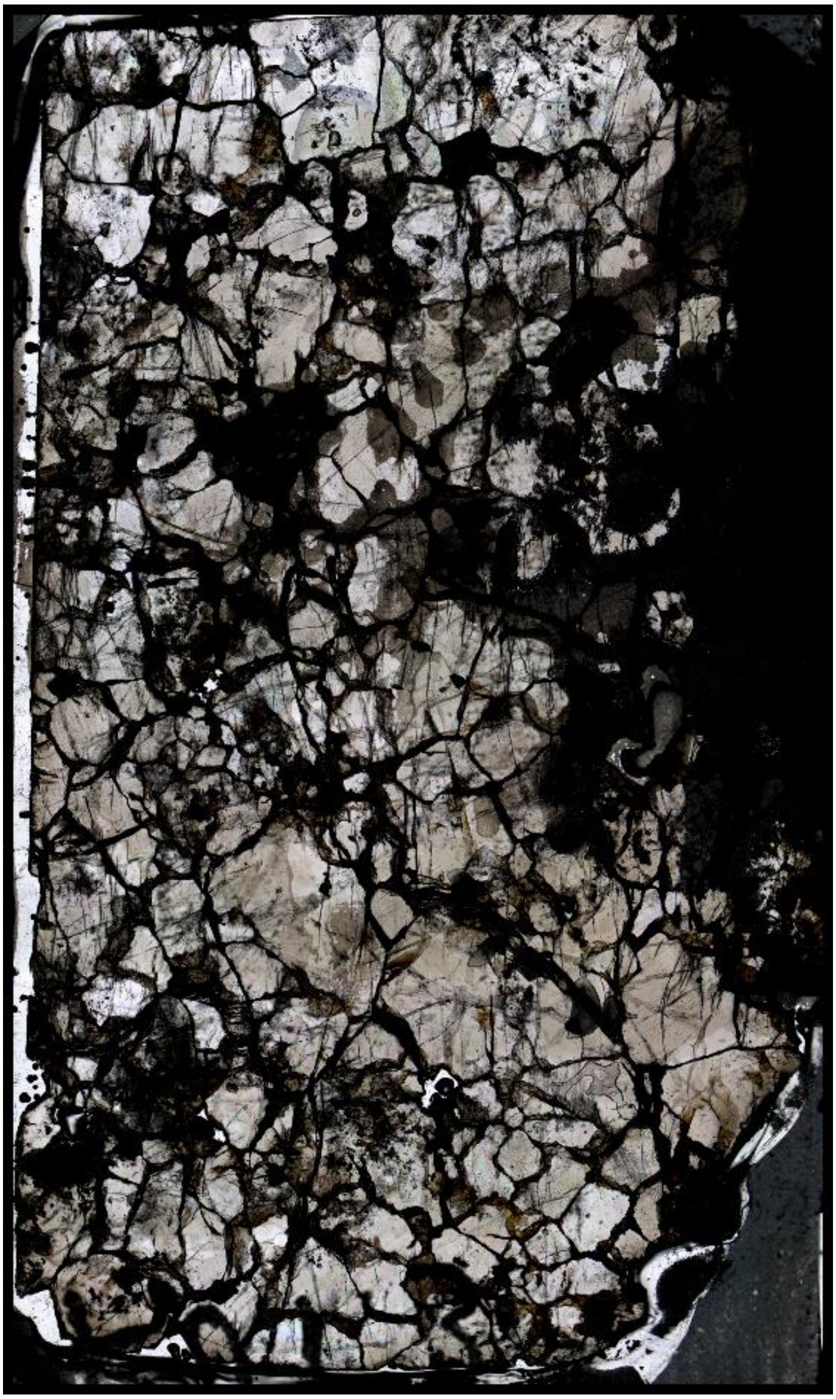

Figure 29. *High-resolution scan of sample KUI3 representing type 4 recrystallized quartz vein (V_4).*

Petrography in the type 4 quartz veins (V_4) is generally quite ambiguous, as many FIAS form neither clearly defined trails nor clusters. High invariabilities within individual FIAs occur in many cases due to necking down of the inclusions. Several gaseous phases exist in these fluid inclusions affected by necking (Fig. 30). There is also huge variability in the size of different inclusions within single FIAs, as can be seen in Fig. 31. In many occasions most of the inclusions are less than 1 µm in size, with only occasional presence of ~10 µm inclusions.

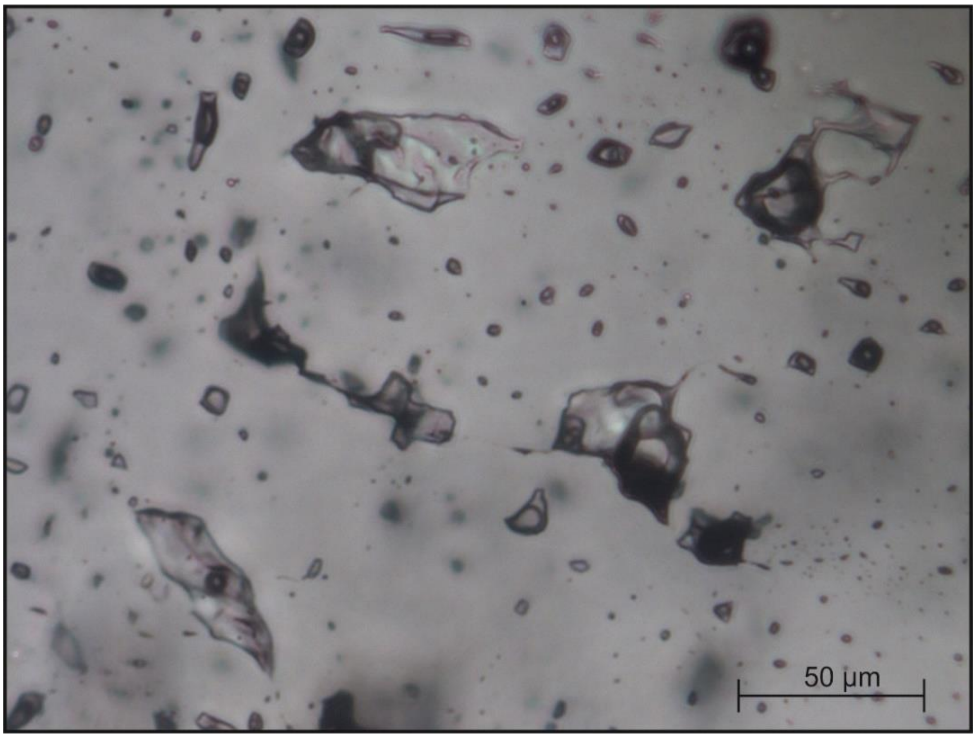

Figure 30. *FIA of highly variable liquid-vapor ratios due to necking down of the inclusions.*

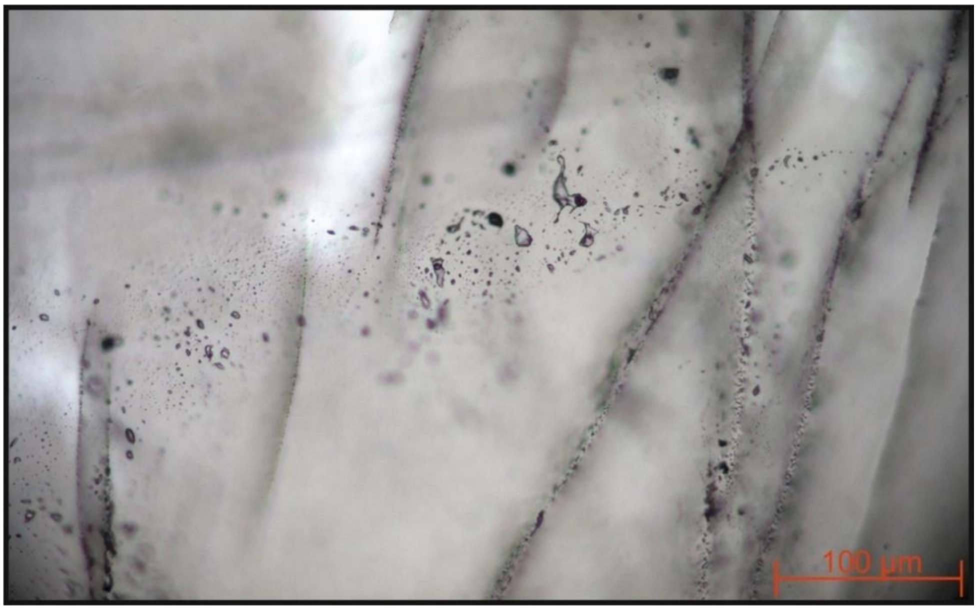

Figure 31. *Typical appearance of trails in V_4. Sizes of the inclusions within FIA are highly varying.*

4.2.1. Fluid inclusion types

Fluid inclusions were divided into different types based on their petrographic and microthermometric properties. Type A, B, E and F represent aqueous-dominated inclusions, although later Raman studies revealed that some of these also have traces of hydrocarbons and in some cases N_2 in their gas phases. However, in these aqueous-rich inclusions the content of other gas species than H_2O is presumed to be so low that their presence will have only minor to no effect on the salinity calculations.

Type C inclusions are mostly 3-phase aqueous-carbonic inclusions at room temperature (~24 °C). In some cases the presence of CO_2 vapor could only be observed during cooling of the inclusions, as the partial homogenization temperature of the carbonaceous phase can be below that of room temperature. Only one FIA presenting Type G inclusions was observed and they consist of vapor-rich (>90 % of vapor) to full-vapor CO_2 inclusions.

Type D inclusions are classified also as aqueous-carbonic bearing inclusions. They show distinct differences to those of classified as aqueous inclusions in both petrographic and microthermometric studies, as well as to those aqueous-carbonic fluid inclusions of type C. The appearance is not a typical 3-phase inclusion as is in the type C inclusions. The appearance of the vapor phase is similar to those classified as H_2O+CH_4 inclusions in some earlier fluid inclusion studies (e.g. Poutiainen and Partamies 2003b). During heating-cooling experiments in microthermometry, no changes could be observed in the vapor phase even at the operational limit of -196 °C.

The key characteristic features of all different type of fluid inclusions observed during this study are listed in the next chapters. Volumetric proportions of the inclusions have been optically estimated at room temperature (~24 °C) and are described with abbreviations. L refers to liquid phases and V refers to vapor phase. In cases of aqueous-carbonic inclusions, aqueous liquid phase is reported as $L_{(aq)}$ and carbonaceous liquid phase as $L_{(car)}$. The volumetric proportions are reported as volume percent of liquid phase (e.g. $L_{80}V$ refers to inclusion with 80 vol. % of liquid, 20 vol. % of vapor).

4.2.1.1. *Type A fluid inclusions*

The aqueous-rich type A inclusions are highly saline with the average measured salinity of ~20 wt. % NaCl equivalent and they are present in all different vein types except in the latest V_4. Total homogenization temperatures range from 184 °C to 329 °C, and they are showing variation between each vein type, as the highest values of 329 °C occur V_1, whereas in V_2 and V_3 the measured values were 184 °C and 244 °C, respectively. Liquid-vapor ratios are fairly constant $L_{80–90}V$. Appearance of the liquid phase is generally clear, with slightly reddish to greenish tint. Some of the FIAs representing type A fluid inclusions contain possible daughter minerals, which are often needle shaped (Fig. 32). They were proven to be nahcolite and strontianite by the later Raman laser analyses. These solids were not, however, observed in every inclusion within the same FIA, which indicates they could in fact be accidental solids precipitated in the inclusions. Sizes of type A inclusions range from less than 1 µm up to 30 µm. The smaller inclusions (<1–5 µm) are generally regular shaped with occasionally occurring negative crystal shapes, whereas many of the larger inclusions are somewhat irregular and planar.

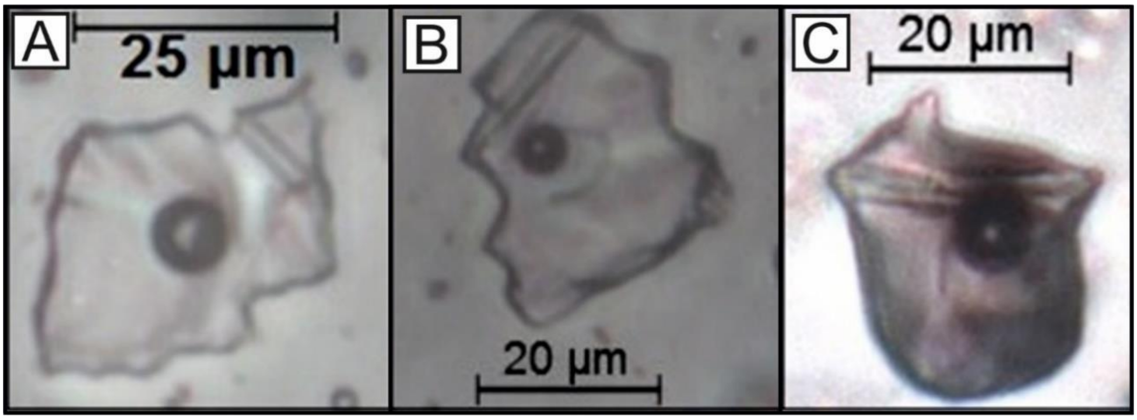

Figure 32. *Type A $L_{80–90}V$+S fluid inclusions containing possible daughter minerals.*

4.2.1.2. *Type B fluid inclusions*

Type B inclusions are moderate salinity (~8–12 wt. % NaCl equivalent) aqueous-rich inclusions that were discovered in V_1, V_2 and V_4. Total homogenization temperatures range from 164 °C to 394 °C, and are noticeably lower in V_2 than in V_1 and V_4.

Petrographically this fluid type is very similar to those of type A. At a room temperature they appear as 2-phase $L_{80}V$ inclusions with occasionally occurring different shaped and sized transparent accidental solids (Fig. 33). The sizes of the type B fluid inclusions are generally ranging from less than 1 µm to 20 µm, with their average sizes being smaller than in type A inclusions. In V_1 these occurred always as clear defined large trails, whereas in V_2 they were observed in a tension gash fractures, where they were oriented parallel to the main stress direction.

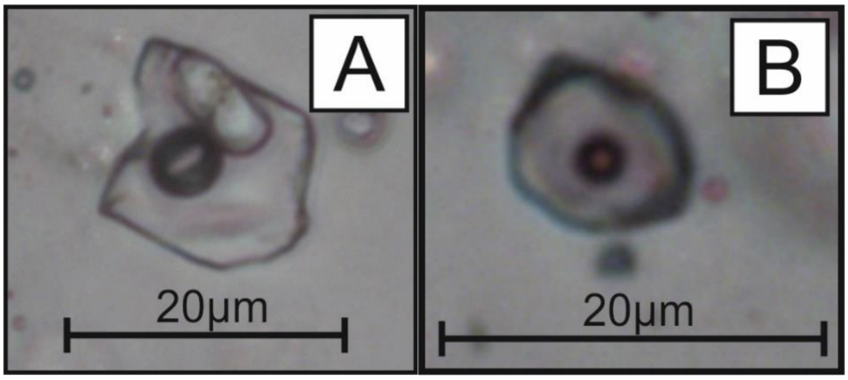

Figure 33. *A) Type B aqueous inclusion containing unidentified relatively large accidental solid. B) Typical appearance of type B aqueous fluid inclusion.*

4.2.1.3. Type C fluid inclusions

Type C inclusions are low to moderate salinity (~4–10 wt. % NaCl equivalent) and they appear typically as 3-phase $L_{(aq)}+L_{(car)}\pm V_{(car)}$ at a room temperature (Fig. 34). They were observed in V_1, V_2 and V_4. Total homogenization temperatures range from 276 °C to 426 °C, meaning the homogenization occur generally at notably higher temperatures than in aqueous fluid types.

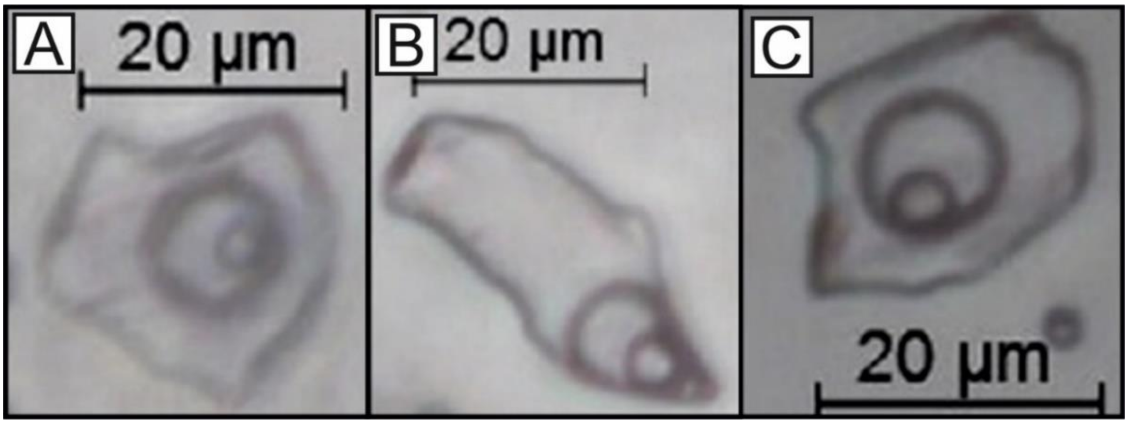

Figure 34. *Type C 3-phase aqueous-carbonic inclusions.*

The partial homogenization temperatures of carbonaceous-phase are highly variable within some FIAs, ranging from 16.6 °C to 26.4 °C, meaning that some of the inclusions are only showing as 2-phase $L_{(aq)}$+$L_{(car)}$ at the room temperature. In some, mostly in the smaller inclusions, the carbonic vapor bubble is moving rapidly in Brownian motion. Some of these type C inclusions contain accidental unidentified solids, which are occasionally opaque minerals. The liquid-vapor ratios are generally $L_{60-80(aq)}L_{10-20(car)}V$. However, there is much variation between different FIAs. Sizes of the inclusions are ranging from less than 5 µm up to 50 µm.

4.2.1.4. Type D fluid inclusions

The type D inclusions are mostly liquid-rich with low (-1.07–1.50 °C) ice melting temperatures, corresponding to salinities of 1.85 to 2.57 wt. % NaCl equivalent. Total homogenization occurs between temperatures of 337 °C to 391 °C. The liquid phase is reddish to yellowish with higher relief when comparing to aqueous-rich inclusions of type A and B. The liquid-vapor ratios vary a lot even within the same FIA (Fig. 35). Phase ratios of inclusions within the same FIA generally ranges from L_{100} to vapor-rich $L_{<30}V$. Appearance of the vapor phase is very dark, and it shows no change during cooling to the instrument maximum (-196 °C). This would indicate that the vapor phase consists of other gas species than CO_2 or H_2O, most likely hydrocarbons and/or N_2. Both, the liquid-rich and vapor-rich inclusions have similar, low ice melting temperatures in the $liquid_{(aq)}$.

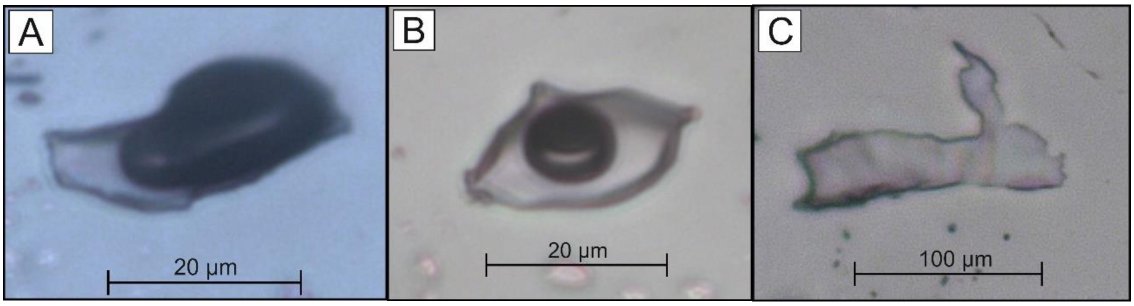

Figure 35. *Type D inclusions of highly variable phase proportions. A) Vapor-rich type D inclusion. B) ~$L_{60}V$ type D inclusion. C) L_{100} type D inclusion.*

Type D inclusions are in all observed crosscutting sequences older than the adjacent fluid inclusion assemblages. They are also often deformed in direction parallel to the direction of the trail. Deformation of the shapes and microstructures of fluid inclusions in quartz veins indicates weak plastic deformation of the quartz (Tarantola et al. 2010). The fact that type D inclusions are in all situations older than the adjacent trails and that these are the only ones with clear deformation features indicates that they represent a very early feature in the analysed quartz veins.

The classification of these type D inclusions is however a bit problematic, since situationally they consist of only the liquid-phase without any vapor-phase present. In those situations they could be easily simply just mapped as aqueous-rich low salinity inclusions, such as the type E inclusions. However, the presence of the dark vapor phase in some of the inclusions within all the observed FIAs distinctly differentiates these from the type E inclusions. Added the fact that the presence of these is similar to those of primary re-equilibrated fluid inclusions in Pampalo reported by Molnàr et al. (2016a). Similar type of re-equilibrated early H_2O+CH_4 fluids have also been observed in fluids in Rämepuro prospect (Poutiainen and Partamies 2003b). Therefore, the microthermometry data of this type of inclusions should be approached with caution, since if they are also in fact re-equilibrated inclusions, it would make the microthermometry results equivocal and non-reliable.

4.2.1.5. Type E fluid inclusions

Type E fluid inclusions are low-salinity (~1–4 wt. % NaCl equiv.) and their sizes are generally very small, ranging from <1 µm to 5 µm. Total homogenization temperatures of type E fluids are generally the lowest of all fluid types in this study, although the measured Th(tot) are highly variable as they range from as low as 54 °C to 286 °C. In all observed crosscutting sequences type E fluids were found to be younger than adjacent fluid types, which supports their late nature. These young fluids were observed in V_1 and V_4. Their shapes are generally irregular and planar, however, the inclusions of ~1 µm in size are negative crystal shaped (Fig. 36).

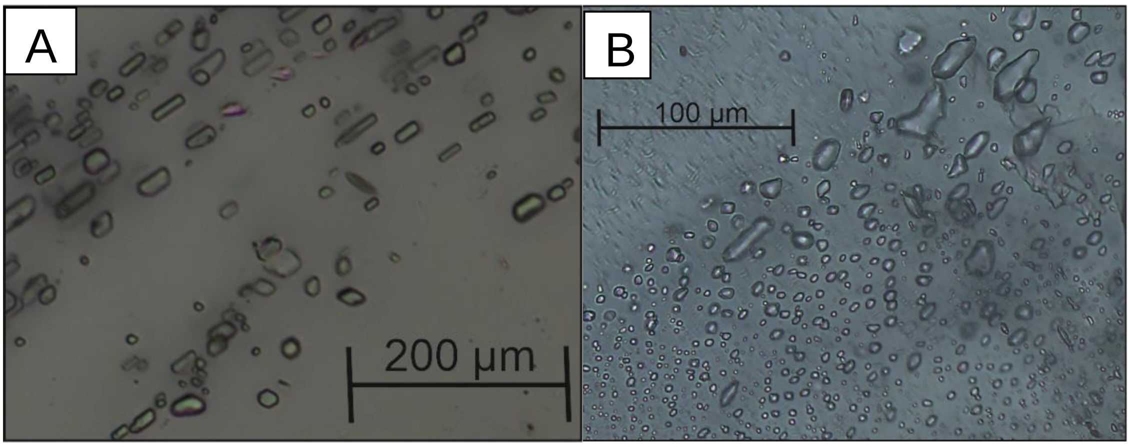

Figure 36. *L_{100} Type E low salinity inclusions. In this rare occasion, the inclusions have negative crystal shapes.*

Essentially, all type E fluid inclusions are pure aqueous liquid inclusions (L_{100}). However, some of the inclusions within single FIA contain inclusions with ~5-10% of vapor phase, which were used for the homogenization temperature measurements. The presence of those inclusions that contain the vapor phase is similar to the aqueous inclusions of type A and B, and they clearly differ from those of type D inclusions. Due to their lack of the vapor phase and very small size it was not possible to analyse them further with the Raman laser or LA-ICP-MS. The homogenization temperatures vary a lot, indicating that at least some re-equilibration has occurred. As all of the FIAs representing type E inclusions were not observed crosscutting other FIAs, it is also possible that the one of the classified type E FIA (KUI7-C3 FIA6), with suspiciously high homogenization temperatures (average 286 °C) is in fact those of the early type D re-equilibrated inclusions.

4.2.1.6. Type F fluid inclusions

Type F inclusions were only found in V_1. They form clusters around large green, most probably chlorite melt inclusion. It is also possible that these are originally very large fluid inclusions that have broken and leaked and then filled with chlorite-bearing fluids in a later fluid event or that there originally has simply been a cavity within the quartz.

According to Touret (2001), clusters are in most cases formed by transposition of a former, larger cavity. Total homogenization occurs at temperatures from 159 °C to 193 °C.

Liquid-vapor ratios are highly variable, and sizes of the inclusions are ranging from <1 µm to 5 µm. They are mostly all-liquid inclusions (L_{100}), however, as can be seen in Fig. 37, the largest inclusions have liquid and vapor phases with an average $L_{90}V$ ratio. Salinities are moderate, yet quite variable, as the measured salinities of two different FIAs are 6.53 and 13.87 wt. % NaCl equivalent. The salinities are therefore yielding similar values than type B aqueous inclusions. Due to the very small size of these type of inclusion, they could not be further analysed with Raman or LA-ICP-MS.

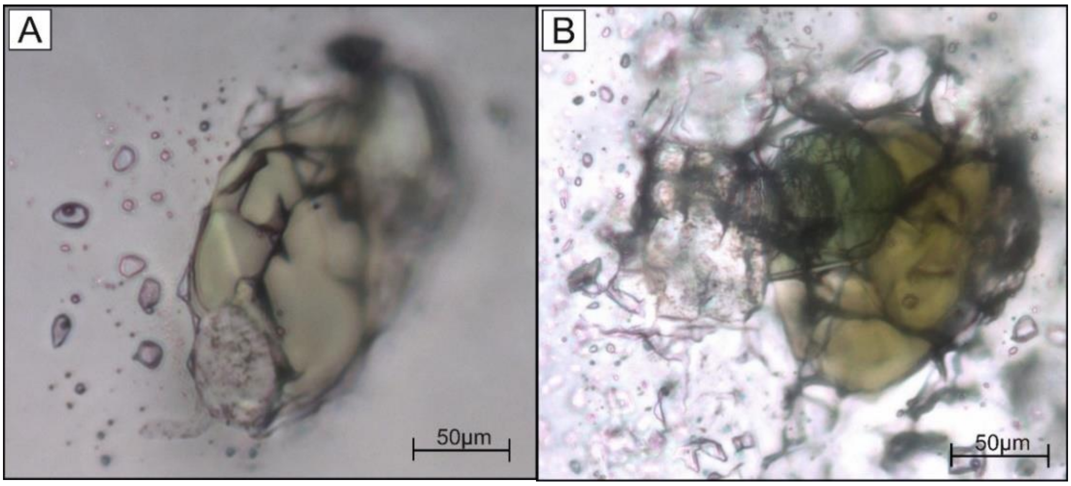

Figure 37. *Type F inclusions appearing as halos around interpreted chlorite melt inclusions. During cooling and heating these melt inclusions, several bubbles appeared. The ice melting temperatures of the melt inclusions appeared to be very similar as in the inclusions around them.*

4.2.1.7. Type G fluid inclusions

These mainly full-vapor inclusions were found only in sample KUI8, representing V_1. As no certain evidence of any re-equilibration was observed in this type of fluids, they presumable record immiscibility during their entrapment (Goldstein and Reynolds 1994). Total homogenization occurs at over 400 °C. From some of the inclusions containing 10-20 % of liquid, the ice melting temperatures could be measured. This is not however very accurate since the variable nature of these inclusions. Raman studies revealed that the gas phase consist of N_2 and CH_4 in addition to the CO_2, however the triple point of CO_2 was measured very close to -56.60 °C in microthermometric studies, which would point toward other gas species than CO_2 being really low content.

The optical appearance of most of these inclusions is completely black (Fig. 38), however some of the inclusions contains clearly liquid phase which could been only recognized during heating-cooling studies by microthermometry. The sizes of this type of inclusions range from 5 µm up to 30µm.

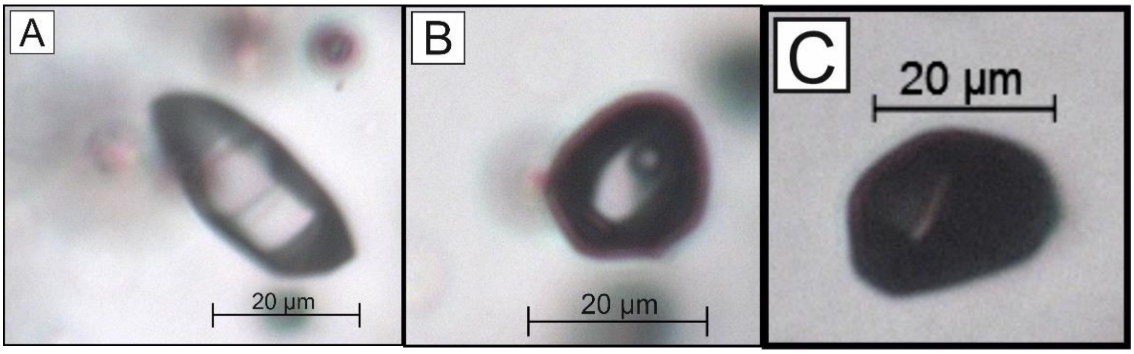

Figure 38. *All of the inclusions in the pictures are from the same FIA. This shows the variable appearance of these type of inclusions. A) Not detectable vapor phase in this inclusion. B) Possibly aqueous-carbonic inclusion with optically hidden rim of* H_20 *around the inclusion. C) Full-vapor inclusion.*

4.3. Microthermometry

The combined petrographic, microthermometric and Raman data are presented in the Table 6 below. In the table are shown the average values of each FIA. Raman data is incomplete due to the problems arised with the hardware and software linked to the Raman laser. Total homogenization temperatures are not measured of all of the inclusions for the simple reason that for the possibility of exploding of fluid inclusion the whole chip had to be observed for phase changes at the same time. This process did not allow reliable measurements of more than 4-5 FIAs per chip.

***Table 6**. Combined petrographic, Microthermometric and Raman data of the analysed FIAs. The reported values are average values of FIAs. T_m(Car)=melting temperature of solid carbonaceous-phase, T_m(ice)=final ice melting temperature, T_m(Cla)=Clathrate melting temperature, T_h(Car)=partial homogenization of carbonaceous-phase, T_h(tot)=total homogenization temperature.*

Sample	FIA	n	Petrography/comments	Phase props (at room T)	T_m(Car) (°C)	T_m(ice) (°C)	T_m(Cla) (°C)	T_h(Car) (°C)	T_h(tot) [a] (°C)	$NaCl_{eq}$ (wt.%)	Method	Gas Species	FI type
Type 1 quartz veins													
KUI7-C1	1	10	Small to large trails. Nahcolite daughter minerals	$L_{80-90}V+S$		-16.30			329	20.24	BULK	C_3H_8	A (Aqueous)
KUI7-C1	2	7	Small to large trails. Nahcolite daughter minerals	$L_{80-90}V+S$		-17.96			329	20.94	BULK	C_3H_8	A (Aqueous)
KUI7-C1	3	6	Late secondary trails	$L_{100}/L_{95}V$		-0.70			190	1.22	BULK	n/a	E (Aqueous)
KUI7-C1	4	6	Halos around chlorite melt inclusions	$L_{100}/L_{90}V$		-9.94			193	13.87	BULK	n/a	F (Aqueous)
KUI7-C1	5	5	Possibly PS trail	$L_{60-80}/(L)+V$	-56.60	-9.04	6.00	31.00	380	8.70	Q2	n/a	C (Aqueous-carbonic)
KUI7-C1	6	4	Small trail, younger than crosscutting FIA5	$L_{60-80}V\pm S$		-19.06			n/a	21.73	BULK	n/a	A (Aqueous)
KUI7-C1	7	7	Possibly PS trail	$L_{70-80}L_cV^*$	-57.40		5.53	22.92	330	6.12	Q2	$CO_2+C_3H_8$	C (Aqueous-carbonic)
KUI7-C1	8	5	Small, isolated trails	$L_{40-60}L_cV$	-56.70		5.26	28.76	370	6.12	Q2	$CO_2+C_3H_8$	C (Aqueous-carbonic)
KUI7-C3	1a	11	Large trail	$L_{85}V\pm S$		-4.09			n/a	6.59	BULK	$C_3H_8+N_2$	B (Aqueous)
KUI7-C3	1b	7	Large trail	$L_{60}V$		-8.75			386	12.57	BULK	$C_3H_8+N_2$	B (Aqueous)
KUI7-C3	2	10	Secondary trails	$L_{80-90}V/L$		-5.92			n/a	9.10	BULK	n/a	B (Aqueous)
KUI7-C3	3	7	Small trails	$L_{60-80}L_cV$	-56.60		3.88	25.97	n/a	8.00	Q2	n/a	C (Aqueous-carbonic)
KUI7-C3	4	7	Small, possibly PS trails	$L_{30-40}V$		-8.72			388	12.52	BULK	n/a	B (Aqueous)
KUI7-C3	5	6	Late secondary trails	$L_{100}/L_{90}V$		-3.55			n/a	5.79	BULK	$C_3H_8+N_2$	E (Aqueous)
KUI7-C3	6	5	Late secondary trails,	L_{100}		-0.76			286	1.33	BULK	n/a	E (Aqueous)
KUI7-C3	7	5	Small trails/isolated inclusions	$L_{80}L_c\pm V$	-56.70		5.20	18.96	421	6.56	Q2	CO_2	C (Aqueous-carbonic)
KUI7-C4	1	17	Large secondary trail, accidental solids	$L_{100}/L_{80-90}V\pm S$		-8.44			314	12.21	BULK	$C_3H_8+N_2$	B (Aqueous)
KUI7-C4	2	6	Deformed early trails, possibly re-equilibrated	$L_{100}/L_{80}V$		-1.50			337	2.57	BULK	$C_3H_8+CH_4+N_2$	D (Aqueous-carbonic)
KUI7-C5	1	14	Halos around chlorite melt inclusions	$L_{90}V\pm S$		-4.05			159	6.53	BULK	n/a	F (Aqueous)
KUI7-C6	1	7	Late secondary trails	$L_{100}/L_{85}V$		-2.52			54	4.22	BULK	n/a	E (Aqueous)
KUI7-C6	2	12	Trail containing accidental needle-shape minerals	$L_{100}/L_{70-95}V$		-13.26			n/a	17.13	BULK	n/a	A (Aqueous)
KUI7-C6	3	16	Trail, older than crosscutting FIA1	$L_{90}V\pm S$		-14.18			n/a	17.94	BULK	n/a	A (Aqueous)
KUI8-C1	1	5	Secondary trails	L_xL_c	-57.42			20.10	n/a	n/a	n/a	n/a	C (Aqueous-carbonic)
KUI8-C1	2	4	Secondary trails	Variable	-56.60		6.00	28.7	n/a	4.42	Q2	n/a	C (Aqueous-carbonic)
KUI8-C2	1	8	Trail of vapor-rich inclusions, younger than FIA2	$V_{80-100}\pm L$	-56.60	-4.00			>400	n/a	n/a	$CO_2+N_2+CH_4$	G (Carbonic)
KUI8-C2	2	10	Trail of more liquid rich inclusions than in FIA1	$L_{85-90}V$		-3.18			164	5.23	BULK	$C_3H_8+CO_2$	B (Aqueous)
KUI8-C2	3	4	Sort of isolated small trails	$L_{60}V$		-7.00			n/a	10.49	BULK	n/a	B (Aqueous)

Type 2 quartz vein

KUI5-C1	1	4	Possibly PS trails in regrowth quartz	$L_{80}L_cV\pm S$	-57.05		4.13	28.7	354	8.50	Q2	n/a	C (Aqueous-carbonic)
KUI5-C1	2	10	Small trails cutting FIA4 parallel	$L_{80}L_cV\pm S$	-56.86		7.94	26.50	354	6.67	Q2	C_3H_8+N_2	C (Aqueous-carbonic)
KUI5-C1	3	3	Cluster	$L_{80}V$		-14.3			n/a	18.04	BULK	n/a	A (Aqueous)
KUI5-C1	4	3	Large secondary trails	$L_{80}L_c$	-62.00		6.50	n/o	289	n/a	n/a	n/a	C (Aqueous-carbonic)
KUI5-C2	1	5	Ambiguous petrography, small trails or clusters	$L_{80}L_cV$	-56.55		2.90	24.21	305	10.36	Q2	n/a	C (Aqueous-carbonic)
KUI5-C2	2	5	Trail of very small inclusions	$L_{75-80}L_cV$	-56.90		3.50	27.64	426	11.05	Q2	n/a	C (Aqueous-carbonic)
KUI5-C2	3	8	Younger than FIA4, accidental solids (halite?)	$L_{90}V$		-16.84			184	20.10	BULK	n/a	A (Aqueous)
KUI5-C2	4	4	Inclusions elongated in direction of trail.	$L_{75-85}L_cV$	-56.92		n/o	29.92	323	n/a	n/a	n/a	C (Aqueous-carbonic)
KUI5-C3	1	4	Small trails of mostly very small <1µm inclusions	$L_{5-80}L_c\pm V$*	-56.75		n/o	17.84	n/a	n/a	n/a	n/a	C (Aqueous-carbonic)
KUI5-C3	2	3	Cutting tension gash-type inclusions, younger	$L_{80}L_cV$	-57.49		n/o	24.37	n/a	n/a	n/a	n/a	C (Aqueous-carbonic)
KUI5-C3	3	2	Trail, FIs highly elongated in the direction of trail	$L_{40}L_c\pm V\pm S$	-57.19		5.27	20.13	n/a	n/a	n/a	n/a	C (Aqueous-carbonic)
KUI5-C4	1	6	Tension gash, parallel to main stress direction	$L_{90}V$		-4.10			194	6.59	BULK	n/a	B (Aqueous)
KUI5-C5	1	3	Small possibly PS trail	$L_{80}L_cV\pm S$	-57.08		2.72	28.59	n/a	12.19	Q2	n/a	C (Aqueous-carbonic)
KUI5-C5	2	3	Small possibly PS trail	$L_{75}L_c\pm S$	-58.96		3.65	8.73	n/a	9.50	Q2	n/a	C (Aqueous-carbonic)

Type 3 tourmaline-carbonate-quartz vein

KUI6-C1	1	4	Large secondary trails	$L_{80}V$		-14.97			244	18.61	BULK	n/a	A (Aqueous)
KUI6-C1	2	3	Secondary trail consisting of very small inclusions	$L_{90}V$		~-23			n/a	n/a	n/a	n/a	A (Aqueous)
KUI6-C1	3	4	Secondary trail	$L_{90}V$		~-23			n/a	n/a	n/a	n/a	A (Aqueous)
KUI6-C1	4	4	Clusters/trails of possibly re-equilibrated fluids	$L_{80}V/L$		-1.07			391	1.85	BULK	n/a	D (Aqueous-carbonic)

Type 4 quartz vein

KUI3-C1	1	6	Trails, no changes to vapor phase during cooling	$L_{50-70}V\pm S$		-8.62			n/a	12.41	BULK	n/a	B (Aqueous)
KUI3-C1	2	9	Possibly re-equilibrated with varying L/V ratios	$L_{100}/L_{80}V$		-6.46			267	9.95	BULK	n/a	B (Aqueous)
KUI3-C1	3	8	Late secondary trails	L_{100}		-0.69			n/a	1.21	BULK	n/a	E (Aqueous)
KUI3-C1	4	2	Sort of isolated inclusion close to FIA5	$L_{45}L_cV$	-57.39		5.98	23.67	351	3.83	Q2	n/a	C (Aqueous-carbonic)
KUI3-C1	5	5	Trail, several opaque solids.	$L_{40-70}V\pm S$		-8.00			393	11.70	BULK	C_3H_8+N_2	B (Aqueous-carbonic)
KUI3-C6	1	6	Petrography ambiguous, many leaked inclusions	Variable		-5.83			394	8.98	BULK	C_3H_8+N_2	B (Aqueous)
KUI3-C6	2	6	Petrography ambiguous	Variable	-56.90		4.87	21.75	276	6.93	Q2	n/a	C (Aqueous-carbonic)
KUI3-C6	3	4	Possibly re-equilibrated fluids	$L_{30}V$		-0.77			316	1.34 [b]	BULK	n/a	C (Aqueous-carbonic)

[a] All observed temperatures of homogenization were from liquid to vapor. [b] No clathrates observed. Salinity calculated based on ice-melting temperature.

In those FIAs that contain variable liquid-vapor ratios, the homogenization temperatures are likewise inconsistent and variable. In situations with consistent liquid-vapor ratios, the homogenization temperatures were also quite consistent. For example particular FIAs of type B fluid inclusions appeared as highly homogenous in microthermometric studies. As can be seen in Fig. 39, the total homogenization temperatures are very consistent in this particular FIA. The complete microthermometry data can be found in Table 6.

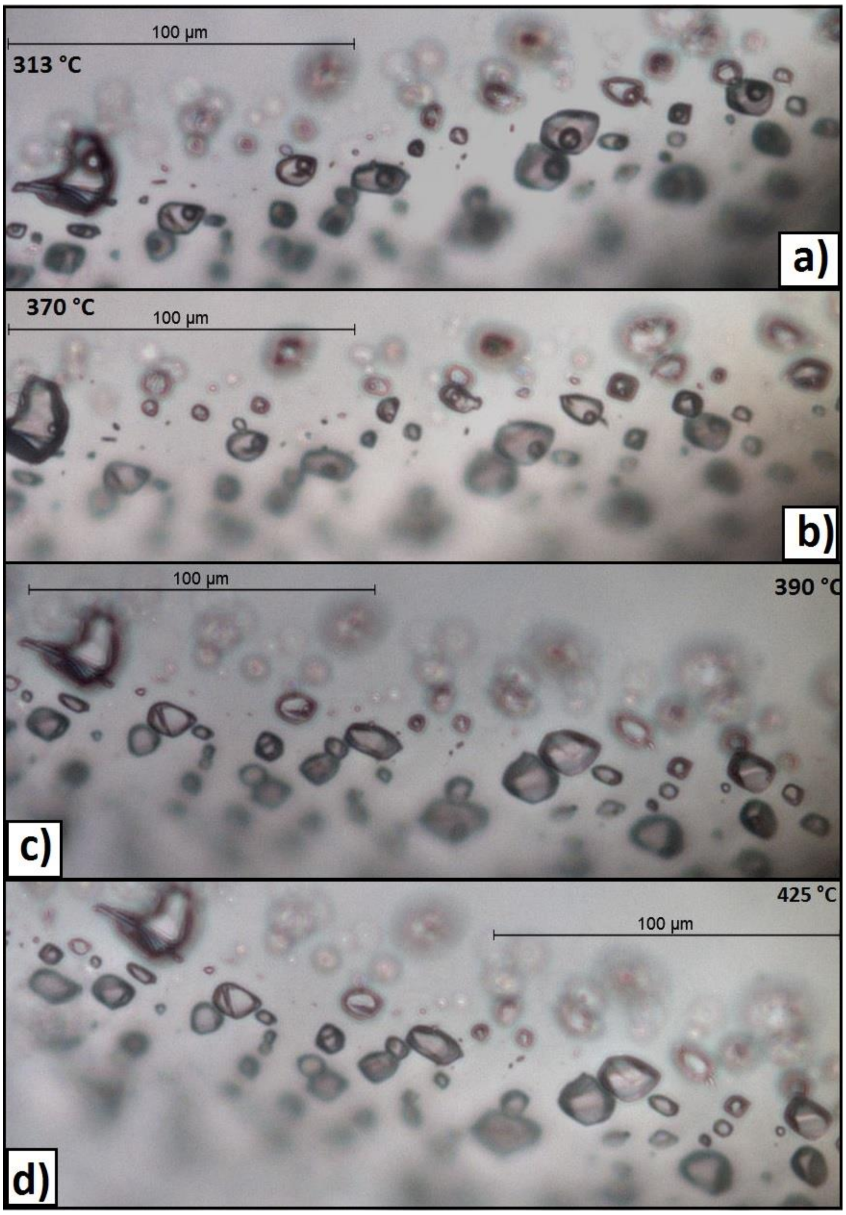

Figure 39. *Type B aqueous inclusions (KUI7-C3-FIA1) with very consistent Th_{tot} temperatures. At 390 °C almost all of the inclusions have been homogenized and finally at 425 °C all of them have been homogenized. Orientation of the trail is slightly turned due to the movement of the chip on the cooling-heating stage.*

In the potentially re-equilibrated type D aqueous-carbonic inclusions no changes were observed in the vapor phase even when they were frozen up to the instrumental minimum temperature of -190°C (Fig. 40). On the contrary, upon freezing the aqueous-rich inclusions (type A–B, E–F), the vapor bubble disappeared completely when the aqueous liquid was fully frozen at -40–-60 °C (Fig. 41).

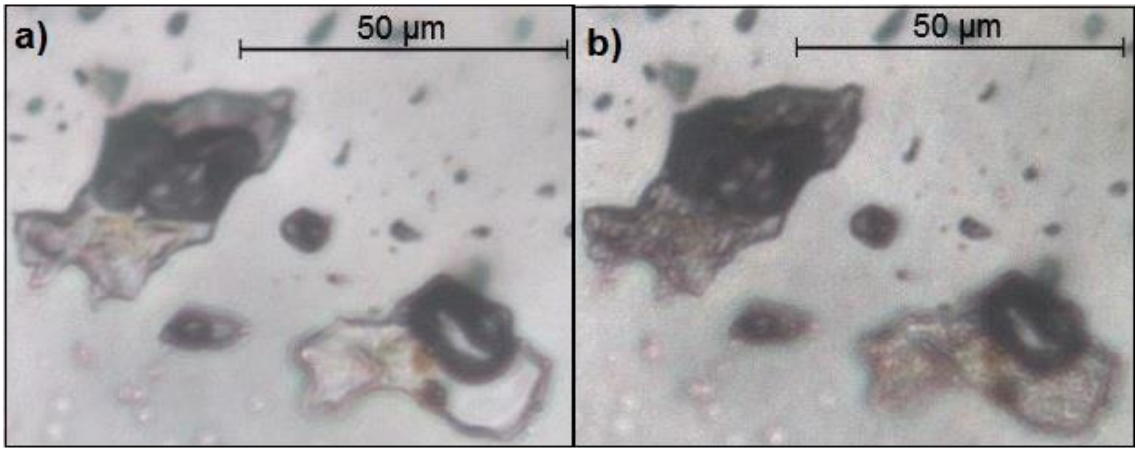

Figure 40. *a) Type D inclusions at room temperature. Note several brown solids in inclusions, which are potentially hematite. b) At -190 °C the liquid H_2O is completely frozen and has brownish appearance. No changes observed within the vapor phase during heating or cooling.*

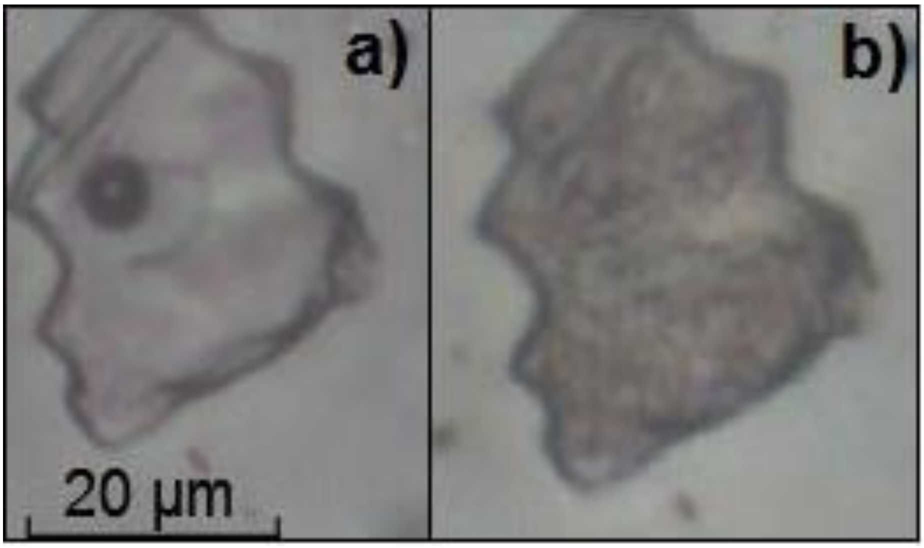

Figure 41. *a) Type A $L_{90}V$+S inclusion at room temperature. b) Same inclusion frozen approximately at -47 °C. Vapor phase is not visible when liquid phase freezes completely as is typically observed in these type A aqueous inclusions.*

The aqueous-carbonic type C inclusions have generally the highest homogenization temperatures, ranging from ~260 °C up to 440 °C (Fig. 42). Homogenization temperatures of aqueous inclusions are generally lower, ranging from the lowest of 40 °C measured in late type E inclusions to the highest measured 394 °C in type B aqueous inclusions. The homogenization temperatures of type C aqueous-carbonic inclusions are quite similar in all different vein types they are present. Larger variation occurs in the aqueous fluids of type B, which show similar values in V_1 and V_4 (~300–420 °C) (Fig.

44), whereas in V₂ the measured homogenization temperatures are significantly lower (~160–240 °C) (Fig. 43). Aqueous type A inclusions homogenize at higher temperatures in V₁ (~190–370 °C) than in V₂ (~150–230 °C) and V₃ (~200–270 °C) (Figs. 42, 43, 44).

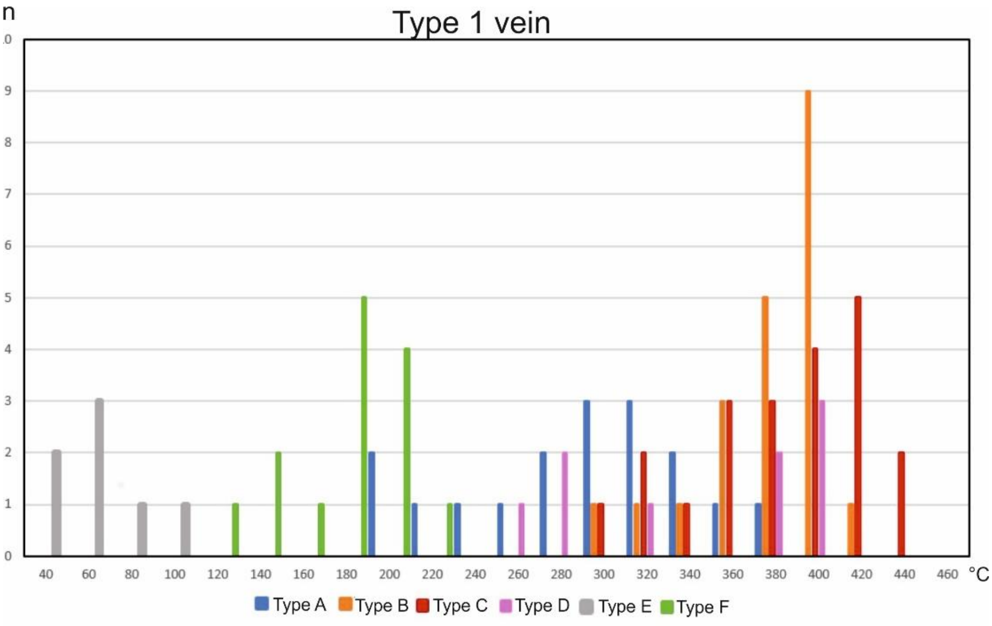

Figure 42. Total homogenization temperatures for different fluid inclusion types measured in V_1. Aqueous-carbonic type C inclusions homogenize at the highest temperatures, although type B and D inclusions are overlapping with type C inclusions.

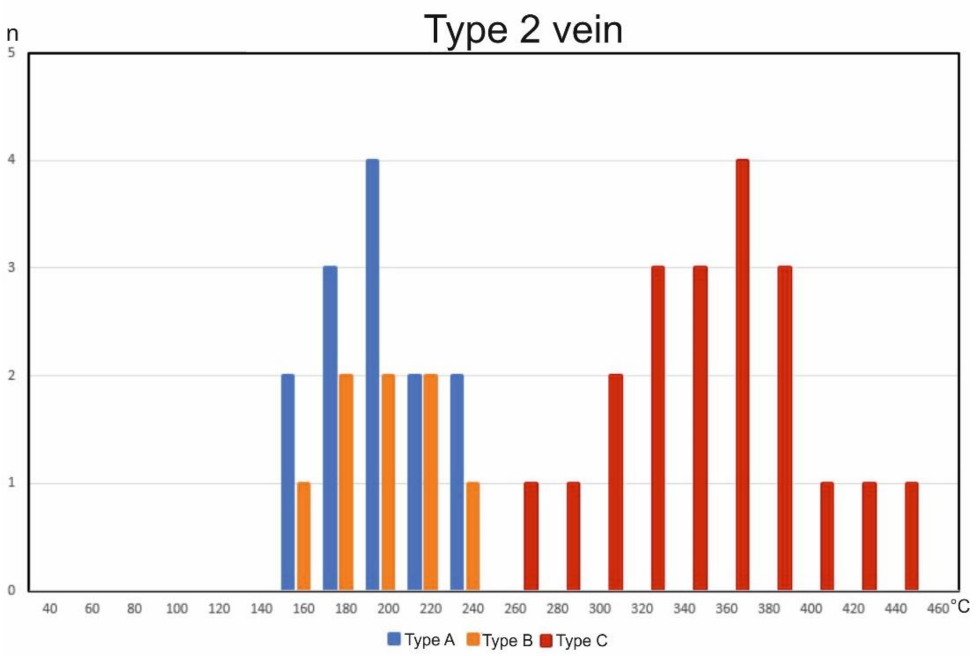

Figure 43. Total homogenization temperatures measured in V_2. In this vein type, type C aqueous-carbonic inclusions have clearly higher homogenization temperatures than aqueous types A and B.

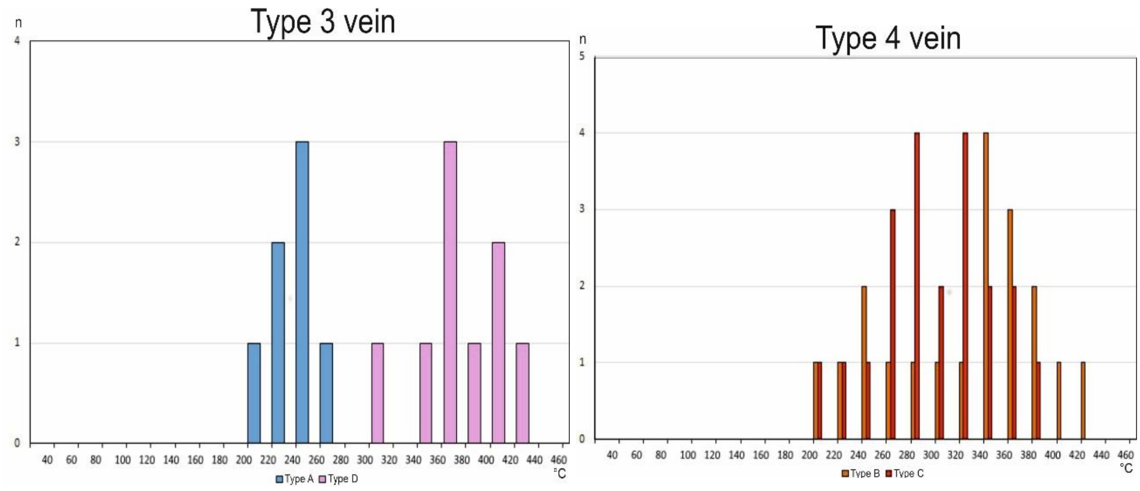

Figure 44. *Total homogenization temperatures measured in V_3 and V_4. The homogenization temperatures of type A and type D clearly differs in V_3. The homogenization temperatures of type B and type C fluids in V_4 are greatly overlapping with each other.*

Fig. 45 shows the total homogenization temperature by salinity. The plotted values are average values of each FIA. Only FIAs for which it was possible to measure both salinity and homogenization temperatures are plotted. The total homogenization temperatures of single FIAs within different fluid types are varying a lot, especially for fluid type E.

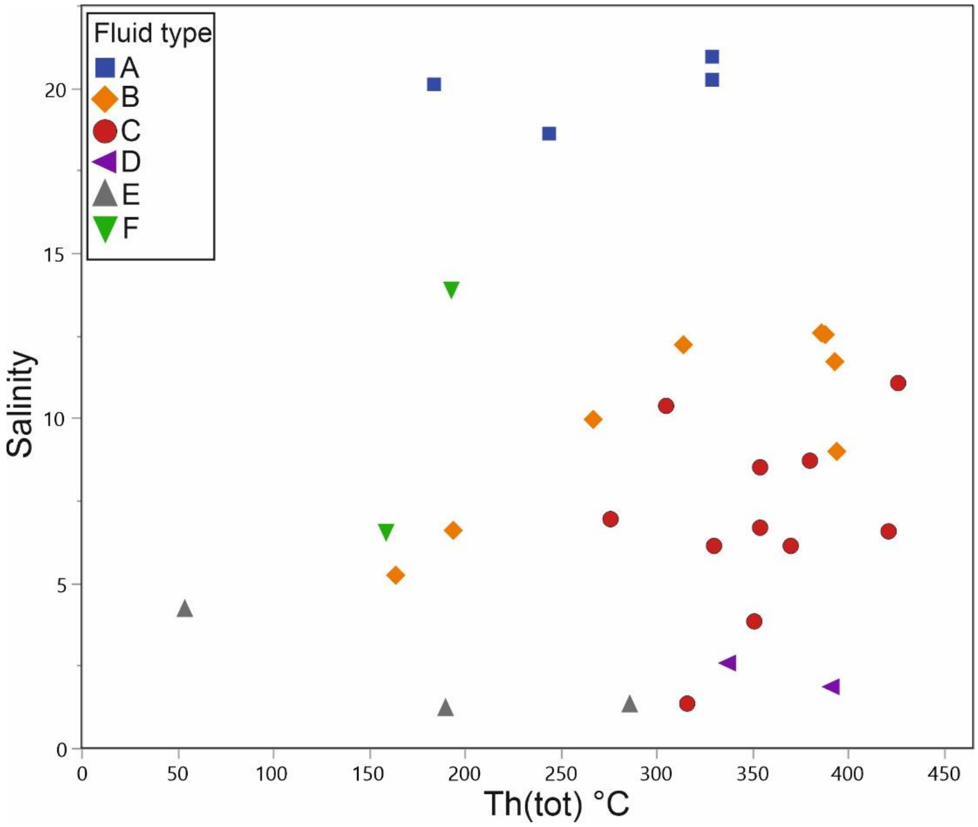

Figure 45. *Diagram showing salinity (NaCl eq. Wt. %) to average total homogenization temperature.*

4.4. Raman spectrometry

Fig. 46 shows the typical examples of different acquired Raman spectra. The propane peak is consistently seen in different analyses, although it is quite unnoticeable compared to the highest peak that was obtained in fluid inclusion assemblage representing type D inclusions. The typical 2-peak fermi diad of CO_2 is clearly visible in the aqueous-carbonic fluids (Fig. 46). The possible daughter mineral nahcolite was discovered in type A aqueous inclusions (Fig. 46). The Raman spectra of of aqueous type B inclusions show traces of N_2 and C_3H_8 peaks in addition to H_2O (Fig. 46).

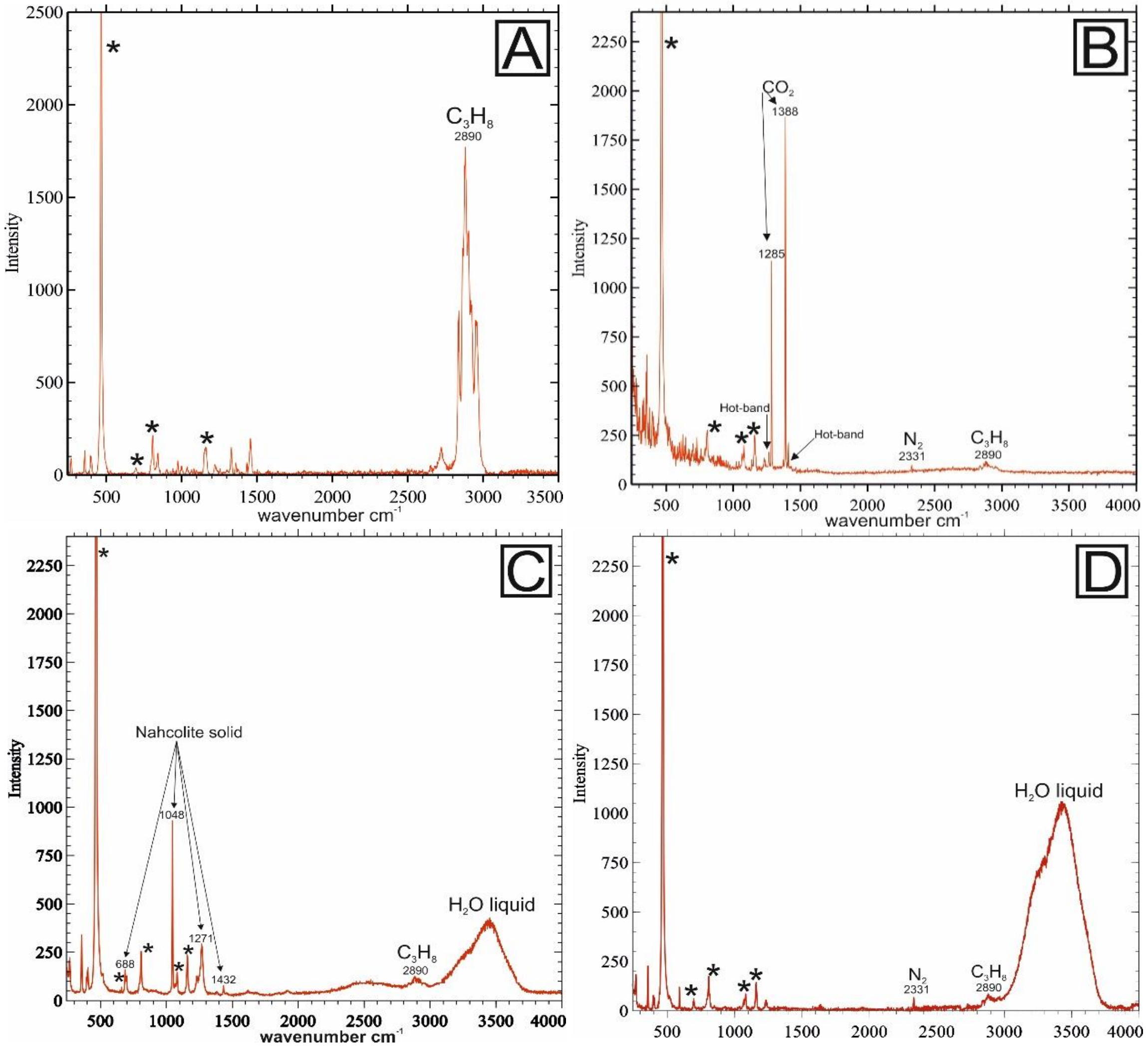

__Figure 46.__ Raman spectra from selected analyses of individual fluid inclusions. Signal from host (quartz) is marked with asterisk. A) Raman spectra of type D inclusion (KUI8-C2-FIA2) is showing that the vapor-phase of the inclusion consists almost entirely of propane. It is also possible that due to CH_4 and C_3H_8 peaks overlapping, the methane could not be identified. B) Raman spectra of type G CO_2 vapor-rich inclusion. Small peaks of N_2 and C_3H_8 confirming the presence of other gas species prior to CO_2. C) Nahcolite solid in type A aqueous fluid. D) Raman spectra of type B aqueous inclusion. Also showing small peaks of N_2 and C_3H_8. Unidentified peak at 1220 is possibly from small Mg-sulfate solid in inclusion. Most of the peaks of Mg-sulfate however are overlapping with those from quartz, so it could not be confirmed for certain.

4.5. LA-ICP-MS analyses of fluid inclusions

4.5.1. Reliability of the LA-ICP-MS data

To obtain the most possible representative fluid inclusion peak from LA-ICP-MS analyses, the analysed inclusion should occur as isolated and not be under other inclusions. The ideal situation, in reality, is rarely the case, since fluid inclusions usually appear as very tightly packed trails. Also, the depth of the inclusions is a decisive factor on how well the ablation will work out. Inclusions too close to the surface of a chip in many cases exploded or leaked and thus were not included in the measurements. In the samples of this study the optimal depth from the surface for successful ablation turned out to be at 40–80 µm from the surface.

All the LA-ICP-MS spectra were gone through manually to determine whether there is a peak in reality or the calculated values are just artifacts. Some of the analysed elements e.g. Fe and Mg caused problems due to their high background values. Measuring of sulphur was also problematic, as only in rare cases a sulphur signal could be seen. In most cases the sulphur values appeared to be completely random, giving high values when there was no detectable sulphur peak at all. For that reason the sulphur is excluded from the data tables. Au concentrations measured were in some cases over 1 ppm, although in those situations no clear gold peaks were observed apart from some of the false peaks caused by chip of loose quartz flying into the detector during ablation (Fig. 47). Good Au signals yielded concentrations of 0.11–0.58 ppm.

In an ideal ablation peak the Si peak from the matrix quartz is as constant as possible and inclusion peak appears as a sharp, short peak (Fig. 47). In case the inclusion explodes and starts leaking during the ablation, the inclusion peak will appear as wide and it may not be completely reliable. Several times the host quartz cracked during pre-drilling or ablation, causing a large crater forming in the host quartz (Fig. 47). In these cases, the LA-ICP-MS spectrum consist of elemental data from several different inclusions and also from the quartz, and they were, of course, discarded.

Attention must be paid also for the situations where false peaks will show as a result of particles of loose quartz flying into the detector during drilling. In these occurrences the Si peak will rise rapidly and will affect the concentrations of different elements (Fig. 47). All measurements where these random rapid peaks of Si occurred were discarded. In cases where inclusions were too vapor rich getting any signal from other elements than sodium turned out to be impossible and therefore getting usable data of inclusions containing ≥ 40 % of vapor turned out to be impossible (Fig. 47). Also with inclusion of very low salinity, getting reliable inclusion peaks was not possible. In total, 155 different holes were ablated, out of which 90 yielded peaks good enough to be used, meaning the rate of successful ablation was 58 %.

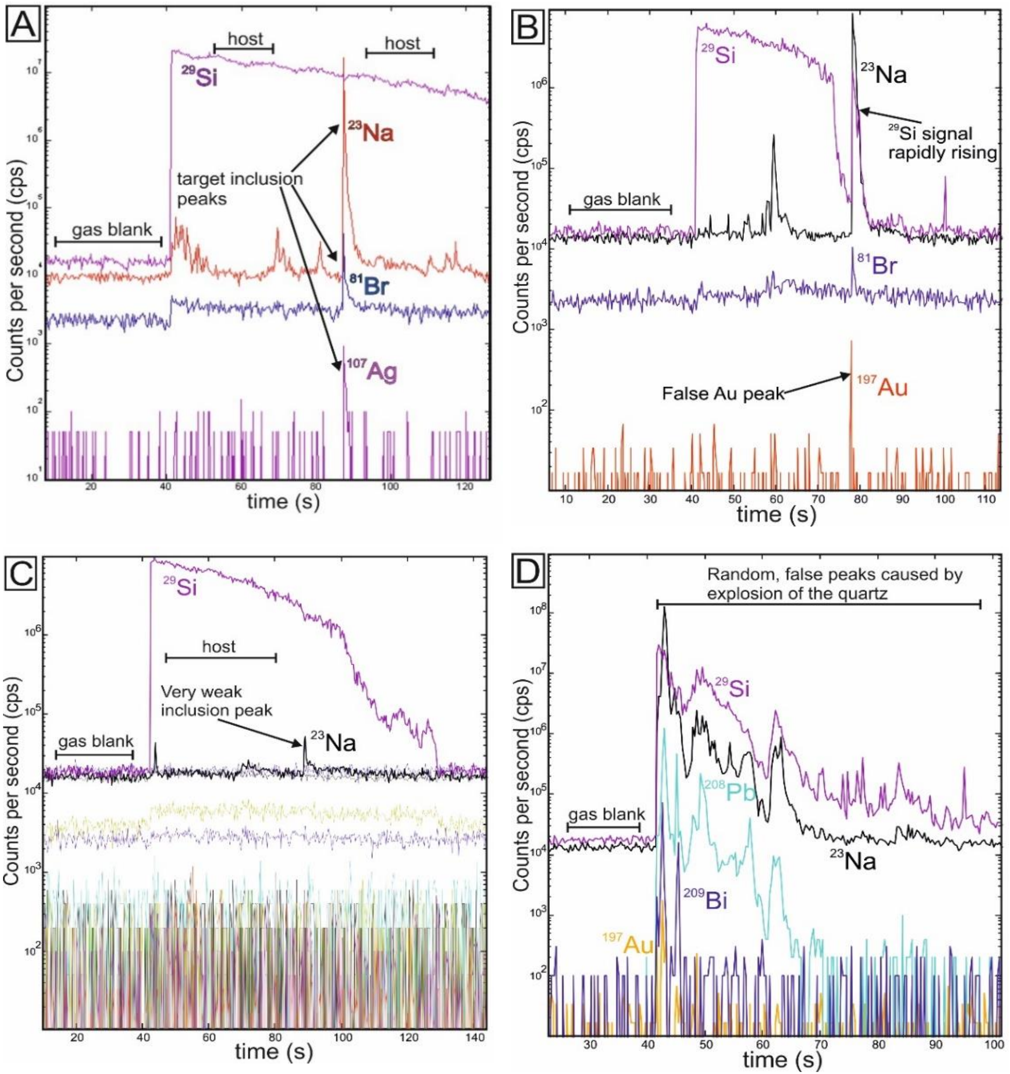

***Figure 47**. A) An example of successful LA-ICP-MS signal of fluid inclusion. Fluid inclusion peak is highly reliable since all the other peaks are very neatly lined up with the target inclusion peak and Si peak from the host quartz stays stable. B) An example of false gold peak in LA-ICP-MS spectra caused by chip of loose quartz flying into the detector during drilling. This results too high content of rare elements such as Au and Bi to be calculated. Results like these were discarded. C) Full LA-ICP-MS spectra from 50 µm vapour rich (>50 %) inclusion. D) Random spectra caused by quartz exploding during the drilling. These measurements were useless and were discarded.*

4.5.2. Fluid inclusion geochemistry

In the Table 7 are shown the average concentrations of analysed elements of the fluid inclusion analyses by different FIAs. Values are given with three significant figures. Values over 10000 were rounded to nearest hundred and values over 100000 to nearest thousand for the clarity reasons. Sulphur data is removed, as real sulphur peaks were detected only in few inclusions and the acquired sulphur data would be therefore equivocal and incomplete. The aqueous inclusions of type A were further divided into type A1 and A2, and type B inclusions into type B1 and B2 based on the differences in the geochemistry. Also aqueous-carbonic type C inclusions were divided into C1, C2, C3, C4 and C5 based on the geochemistry.

Lithium shows highest concentrations in type 1 vein, where type A1 inclusions have concentrations of 2730–2880 ppm (Fig. 48) (Table 7). In the other fluid types in the V_1 the concentrations of Li are varying a lot, especially in the aqueous-carbonic inclusions of type C1 and C3. In C1 inclusions the concentrations are varying from 260 ppm to 570 ppm, whereas in C3 inclusions the measured values give range of 852–2304 ppm. In all the other vein types the Li contents are significantly lower, ranging from as low as 1.15 ppm measured in type D inclusion in V_3 to 99.5 ppm measured in type C2 inclusion in V_2 (Fig. 50).

Boron concentrations of the type A1 inclusions (383–693 ppm) are also higher than the average concentrations of the different analysed FIAs. However, when comparing the Li/B ratios of the type A1 inclusions in V_1 to the other FIAs in different vein types, there are significant differences. For example, although in the fluid type C2 in V_2 the concentration of B is quite similar to the values in A1 inclusions (245–752 ppm), the Li is remarkably lower in the C2 inclusions (8.78–98.2 ppm) (Fig. 49).

Table 7. *Average elemental concentrations (µg/g) and molar Cl/Br-ratios of the measured FIAs, classified by interpreted corresponding vein type. High values marked with asterisk are caused most likely by solids in the analysed inclusions. Not analysed (n/a) were marked in situations where no detectable peak were obtained yet the measured values were above the detection limit.*

Sample	FIA	n	Type	Li	B	Na	Mg	Cl	K	Ca	Ti	Fe	Cu	Zn	As	Br	Rb	Sr	Mo	Ag	Sb	Cs	Ba	W	Au	Pb	Bi	Cl/Br	K/Rb
Type 1 veins (V_1)																													
KUI7-C1	1	5	A1	2730	693	53300	14.7	166000	20600	10100	32.9	n/a	<0.33	265	1194	10900	206	363	<0.31	n/a	30.3	229	96.1	<0.17	<0.11	324	<0.04	35	99
KUI7-C1	2	3	A1	2880	383	45600	12.1	163000	15700	19900	40.5	n/a	<0.08	138	282	13500	186	701	<0.04	<0.03	18.1	232	215	<0.06	<0.02	62	<0.03	28	86
KUI7-C1	5	3	C3	852	645	48200	9.8	41400	2841	<41.5	28.1	338	600	<0.54	238	418	7.93	6.03	1.78	10.6	36.9	4.96	7.19	11.3	0.22	51.9	n/a	64	388
KUI7-C1	7	2	C1	260	768	22400	<0.12	48300	2239	55.5	28.4	n/a	37.0	16.8	444	4776	12.3	81.6	<0.14	1.70	24.9	15.9	13.9	<0.33	<0.07	14.8	n/a	28	220
KUI7-C1	8	6	C3	2304	616	22500	2.96	24000	1929	179	9.94	n/a	213	<0.44	195	1094	7.37	6.08	<0.16	1.54	1.31	5.25	0.73	13.9	0.27	<0.19	n/a	59	307
KUI7-C3	1	3	B1	154	12.9	18000	36.1	54000	704	17600	21.8	n/a	0.86	<0.25	6.25	2392	6.21	134	<0.05	<0.10	1.36	9.34	4.06	<0.35	<0.16	<0.15	89.7*	142	215
KUI7-C3	3	3	C1	570	512	30500	13.0	18500	1336	218	<0.91	n/a	37.5	2.18	309	1010	11.4	39.7	<0.01	0.60	17.3	17.3	7.6	<0.06	<0.13	0.89	<0.08	46	154
KUI7-C3	4	1	B1	202	9.13	22100	2.17	45700	707	24400	35.1	n/a	<0.07	<0.30	20.0	2029	1.74	168	<0.03	<0.09	<0.13	2.80	1.98	<0.06	<0.08	4.96	<0.05	51	408
KUI7-C3	7	4	C1	437	539	23100	1.19	40000	3507	45.3	16.7	n/a	94.6	<0.63	635	1830	16.8	55.5	<0.30	1.09	18.7	18.7	14.7	n/a	<0.07	1.51	<0.12	51	208
KUI7-C4	2	3	D	98.3	2.20	4220	11.3	9065	95.4	1965	13.7	3968	2.47	<0.17	3.63	110	1.05	46.2	1.12	<0.02	0.52	0.80	1.92	2.81	<0.01	<0.02	0.46	204	91
KUI8-C2	2	4	B1	40.7	4.63	9557	0.84	40800	85.8	15500	16.1	17.9	<0.44	n/a	4.25	785	0.92	240	<0.25	<0.18	1.16	0.85	2.64	n/a	<0.06	<0.19	<0.11	125	106
KUI8-C2	3	4	B2	158	675	37600	0.11	22200	2373	<37.0	32.1	n/a	3.55	1.71	257	629	7.50	15.7	<0.09	n/a	8.10	6.77	1.04	2.11	0.11	0.58	<0.05	87	323
Type 2 vein (V_2)																													
KUI5-C1	2	8	C2	8.78	245	20600	0.67	37400	3427	n/a	<2.02	n/a	0.86	172	410	7248	10.9	67.3	<0.30	5.06	4.70	9.96	212	0.35	<0.02	191	0.20	23	304
KUI5-C2	1	7	C2	22.6	310	36000	1.13	74100	6839	<107	<2.22	n/a	0.29	170	632	12200	20.2	132	<0.27	2.93	14.0	18.7	225	<0.32	<0.09	187	<0.10	17	341
KUI5-C2	2	5	C2	20.9	455	35600	0.98	85500	6723	<50.6	n/a	n/a	1.38	216	611	4354	20.3	131	<0.13	2.38	10.6	17.9	256	0.49	<0.07	250	<0.12	46	360
KUI5-C2[a]	4	4	C2	98.2	584	67500	1.63	135000	10800	<49.8	<2.15	n/a	16.1	348	970	12100	27.5	200	<0.21	2.05	<3.77	25.6	456	<0.30	<0.03	213	<0.10	26	391
Type 3 vein (V_3)																													
KUI6-C1	1	3	A2	9.15	3.11	27600	207	124000	1401	40600	7.13	64.7	<0.11	3.89	<0.41	3949	13.2	307	<0.07	<0.10	3.01	10.4	19.5	<0.10	<0.12	<0.06	<0.11	81	108
KUI6-C1	4	4	D	1.15	9.19	5061	1.80	15000	654	1662	n/a	17.1	0.21	10.9	3.91	716	1.13	13.0	<0.08	1.01	1.38	0.88	1.54	<0.05	<0.04	15.1	<0.07	47	449
Type 4 vein (V_4)																													
KUI3-C1	1	3	B1	13.7	30.2	27400	0.99	72800	392	19500	9.53	n/a	0.52	1.13	4.55	1229	6.80	282	<0.07	<0.04	<0.15	14.9	10.9	<0.24	<0.02	<0.05	n/a	135	59
KUI3-C1	2	1	B1	14.6	14.8	26800	0.19	62400	654	10800	<0.56	n/a	0.15	<0.46	0.78	711	3.70	252	<0.10	<0.05	0.68	7.00	6.35	<0.23	<0.02	<0.07	<0.04	198	177
KUI3-C1	4	3	C5	11.2	1000	39800	<0.08	34200	1490	205	<0.63	391	23.2	0.60	442	722	5.6	5.1	<0.09	n/a	13.6	4.9	<0.12	18.3	0.58	<0.05	<0.05	44	278
KUI3-C1	5	2	B1	6.58	71.1	16000	15100*	60800	195	27600	42.8	30400*	2.27	69.3	54.6	1529	6.95	402	<0.06	<0.11	1.76	17.1	16.5	<0.09	<0.04	3.43	<0.09	98	32
KUI3-C6	1	6	B1	39.9	118	21500	1.53	84200	367	15600	<1.13	n/a	<0.19	n/a	<0.89	1912	5.83	238	<0.12	<0.07	<0.29	9.95	2.06	<0.16	<0.03	<0.10	<0.06	142	70
KUI3-C6	3	2	C4	7.84	159	5126	0.13	9116	189	<55.2	<1.15	n/a	7.03	n/a	89.1	805	1.51	4.46	<0.05	1.07	0.78	1.52	6.35	0.67	<0.05	1.73	<0.08	25	109

[a] *No clathrates were observed during microthermometric studies in this aqueous-carbonic fluid and therefore salinity could not be calculated prior to analysis. Due to the similar petrographic properties, salinity of KUI5-C2-FIA2 was used as an estimation.*

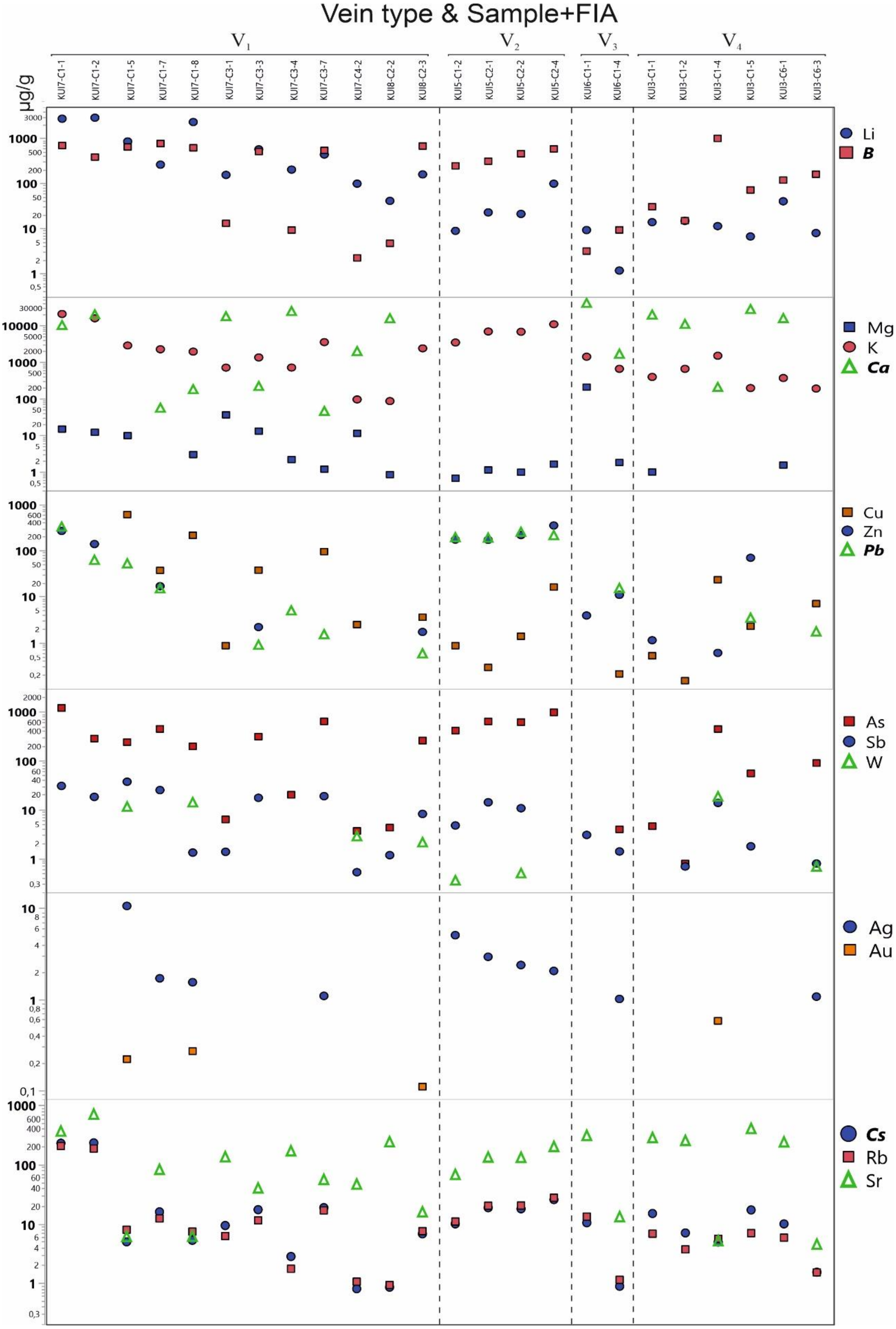

Figure 48. *Elements (y-axis) plotted against sample+FIA and vein type (x-axis). All element values are average concentrations in µg/g of different FIAs.*

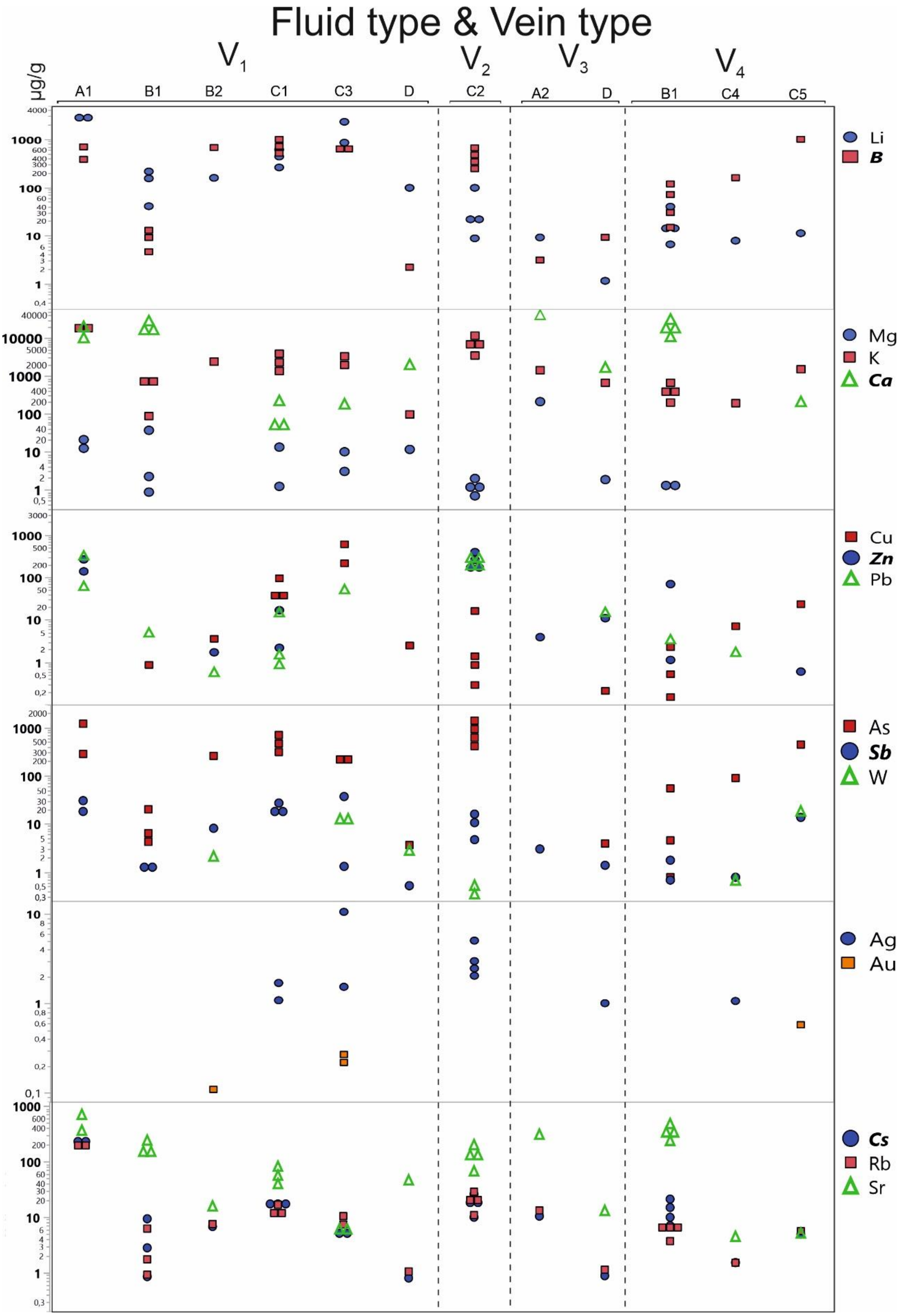

Figure 49. *Elements (y-axis) plotted against fluid type and vein type (x-axis). All element values are average concentrations in µg/g of different FIAs.*

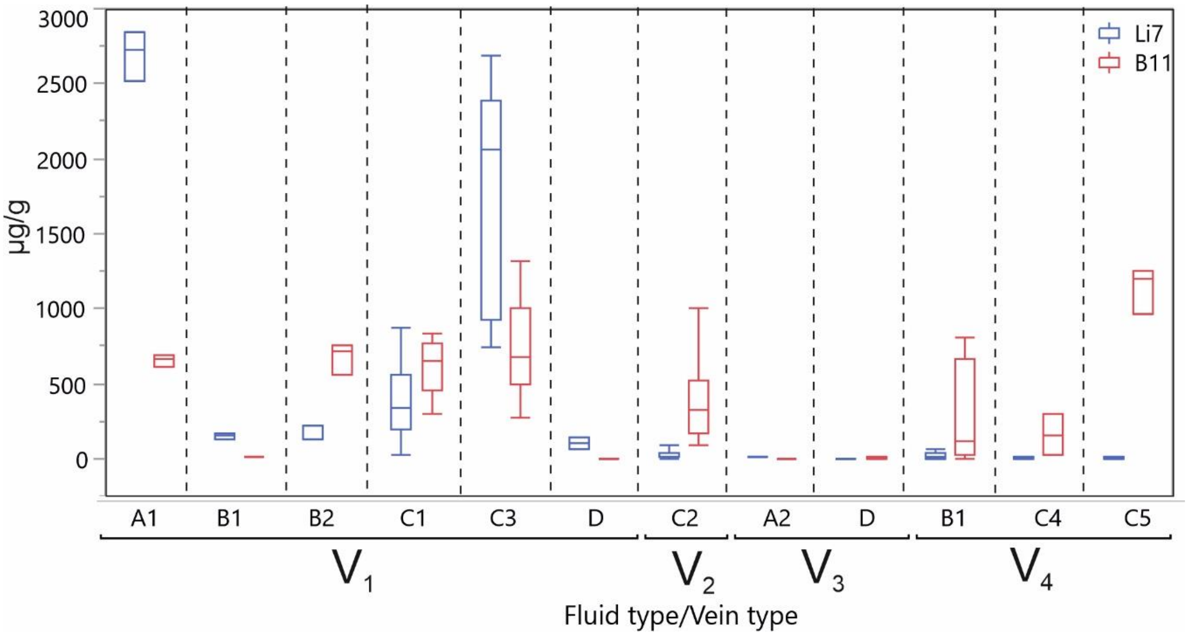

Figure 50. *Box-whisker plot of complete LA-ICP-MS data showing Li and B composition of different fluid types by different vein type. Fluids in* V_1 *are clearly lithium enriched compared to the other vein types. In* V_2 *and* V_4 *B is clearly enriched compared to Li. Both Li and B have very low concentrations in* V_3*. The mostly Li enriched fluid types are aqueous type A1, although some of the aqueous-carbonic type C3 inclusions are partly overlapping with those of type A1.*

Magnesium and titanium concentrations are in general slightly above or below the detection limit in all different fluid types and show no significant difference between different veins. Therefore, the measured values are generally ~10 ppm or below for Mg and ~20 ppm for Ti. An exception occurred in FIA representing type B1 fluids in V_4, where Mg concentration up to 15100 ppm was measured. This anomalously high value is caused by solids in the measured fluids.

Iron did not yield reliable LA-ICP-MS peaks apart from few exceptions and therefore they are generally manually deleted of the final data. However, concentration of 3968 ppm was measured in type D fluid in V_1. FIA representing type C3 fluids in V_1 contain 338 ppm of Fe. Also, the solids bearing FIA of type B1 inclusions with high Mg concentrations in V_4 yielded average value of 30400 ppm of Fe.

Potassium is most enriched in the A1 inclusions, with K content of average 1.69 wt. %. This is not unexpected, as the A1 inclusions are the most saline ones and K can be considered as the most important cation after Na. High concentrations of K are also showing in type C2 inclusions in V_2 with the concentrations ranging from 3427 to 10800 ppm (Fig. 51). This is a bit unexpected, as the salinities of aqueous type A2 and B1/B2 are generally higher. The microprobe data however revealed sylvite crystals in the vein quartz, and therefore it is possible that they originate from these inclusions with high K contents.

Zinc shows clear enrichment in the aqueous-carbonic type C2 fluids in which the measured concentrations are varying between 170 to 348 ppm. Pb is likewise enriched in C2 fluids with measured contents of 187–250 ppm. Elevated concentrations of Zn and Pb were also detected in the aqueous type A1 fluids, in which the measured concentrations were 138–265 ppm and 62–324 ppm, respectively. Zinc is showing clear positive correlation with Cl whereas not as clear correlation trend cannot be seen between Pb and Cl (Fig. 51).

Copper shows quite a bit of variation between different FIAs. The key note is that those FIAs with elevated Zn and Pb values usually yielded Cu concentrations below the detection limit. The most Cu enriched fluids are the C3 fluids, where the measured values range from 213 to 600 ppm. Copper is not showing any correlation at all with the Cl content unlike most of the other elements (Fig. 51).

Arsenic values are generally quite variable. The most constant As values were observed in type C2 inclusions, with concentrations ranging from 410 ppm to 970 ppm. For example in type A1 inclusions the As concentrations were varying from 282 ppm up to 1194. The lowest As concentrations were measured in the aqueous-carbonic type D inclusions (3.63–3.91 ppm) and aqueous type B1 inclusions (0.78–54.6 ppm). Type A2 yielded concentrations below the limit of detection. Arsenic shows clear correlation with the Cl values (Fig. 51). Arsenic is also generally correlating well with most of the elements, with exceptions of Cu, Ag, W.

Calcium concentrations are highly varying, as high Ca concentrations (>10000 ppm) were measured in all aqueous inclusions, with exception of type B2 (<37.0 ppm) fluids. In all aqueous-carbonic fluids the Ca contents are low, as they range from below the limit of detection to 205 ppm. The highest measured value is 40600 ppm in type A2 inclusion in V_3. Calcium is also highly variable between single measured inclusions within some FIAs, which suggest that the fluids in Kuittila are in general rich in accidental Ca-bearing solids.

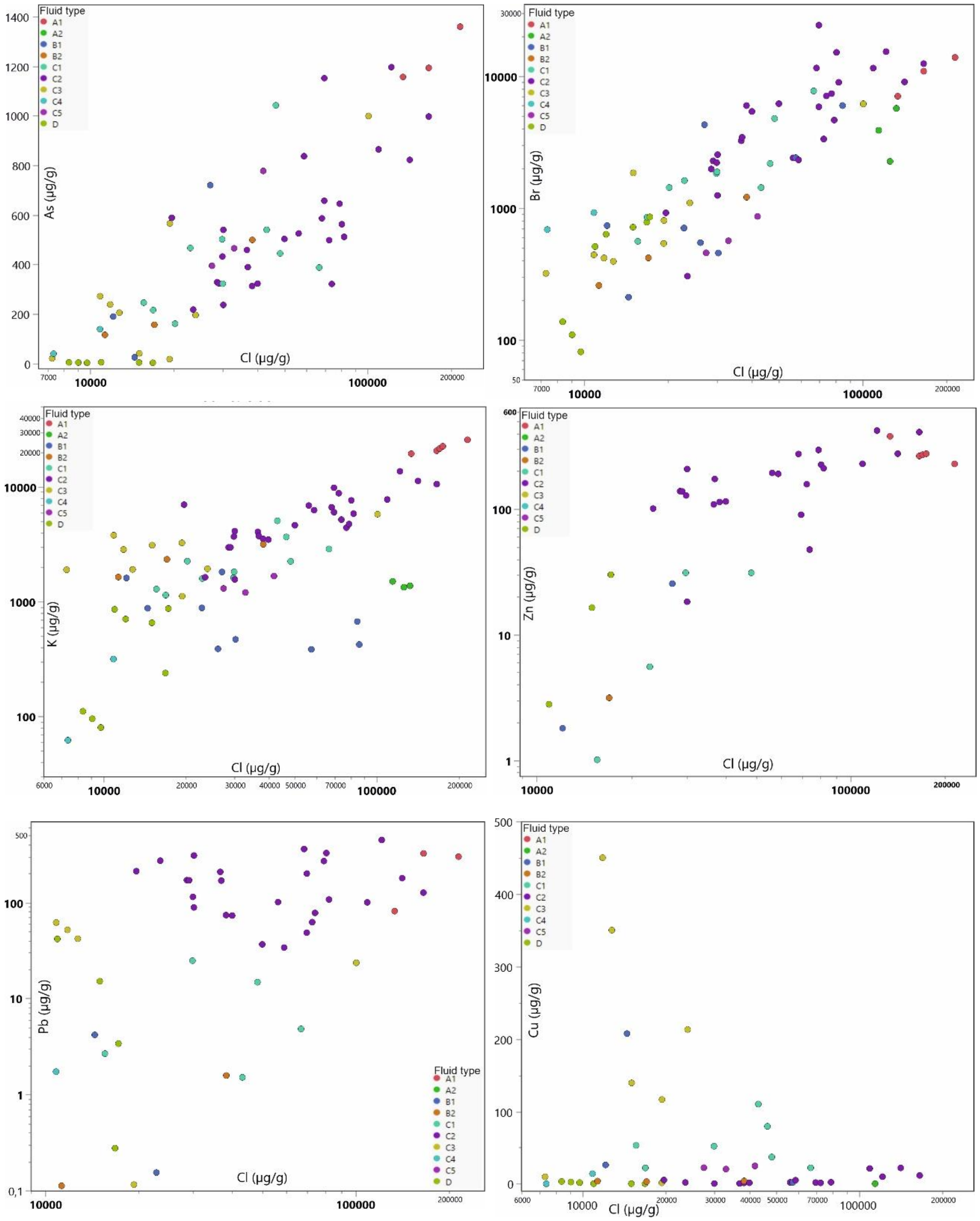

Figure 51. *Elemental distributions of As, Br, K, Zn, Pb and Cu plotted against Cl concentrations. As, Br and K are strongly correlating with the Cl concentration and therefore also to the salinity of the analysed inclusions. Zn is also showing clear correlation with Cl. Unexpectedly Pb is not showing as clear correlation with Cl as Zn. Cu has not correlation at all with Cl.*

Concentrations of strontium are likewise varying quite a lot even between FIAs representing the same type of inclusions. Type A1 fluids contain highest concentrations (363–701 ppm). Aqueous-carbonic inclusions of type C3, C4 and C5 contain lowest contents (4.46–6.08 ppm). Type C2 inclusions yield much higher Sr concentrations than the other aqueous-carbonic fluid types (67.3–200 ppm). Sr is showing positive correlation with Cl and elements like Zn, As, Rb, and also more or less with calcium (Fig. 52).

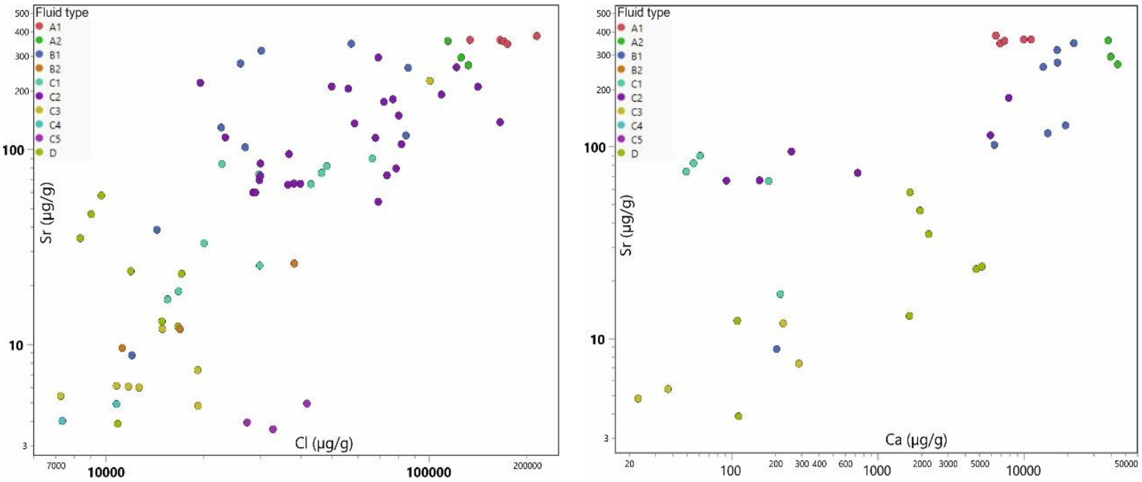

***Figure 52**. Correlation trend between Sr and Cl can be seen on the left. On the right are shown the correlation trend between Sr and Ca, erratic behaviour can be seen especially in type D fluids.*

As could already be quessed by the weak Pb and Cl correlation, lead and zinc do not show strong correlation either, although correlation trend is, however, visible especially in type C2 fluid inclusions (Fig. 53). However, in this graph is not showing the fact that some of the FIAs had only Pb concentrations above the detection limit where Zn yielded values below the detection limit, and vice versa. Although, generally they appear together in the same FIAs. The general trend seems to be so that the inclusions showing high copper contents contain little to none Zn and Pb, and the other way around. Cu does not have any correlation with Zn or Pb (Fig. 53).

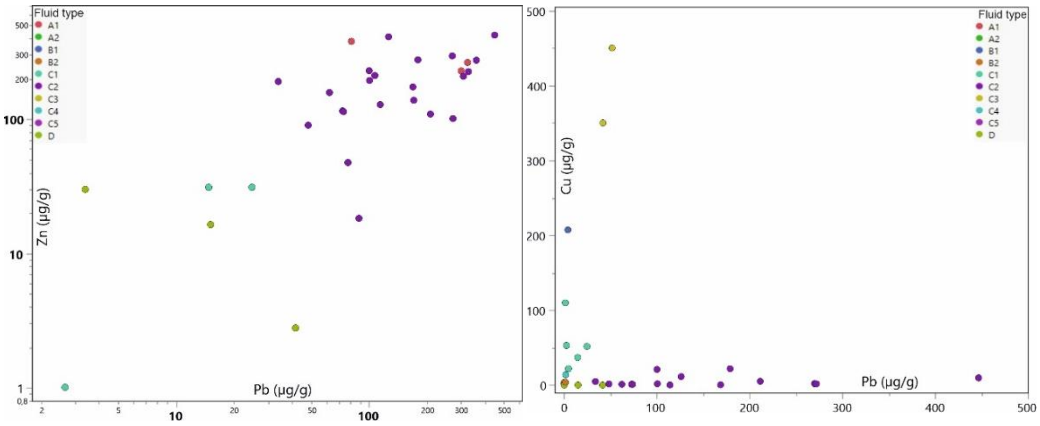

Figure 53. *Elemental distributions of Zn and Cu plotted against Pb. Zn and Pb shows correlation, although not as strong as would be expected. Cu and Pb have no correlation at all.*

High variation in the distribution of Cu, Zn and Pb in different fluid types can be seen distinctively also in the box-whisker plot showing the elemental concentrations divided by different fluid types (Fig. 54). The most Cu enriched inclusions are in type C3 fluids, whereas Zn and Pb is mostly enriched in type A1 and C2 fluids.

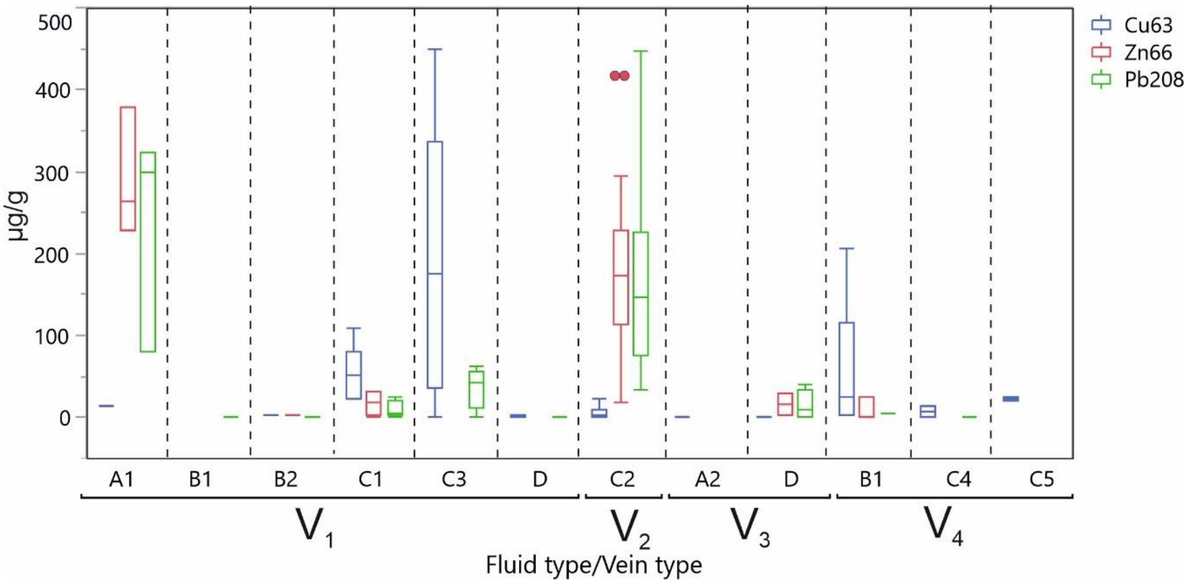

Figure 54. *Box-whisker plots of complete LA-ICP-MS data. Y-axis represents elemental compositions of Cu, Zn and Pb (ppm) and X-axis represents fluid inclusion type and vein type. A1 and C2 fluids are clearly enriched in Zn and Pb compared to Cu, whereas C3 and B1 shows clear enrichment of Cu when compared to Zn and Pb.*

Rubidium is only clearly enriched in type A1 fluids which are showing concentrations between 186–206 ppm. In all other fluid types the measured concentrations are between 1–20 ppm (Fig. 55). Barium shows clear enrichment in type C2 fluids in V_2, where the measured concentrations of different FIAs are 212–456 ppm (Fig. 55). The measured values are well below 100 ppm in all other fluid types, with the exception of type A1 fluid (96.1–215 ppm). Potassium and rubidium show clear correlation between all different fluid types except for the erratic behavior in type B1 fluids (Fig. 56). Anomalously high K and Rb values are however seen in type A1 fluids (Fig. 55). The measured K/Rb ratios of these type A1 inclusions are 86 and 99, meaning they are well below the average crustal values of K/Rb. The K/Rb ratios of type C2 aqueous-carbonic inclusions are 304–391, meaning the values are higher than the crustal average.

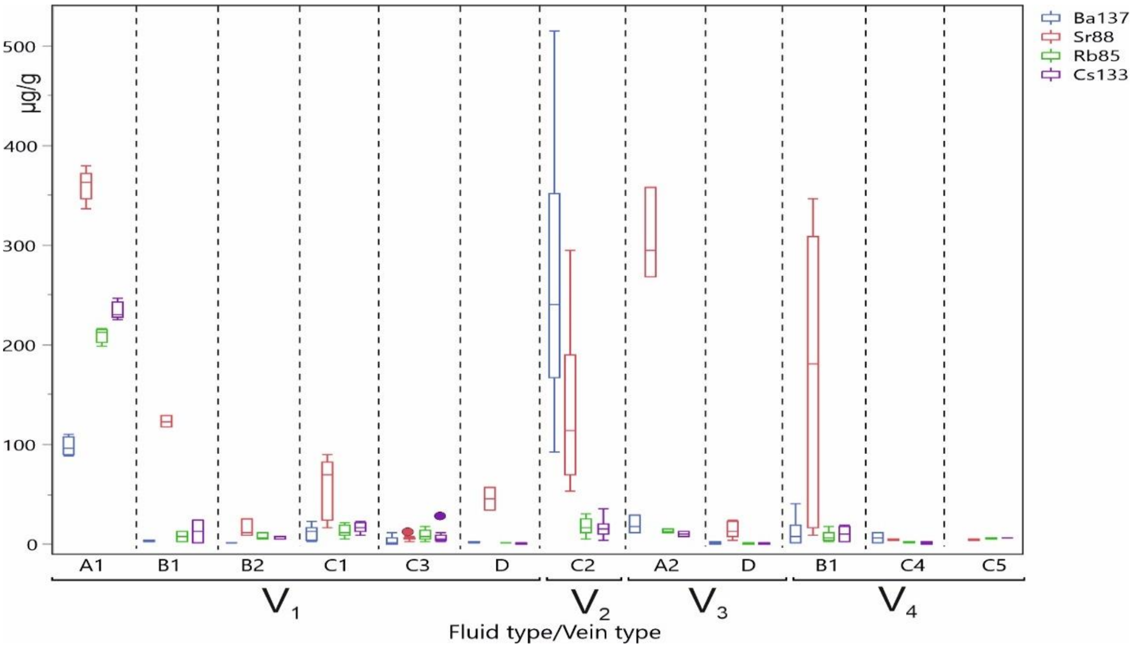

Figure 55. *Box-whisker plot of complete LA-ICP-MS data showing the concentrations of Ba, Sr, Rb and Cs by fluid/vein type. C2 type fluids are clearly Ba-enriched. Aqueous fluid types (A1, B1, A2) have in general clearly higher Sr concentrations than aqueous-carbonic fluids. Type C1 and C2 aqueous-carbonic fluids, however, show elevated Sr concentrations compared to other aqueous-carbonic fluid types.*

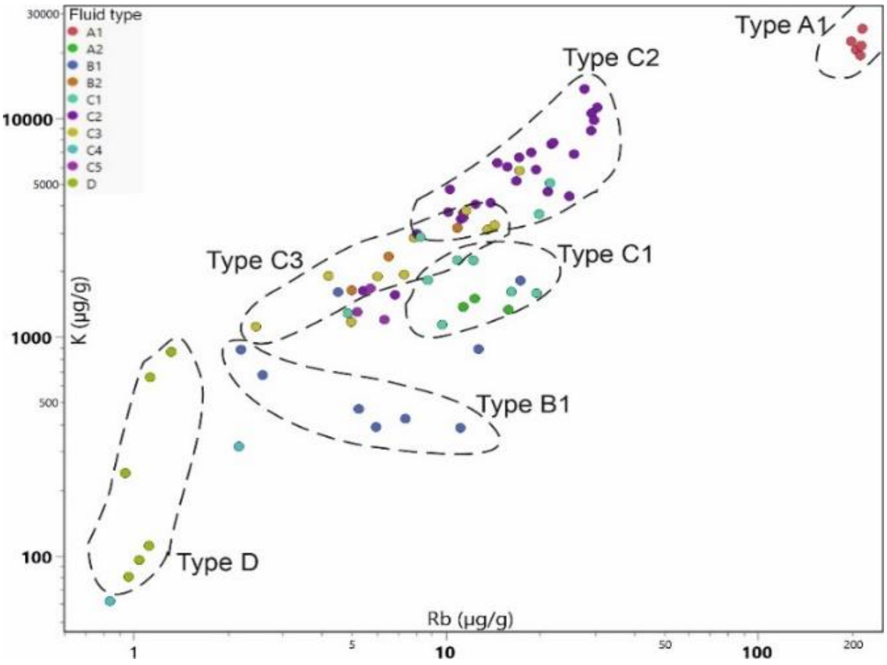

Figure 56*. K and Rb are mainly strongly correlating. Type B1 fluids are, however, showing erratic behaviour. The different fluid types form clearly clusters, showing that the different fluid inclusions of different FIAs are highly similar. The type A1, B1, C1, C2, C3 and D fluids are clearly showing as their own clusters, whereas inclusions of type A2, B2, C4 and C5 are partly overlapping with the other fluid types.*

Cesium shows clear positive correlation with rubidium and potassium (Fig. 57). It can be considered as a good indicator that the data quality is generally good. Erratic behavior of type D and B1, and more or less in C1 inclusions can be seen in K/Cs ratios (Fig. 57).

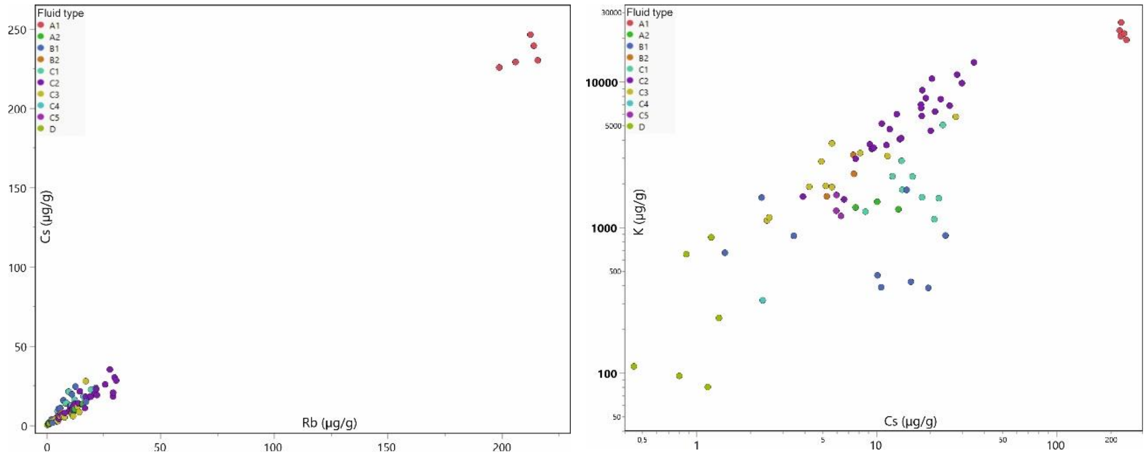

Figure 57. *Strong correlation between Cs and Rb shown on the left. The high Cs/Rb type A1 inclusions are correlating as well, although they appear separately from the cluster of other inclusion types. Correlation of K/Cs shown on the right. B1 fluids show again somewhat erratic behaviour.*

Gold was only observed in C3 aqueous-carbonic inclusions (0.22–0.27 ppm) in V_1 and in C5 aqueous-carbonic inclusions (0.58 ppm) in V_4. Also, in V_1 FIA representing B2 type aqueous inclusions yielded concentration of 0.11 ppm of Au. The FIAs with gold contents show positive correlation with tungsten (Fig. 58). Apart from these gold bearing fluids, notable concentration of tungsten were observed in type D fluids in V_1 (2.81 ppm).

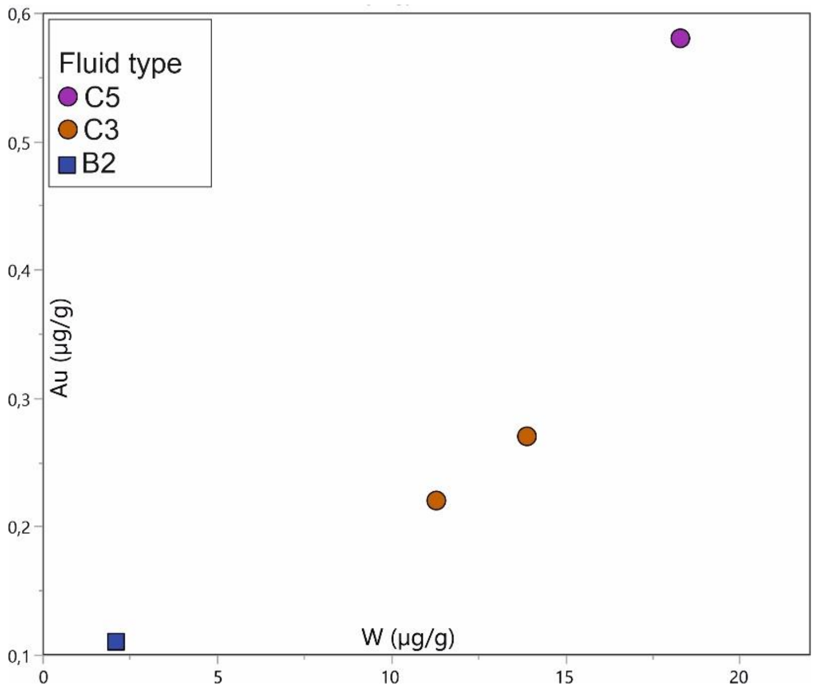

Figure 58. Showing the W to Au by average of FIAs. All of the FIAs containing gold shows clear positive correlation with the tungsten

Silver concentrations above the detection limit were only measured in the type C aqueous-carbonic fluids (Fig. 59). The most constant values were measured in type C2 fluids, where the measured values range from 2.05 ppm to 5.06 ppm. In type C1 and C3 the Ag concentrations are mainly approximately 1 ppm, although in single FIA representing type C3 the average measured value is 10.6 ppm.

Molybdenum concentrations above the detection limit were only measured in two FIAs, representing the type C3 (1.78 ppm) and type D (1.12 ppm) fluids (Fig. 59). Both of these FIAs with detectable Mo contain also considerable amount of W.

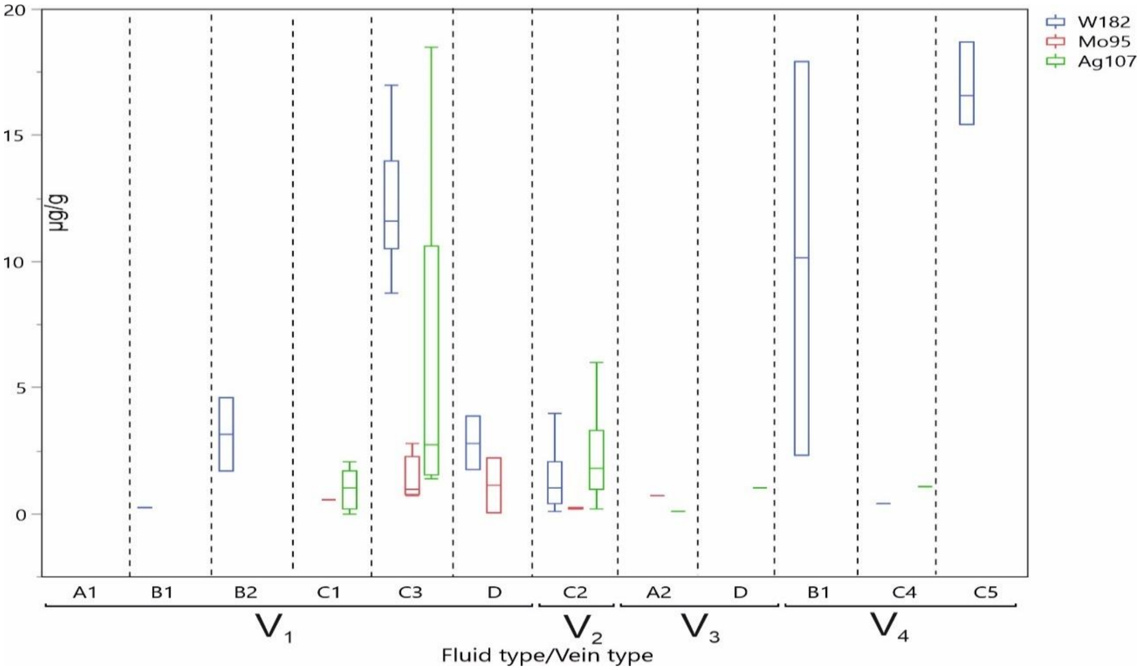

Figure 59. *Box-whisker plot of complete LA-ICP-MS data showing the concentration of W, Mo and Ag by fluid and vein type.*

Bismuth is generally below the detection limit. However, single FIA of aqueous type B1 fluids in V_1 yielded value of 89.7 ppm. Concentration this high compared to all the other FIAs can be considered to be caused by solids in the analysed inclusion.

Cl/Br ratios are quite variable, although common thing is that they are in all FIAs notably low, with the ratios ranging from 17 to 204. The highest average Cl/Br ratio of FIA were measured in the type D inclusions in V_1 and the lowest ratio in type C2 fluids in V_2. K/Rb ratios range from 32 measured in FIA representing type B1 fluids in V_4 up to 449 in type D fluids in V_3. In aqueous-carbonic fluids, especially in type C2 the values are invariably above 300, as they are ranging from 304 to 391, whereas in aqueous fluids they are commonly below 100.

5. DISCUSSION

5.1. Sample representativeness

One of the reasons for EPMA studies was to compare the mineralogy of the samples to the selected quartz veins prior to classification done by Sorjonen-Ward (1993) and the ore mineral petrogenesis of the whole Hattu schist belt, which is published by Molnár et al. (2016b). Also, according to Nurmi et al. (1993), ore minerals related to gold mineralization in Kuittila prospect are gold, electrum, dyscrasite, silver, Au-Ag-Bi-Pb-Fe tellurides, bismuth; pyrite & pyrrhotite; minor Cu-Zn-Pb sulphides, molybdenite, scheelite, pentlandite, ilmenite & rutile. Alteration minerals in ore zone contain quartz, albite, biotite, muscovite, calcite, K-feldspar & epidote (Nurmi et al. 1993).

Early Mo-W quartz veins (V_1)

No scheelite or molybdenite were found in the thick sections of this supposed early stage quartz vein type. Molybdenite was observed however in the field in the vein representing this sample (pers. comm. Fusswinkel 2017). It should be taken into consideration that since the sample preparation was done so that the samples would be best possible for fluid inclusion studies, the fact that there are simply not any scheelite or molybdenite present in this specific sample does not rule out that this would not represent the early Mo-W type of quartz vein. Many of the typical ore related alteration minerals are present; biotite, calcite, albite and K-feldspar. One very fine grained chalcopyrite was found, which is not unexpected, as according to earlier studies (Molnár et al. 2016b; Sorjonen-Ward 1993) the paragenesis of chalcopyrite has started already at the same time with the tungsten-molybdenum mineralization. Abundance of galena have been only reported in the vein belonging to the main gold-sulphide-telluride stage. The fact that the samples representing V_1 also contained galena in secondary cracks indicate that the fluids related to the later main gold stage have circulated through type 1 veins and are now overprinting the primary features. However, it is also possible that this is a vein related to the main gold mineralizing stage, as the paragenesis of scheelite and molybdenite have continued even after the earliest mineralizing stage.

Barren quartz vein (V_2)

The main charasteristic of this type of vein is the presence of coarse grained chalcopyrite. As the earlier studies suggest, the precipitation of chalcopyrite have lasted from the earliest Mo-W-stage until the latest gold-telluride-sulphide stage. The presence of sphalerite and native bismuth are suggesting that this interpreted barren vein could very well be related to the gold mineralization stages and therefore it should not be considered as barren vein type without doubt.

Tourmaline-carbonate-quartz vein (V_3)

Carbonate minerals are more abundant in the V_3 than in the other vein types. The carbonates are massively filling the fractures and cracks on quartz and they are controlling mainly the ore mineralization. Pyrite has been mostly oxidized into iron oxides. In the EPMA was seen that some of the pyrite grains show healthy pyrite surrounded by oxidized rim. REE–minerals are common, they can be found both as anhedral monazite grains, as well as filling textures in carbonates. Apatite is common mineral on this type of vein and it is most likely the cause for REE–mineralization. Most of the ore minerals that have been linked with the gold mineralization within the Hattu schist belt are lacking in this vein type. For example galena and chalcopyrite were absent.

Auriferous quartz vein (V4)

Despite careful microscope and microprobe studies, no gold was found in the analysed sample KUI3 representing the interpreted auriferous quartz. It is not however directly proving that this vein type is not related to the gold mineralization, as the presence of silver and arsenic-bearing minerals is a clear characteristic differentiating this vein type from the others. In paragenesis presented by Molnár et al. (2016b), arsenopyrite is essentially linked with the main gold-sulphide-telluride stage. Also the presence of native bismuth in K-feldspar will support the auriferous context of this vein type. However, without observing any gold-telluride assemblages it cannot be said for certain that this would be for certain linked to the main gold stage mineralization. It is also possibility that this vein type is also related to the early Mo-W-Au stage of mineralization.

5.2. Characteristics of the fluids in quartz veins in the Kuittila tonalite

In total, seven different fluid inclusion types were identified in this study based on their petrographic and microthermometric characteristics. They are described in detail in chapter 4.2.1. Fluid inclusion types. In contrast to the earlier fluid inclusion study of Kuittila done by Bornhorst and Wilkin (1993), the data of this study proves that there is much more variety within the fluid inclusion assemblages than observed in the earlier study. By the presence of 3-phase aqueous-carbonic inclusions and confirmed with the Raman laser measurements, the abundance of aqueous-carbonic inclusions in the quartz veins in Kuittila tonalite is evident. As was already suspected by the lower T_m(Car) temperatures than of CO_2 and confirmed by Raman laser studies, in addition to H_2O and CO2, there are C_3H_8, CH_4 ±N_2 volatiles in the gaseous phase. It can be discussed whether the high peaks of propane are caused by some changes to the inclusions during sample preparation or by the effect of heating of the Raman laser or is it the original composition of the gaseous phase. Hydrocarbons heavier than methane are relatively rarely found in fluid inclusions, although some studies point out their presence (e.g. Bray et al. 1991). Also, the Raman spectra for propane are possibly overlapping with that of methane and for that reason the methane peak could not be identified in all cases.

The highest measured homogenization temperatures are in line with those of Pampalo fluids reported by Molnár et al. (2016), although generally those reported in this study are a bit higher. However, the fluid inclusions yielding highest total homogenization temperatures in Pampalo were potentially re-equilibrated inclusions, meaning the data is not undoubtedly comparative. The type D inclusions presenting the early aqueous(-carbonic) re-equilibrated inclusions observed in this study remind a lot of those re-equilibrated in the study done by Molnár et al. (2016). They both share the characteristics of having low salinity, high homogenization temperatures and re-equilibration textures. Re-equilibration textures of the early H_2O-CH_4 fluids have also been mentioned in samples of Rämepuro in a study by Poutiainen and Partamies (2003b). The petrological features as well as microthermometric data of the type D inclusions in this study are similar to those in Poutiainen and Partamies (2003b) study. The reported Tm(H2O) are similar, ranging from -5.8 to -2.6 and homogenization temperatures range from 225 °C to 355 °C. As it has been observed in earlier fluid inclusion studies in the Hattu schist belt, the CH_4-bearing fluids are likely the earliest also in Kuittila, as they show deformation features which are lacking in the other type of fluids.

The homogenization temperatures of aqueous type A inclusions in this study have similar range to the aqueous inclusions in Kuittila studied by Bornhorst and Wilkin (1993). However, the salinities of type A inclusions are much higher than in any of the fluid types observed in the earlier studies. Salinities of type B inclusions are closer to the range of the aqueous inclusions reported in the earlier study, although the type B inclusions observed in this study generally homogenize at higher temperatures. However, type B fluids in tension gashes observed in V_2 yield similar Th(tot) and salinities as was measured in the fluids occurring in the early veins and main gold stage veins in the earlier study by Bornhorst and Wilkin (1993). Also, the late type E inclusions are similar, low salinity aqueous inclusions as has been observed earlier in late stage quartz veins, although homogenization temperatures are more variable in this study. The homogenization temperatures of aqueous-carbonic inclusions are much higher than the highest measured from the aqueous inclusions observed in study by Bornhorst and Wilkin (1993).

Type A inclusions contain nahcolite solids, which in places are systematically present within the same FIA, which makes it look like they were daughter minerals. However, nahcolite solids were not found in every inclusion within the same FIA. This might point out that they originate as accidentally trapped solids which could be similar to those observed in earlier study by Hoshino et al. (2006), where accidentally trapped solids were formed while the fluids were immiscible below the nahcolite melting temperature at 270 °C. According to Hoshino et al. (2006) this would indicate that the liquids prior to their immiscible state might have contained high Na^+ and low Cl^- yielded by an interaction of a low -salinity fluid and Na-bearing minerals such as plagioclase in the host metamorphic rocks below the fractures now occupied by quartz if nahcolite precipitated from boiling fluids.

The suspiciously high homogenization temperatures of some of the FIAs that are classified as type B fluids in V_1 and V_4 raises doubts whether in fact some of them are misidentified and could, in reality be aqueous-carbonic fluids of type C. During freezing-cooling experiments no evidence of carbonaceous nature of these fluids was not observed. However, due to the small nature in general of these fluids, it is possible that the carbonaceous-phase was simply undetectable in the microthermometry. By the measured total homogenization temperatures, the minimum temperature for the entrapment of type C and type B inclusions in V_1 and V_4 have been ~260–440 °C, with the average temperature being closer to 360–380 °C. For the later aqueous type A inclusions the minimum temperature for the entrapment have been significantly lower, with the average temperature being between ~200–260 °C. The total homogenization temperatures of type D fluids cannot be trusted, as it seems likely that they are affected by re-equilibration and therefore the temperatures are not equitable.

5.2.1. Chronology of the fluids

Based on the petrography, it is hard to reconstruct the evolution of the fluids as most of the FIAs were not found crosscutting each other and also even in the cases when they were, it is as likely that they were trapped coevally than proving any significant time sequence. However, petrological evidence of the deformation features as well as several crosscutting sequences observed of the type D inclusions that were not observed in the other fluid types would suggest their early nature among the fluids in the Kuittila zone. Also, the late nature of the low salinity type E fluids seems apparent based on the crosscutting sequences. FIAs of type C aqueous-carbonic inclusions were found crosscutting some of the type B aqueous inclusions in V_2. In these situations the type C inclusions were found to be likely younger than the aqueous ones, although due to more or less unclear crosscutting sequences it is also possible that they have been trapped rather coevally. The fact that the homogenization temperatures of type C and B fluids are strongly overlapping favours their potentially coeval entrapping. Also, in V_2, type A fluids were found crosscutting type C inclusions pointing toward the fact that type A inclusions are younger than type C.

The potential time sequence of the different fluid types is therefore following, from older to younger: 1) Type D - aqueous+hydrocarbon bearing fluids, 2) Type B - moderate salinity aqueous fluids, 3) Type C - aqueous-carbonic fluids, 4) Type A - high salinity aqueous fluids, 5) Type E - late aqueous fluids. Entrapping times of type F and G fluids are unknown, although the fact that type F inclusions occur as clusters around the likely chlorite melt inclusions would suggest their potential early presence.

5.3. Implications of the geochemistry of the fluids

The geochemical data obtained is more or less perplexing in the sense that there are no clear geochemical tracers of different fluid types pointing toward the source of the fluid. For example, type C2 fluids show magmatic signatures, as they contain high concentrations of Zn and Pb along with moderately high concentrations of K, all of which are considered as tracers for magmatic origin of the fluids. However, the same fluid type has low Cl/Br ratios and high As concentrations which are generally thought to be attributes for metamorphic fluids (Table 8). This suggests a high degree of fluid mixing between the magmatic fluids and most likely of fluids originating from the country metavolcanites and metasediments.

The base metals are generally lacking in the aqueous-dominated inclusions, with an exception of type A1 fluids, which contain considerable amounts of Zn and Pb (Table 8). This is not unexcepted, since base metals are generally transported as Cl-complexes and the type A fluids represents high salinity brines of relatively late stage.

Type A1 and type C2 fluids have clearly lower Na/K molar ratios than other fluid types. Whereas in type C1 and C3 fluids it is ranging from ~20 to 60 and in type D even from ~90 to 180. The measured values in type A1 and type C2 fluids are very consistently ranging from ~4 to 8 and ~8 to 14 respectively. Earlier studies have shown that the Na/K molar ratios will reduce with decreasing temperature (Rusk et al. 2004). The highly variable range in type C1, C3 and D fluids could indicate that high-salinity brines were trapped in the quartz veins under a wide range of pressures and temperatures. In case albite and K-feldspar are in equilibrium with the hydrothermal fluid, then the Na/K ratios of the fluid are fixed at any given pressure and temperature by the alkali exchange reaction (Rusk et al. 2004).

Table 8. *Average elemental concentrations (µg/g) of different fluid types as measured in different vein types. FIAs with anomalously high values caused most likely by solids in the analysed inclusion were deleted and are now marked with asterisk. Not analysed (n/a) were marked in situations where no detectable peak were obtained yet the measured values were above the detection limit. For elements where the analysed values were close to the limit of detection, in some situations some of the FIAs yielded values slightly above the detection limit, whereas others yielded values below detection limit. In these cases the concentrations for those FIAs below limit of detection were included in the average calculations as half of the value of limit of detection.*

Fluid type	Vein type	Li	B	Na	Mg	Cl	K	Ca	Ti	Fe	Cu	Zn	As	Br	Rb	Sr	Mo	Ag	Sb	Cs	Ba	W	Au	Pb	Bi	Cl/Br	K/Rb
Aqueous fluids																											
A1	V_1	2805	538	49500	13.4	165000	18200	15000	36.7	n/a	<0.33	202	738	12200	196	532	<0.31	n/a	24.2	231	156	0.12	<0.11	193	<0.04	32	93
A2	V_3	9.15	3.11	27600	207	124000	1401	40600	7.13	64.7	64.7	3.89	<0.41	3949	13.2	307	<0.07	<0.10	3.01	10.4	19.5	<0.10	<0.12	<0.06	<0.11	81	108
B1	V_1	132	8.89	16600	13.0	46800	499	19167	24.3	n/a	0.37	<0.30	10.2	1735	2.96	181	<0.25	<0.18	0.86	4.33	2.89	<0.35	<0.16	1.71	<0.11*	106	243
B1	V_4	18.7	58.5	22900	0.90	70100	402	18375	13.3	n/a*	0.76	0.68*	15.1	1345	5.82	294	<0.12	<0.11	0.67	12.2	8.95	<0.23	<0.04	0.89	<0.09	143	85
B2	V_1	158	675	37600	0.11	22200	2373	<37.0	32.1	n/a	3.55	1.71	257	629	7.50	15.7	<0.09	n/a	8.10	6.77	1.04	2.11	0.11	0.58	<0.05	87	323
Aqueous-carbonic fluids																											
C1	V_1	422	606	25300	4.75	35600	2361	106	15.2	n/a	56.4	6.43	463	2539	13.5	58.9	<0.30	1.13	20.3	17.3	13.4	<0.33	<0.13	5.73	<0.12	42	214
C2	V_2	37.6	399	39900	1.10	83000	6947	<107	<2.22	n/a	4.66	227	656	8976	19.7	133	<0.30	3.11	7.80	18.0	287	0.29	<0.09	210	0.09	28	349
C3	V_1	1578	631	35400	6.38	32700	2385	99.9	19.0	n/a	407	<0.54	217	756	7.65	6.06	0.93	5.96	19.1	5.11	3.96	12.6	0.25	26.0	n/a	62	348
C4	V_4	7.84	159	5126	0.13	9116	189	<55.2	<1.15	n/a	7.03	n/a	89.1	805	1.51	4.46	<0.05	1.07	0.78	1.52	6.35	0.67	<0.05	1.73	<0.08	25	109
C5	V_4	11.2	1000	39800	<0.08	34200	1490	205	<0.63	391	23.2	0.60	442	722	5.6	5.1	<0.09	n/a	13.6	4.9	<0.12	18.3	0.58	<0.05	<0.05	44	278
D	V_1	98.3	2.20	4220	11.3	9065	95.4	1965	13.7	3968	2.47	<0.17	3.63	110	1.05	46.2	1.12	<0.02	0.52	0.80	1.92	2.81	<0.01	<0.02	0.46	204	91
D	V_3	1.15	9.19	5061	1.80	15000	654	1662	n/a	17.1	0.21	10.9	3.91	716	1.13	13.0	<0.08	1.01	1.38	0.88	1.54	<0.05	<0.04	15.1	<0.07	47	449

Some of the fluid types, especially B1, A2 and D show erratic behaviour, as Br and K show negative correlation with Cl content. Despite the fact that the data of type D inclusions should be approached with caution because of the more or less ambiguous data, the fact that clear tungsten peaks were observed in these type of inclusions is still a clear sign of the W signature in these early fluids. Even thought reliable gold signal could not been obtained of this fluid type, it is likely based on the presence of W and Mo in type D fluids. The lack of gold in the analyses could be because of the really low salinity of inclusions of this type. The type D inclusions in V_1 have the highest molar Cl/Br ratios of all inclusion types. It is possible that the high molar Cl/Br ratios are explained by the early nature of these fluids, which could be the reason why the contribution of metamorphic fluids have been less and therefore they are potentially best representing the composition of the magmatic fluids.

It is notable that the aqueous-carbonic type C fluids, which were further divided into type C1, C2, C3, C4 and C5 based on the geochemistry, show significant differences in their composition. The most notable difference is in their base metal values, as type C3 (as well as C1 and C5, although less) fluids are clearly enriched in Cu, whereas type C2 fluids have low Cu contents compared to type C3 fluids, but are instead characterized by high Pb and Zn values. Also barium concentrations is remarkably higher in type C2 fluids than in the other fluid types. The barium-rich type C fluids are present in only in V_2. Differences between the base metal contents of the aqueous-carbonic fluids can be explained by either different fluid source for each type, or that the originally magmatic fluids have undergone different evolution paths. K/Rb ratios of all these aqueous-carbonic type C inclusions are relatively close to the crustal value of 285, however differences arise in K/Ba ratio. K/Ba ratio in type C1 fluids are up to 2000–5000, whereas in type C2 they are ranging from ~10 to 30. K/Ba ratio can be considered as possible indicator for different stages of fractional crystallization in magma, as incorporation of barium into K-feldspar at earlier stages of magmatic evolution results in a compensating depletion of Ba in late-stage differentiates. (Kerrich 1988). This would mean that the Zn and Pb bearing C2 fluids with high Ba concentrations would be the early stage fluids of the magma, whereas the other types would be late stage fluids with more or less contribution of metamorphic fluids in them.

The only detectable peaks of gold were observed in type C3 inclusions in V_1 and C5 inclusions in V_4. They are also the highest W-enriched inclusions analysed. There seems to be certain correlation with the Au and W in the auriferous fluids. Also, one FIA representing type B2 inclusions in V_1 shows tungsten and gold values above the detection limit. However, the gold concentration in this is barely above the detection limit. Silver on the other hand was observed in almost all different type of aqueous-carbonic inclusions (C1, C2, C3 and C4) and therefore it does not seem to be related to the gold concentration of the fluids. The auriferous fluids do not show the typical characteristics of magmatic fluids. On the contrary they have, for example low Zn and Pb concentrations and relatively low K contents. The lack of Zn and Pb in these auriferous type of fluids indicate that the W-Au(-Mo) mineralization is unrelated to the Zn and Pb concentrations in the fluids. Also due to the lack of clear magmatic affinities, it is reasonable to assume that these gold-bearing fluids have been affected considerable amount by metamorphic devolization and fluid-rock reactions with the country rocks.

Even though the auriferous fluids of type C3 and C5 have similar salinities and high W concentrations, differences arise in their Li, Cu and Pb contents. Type C3 fluids contain average of 1578 ppm Li, 407 ppm Cu and 26 ppm Pb, whereas corresponding concentrations in type C5 fluids are 11.2 ppm Li, 7.03 ppm Cu and <0.05 ppm Pb. Silver concentrations are also clearly elevated in type C3 fluids (5.96 ppm), whereas no silver were detected in fluids of type C5. The fact that type C3 fluids are only present in the early Mo-W vein type, whereas type C5 fluids are only present in the later auriferous vein type, suggest that the type C3 fluids are potentially representing the ore fluid for the early Mo-W mineralization and the type C5 fluids are related to the later main gold stages.

The lack of any correlation trend between Cu and Cl suggest that the Cu is likely transported as bisulphide complex rather than with the chloride. As the Zn shows clear correlation to Cl, it can be considered that it has been transported as chloride-complexes. As the gold and tungsten bearing inclusions also contain more or less copper, it is likely that the gold is likewise transported as bisulphide complexes, as which is the case in orogenic gold deposits usually. However, the data on auriferous fluids is too sparce to see any correlation in this matter.

The presence of base metal alloys (for example Cu-Zn-Ni alloy) found in EMPA analyses in V_3 might indicate that some of the fluids transporting these metals have been lacking the sulphur and would have been more likely transported as chloride complex. These alloys lacking the sulphur have been most likely formed in a strongly reducing environment with absent oxygen and low sulphur activities (JiaJun et al. 2008). However, as oxidation of pyrite was observed, it seems more likely that these alloys are simply left overs from sample preparation.

The Cl/Br data is more or less equivalent with the other geochemistry of the certain fluids types. As the earlier studies show, molar Cl/Br ratios should be lower in metamorphic fluids than in magmatic ones, in which they generally yield ratios above 500. As the Cl/Br ratios in all of the analysed fluids in Kuittila range from 17 to 204, the obtained data does not seem to be correlating in that sense, as many of the inclusions show other magmatic attributes. The molar Cl/Br ratios are in similar range than has been observed in Pampalo fluid inclusions by Fusswinkel et al. (2017), where they range from 9 to 150. According to Fusswinkel et al. (2017), the low Cl/Br ratios in Pampalo are most probably caused by the derivation of Br from interaction with organic matter in metasedimentary rocks during metamorphic fluid production. The high abundance of hydrocarbons observed in Kuittila in most of the fluid inclusions confirmed with Raman studies would support this theory.

5.4. Implications of the potential role of the magmatic fluids in orogenic gold forming processes

The fluid inclusion LA-ICP-MS data in this study shows significant differences in the geochemistry to those reported in Pampalo by Fusswinkel et al. (2017). The Pampalo fluids are characterized by low base metal contents, but contain in comparison high As and Sb values, which are typical features for gold forming fluids. In comparison, the fluid inclusions analysed in this study have generally higher base metal compositions and therefore are representing more or less altered magmatic fluids. The most distinct signatures of magmatic fluids are seen in most of the fluids in the early vein types, whereas the typical features of magmatic-hydrothermal fluids are generally lacking in the latest vein type (V_4). Enriched values of Zn were, however, measured in one FIA (KUI3-C1 FIA5) representing type B1 fluids in V_4. However, the abnormally high concentrations of Mg and Fe measured in the same FIA indicate that the analysed spectrum is most likely from a solid rather than fluid inclusion, or that the Mg-Fe-bearing solid is abnormally large within the fluid inclusion in the FIA and therefore the measured values are not comparable with the general data.

The fact that molar Cl/Br ratios of all different fluid types in the Kuittila quartz veins are way lower than the typical values in magmatic fluids indicate that even the earliest fluids with a distinct magmatic fluid affinities have been affected by Br-rich source. The exceptionally low molar Cl/Br-ratios observed in both Kuittila and Pampalo suggest that it is a quite common feature in Hattu schist belt as whole. It seems apparent that the Br-rich fluids delivered most likely from carbonaceous country sediments have had a large impact on the Kuittila tonalite as well.

Both auriferous fluid types C3 and C5 share some of the characteristics observed in auriferous fluids in Pampalo, e.g. high W, low molar Cl/Br ratios, and low to below detection limit values of Zn and Pb. The composition of type C5 fluids in V_4 is closer to the auriferous fluids in Pampalo than the composition of type C3 fluids in V_1. In both, the type C5 fluids in this study and auriferous fluids in Pampalo, Ag concentrations are low and Pb/Zn values are below the detection limit or slightly above, although Cu concentrations are a bit higher in C5 fluids than in Pampalo. Type C3 fluids in the early Mo-W veins on the other hand have significant amounts of Cu and slightly elevated Pb concentrations, both which are lacking in the auriferous fluids in Pampalo. Nevertheless, the general absence of magmatic signatures in the auriferous fluids in Kuittila indicate that the originally magmatic fluids have been affected highly by metamorphic fluids, or that the auriferous fluids have different sources and the gold precipitated in the quartz veins within the Kuittila tonalite is therefore transported from elsewhere. In the latter situation the Kuittila tonalite would have then acted as a trap for the gold bearing fluids that have originated by metamorphic devolization of the country rocks, which have then mineralized in localized sites within the vein network of the Kuittila tonalite. Also, the fact that the geochemistry differs between type C3 fluids, which are potentially representing the ore fluids of the early Mo-W mineralization to those of the C5 fluids in later auriferous veins, raises a question of that if the latter are potentially later differentiates of the same magmatic source that have been simply affected more by metamorphic fluids during their fluid evolution, or are they both delivered from different sources. However, as the magmatic signatures are relatively low even in the auriferous fluids in the early Mo-W veins, the latter seems more likely option. The more or less similar features, especially the low molar Cl/Br ratios, of the gold-bearing fluids in

Kuittila and of those in Pampalo studied by Fusswinkel et al. (2017) would suggest that the source of gold could potentially be the same, most likely country sediments. The fact that the auriferous fluids in Kuittila are lacking most of the magmatic features and at the same time show similarities with the Pampalo fluids suggest that the magmatic imput in the Hattu schist belt does not necessarily have a significant contribution in the auriferous fluids.

6. CONCLUSIONS

The results of this study indicate bimodal distribution of fluids in quartz veins within the Kuittila tonalite. Fluids in V_{1-3} show dominantly magmatic-hydrothermal affinities, whereas more pervasive imput of metamorphic fluids can be seen in V_4. This would suggest that the fluids have evolved during their genesis through metamorphic devolatilization of the surrounding metavolcanites and metasedimentary rocks. The presence of hydrocarbons in most of the analysed inclusions supports the considerable contribution of the potentially Br-rich carbonaceous sediments.

This study revealed that the fluid inclusions in quartz veins hosted by Kuittila tonalite contain much more variety than has been claimed in the earlier studies. The gaseous phase of the inclusions consists of $H_2O \pm CO_2 \pm CH_4 \pm C_3H_8 \pm N_2$. The highly variable elemental compositions as well as variable salinities and in particular Cl/Br ratios of different fluid types indicate that several pulses of fluids have migrated through the Kuittila tonalite with potentially variable origin of the fluids. Some of the fluid types clearly shares the characteristics of magmatic-hydrothermal fluids, whereas some are similar to metamorphic fluids seen in earlier studies. It seems evidential that the magmatic-hydrothermal fluids have been reacted with the surrounding metasediments by variable amounts.

The auriferous fluids show high W signature, and are lacking most of the typical tracers of magmatic fluids. This indicates that the fluids related to the gold mineralization are either transported from elsewhere and trapped in already formed fractures within the Kuittila tonalite, or that even in the early vein forming stages the contribution of metamorphic fluids have been substantial.

Since any primary inclusions could not been observed in this study we cannot say for certain the composition of the quartz forming fluids and their relationship to the gold mineralizing fluids, and whether the same fluids that have formed the quartz veins have also transported the gold or not. This study, however, gives new information about the different fluid evolution stages that can be useful in further studies.

The fact that in this study no gold were observed in the fluids with typical characteristics for magmatic fluids, and on contrary, those with gold signal shared more of the characteristics of metamorphic fluids would suggest that the magmatic fluids are not necessarily involved in the formation of the orogenic gold deposits in the Hattu schist belt and are not therefore mandatory in the formation of orogenic type gold deposits. It seems rather likely that the metamorphic fluids delivered potentially from country metavolcanites and metasediments are the sources for the gold and are precipitated in already formed fractures in the Kuittila zone.

7. ACKNOWLEDGEMENTS

I would like to thank Professor Thomas Wagner for providing me the topic for this thesis and supervising. I would like to give special thanks to Dr. Tobias Fusswinkel, who kindly provided me the samples of this thesis and was also helping me with different analytical methods all the way during this process. The LA-ICP-MS analyses could not have been completed without daily maintaining of the equipment done by Mr. Fusswinkel. I would also like to thank Anselm Loges for helping me with operating the Raman laser spectrometry and also helping me with the Raman data handling. I am also grateful for Dr. Michallik Radoslaw for helping with using the EPMA. I would also like to thank Professor Petri Peltonen for pushing me forward with this work and giving useful hints, not only for the topic of this thesis but writing work in general. Lab-technician Helena Korkka prepared excellent thick section to be used in this study. Lastly, I would like to thank all my fellow colleagues, friends and family members for the great support during this process.

8. REFERENCES

Bakker, R. 2003. Package FLUIDS 1. Computer programs for analysis of fluid inclusion data and modelling bulk fluid properties. Chemical Geology 194, 3-23.

Banks, D. A., Davies, G. R., Yardley, B. W. D., McCaig, A. M., Grant, N. T. 1991. The Chemistry of brines from an Alpine thrust system in the Central Pyrenees: An application of fluid inclusion analysis to the study of fluid behaviour in orogenesis. Geochimica et Cosmochimica Acta, v. 55, pp. 1021–1030.

Banks, D. A., Guiliani, G., Yardley, B. W. D., Cheilletz, A. 2000. Emerald mineralisation in Colombia: Fluid chemistry and the role of brine mixing. Mineralium Deposita, v. 35, pp. 699–713.

Bodnar, R. J. 2003. Introduction to fluid inclusions. In: Samson, I., Anderson, A. and Marshall, D. (eds). Fluid inclusions – analysis and interpretation. Mineralogical Association of Canada, Short Course Series, v. 32, p 1-8.

Bodnar, R. J. 2003. Re-equilibration of fluid inclusions. In: Samson, I., Anderson, A. and Marshall, D. (eds). Fluid inclusions: Analysis and Interpretation. Mineralogical Association of Canada, Short Course Series, v. 32, p 213-230.

Bodnar, R. J., Lecumberri-Sanchez, P., Moncada, D., Steele-MacInnis, M. 2014. Fluid Inclusions in Hydrothermal Ore Deposits. In: Holland, H. D., Turekian, K. K. (Eds.) Treatise on Geochemistry (2nd edition, vol. 13) Elsevier Oxford, pp. 119–142.

Bornhorst, T. J., Wilkin, R. T. 1993. Fluid inclusion data for selected quartz from gold prospect in the late Archean Hattu schist belt, Ilomantsi, eastern Finland. Geological Survey of Finland, Special Paper 17, 317-322.

Bray, C. J., Spooner, E. T. C., Thomas A. V. 1991. Fluid inclusion volatile analysis by heated crushing, on-line gas chromatography; applications to Archean fluids. Journal of Geochemical Exploration 42 (1). pp. 167-193.

Campbell, A. R., Banks, D. A., Phillips, R. S., Yardley, B. W. D. 1995. Geochemistry of Th-U-REE mineralizing magmatic fluids, Capitan Mountains, New Mexico. Economic Geology, v. 90, pp. 1271–1287.

Cartwright, I., Oliver, N. H. S. 2000. Metamorphic fluids and their relationship to the formation of metamorphosed and metamorphogenic ore deposits. In: Spry, G., Marshall, B., and Vokes, F. (eds.) Metamorphosed and Metamorphogenic Ore Deposits. Reviews in Economic Geology, 11. Society of Economic Geologist, Littleton, Colorado, pp. 81-96.

Endomines. 2018. Annual report in Swedish 2017. Accessed online at https://www.endomines.com/index.php/release/?releaseID=2866931.

Eilu, P. 2015. Gold Deposits – Overview on Gold Deposits in Finland. In: Maier, W. D, Lahtinen, R., O'Brien, H. (Editors), Mineral deposits of Finland. Elsevier, Amsterdam, chapter 5.1, pp. 377-403

Frezzotti, M. L., Tecce, F., Casagli, A. 2012. Raman spectroscopy for fluid inclusion analysis. Journal of Geochemical Exploration 112, 1-20.

Fusswinkel, T., Wagner, T., Sakellaris, G. 2017. Fluid evolution of the Neoarchean Pampalo orogenic gold deposit (E Finland): Constraints from LA-ICPMS fluid inclusion microanalysis. Chemical Geology 450, pp. 96-121.

Goldfarb, R. J., Groves, D. I., Gardoll S. 2001. Orogenic gold and geologic time: a global synthesis. Ore Geology Reviews 18. 1–75.

Goldfarb, R. J., Groves, D. I. 2015. Orogenic gold: Common or evolving fluid and metal sources through time. Lithos 233. p. 2-26.

Goldfarb, R. J, Hart, C. J. R., Marsh, E. E. 2008. Orogenic gold and evolution of the Cordilleran orogeny. In: Spencer, J. E., Titley, S. R. (Eds.). Circum-Pacific Tectonics, Geologic Evolution, and Ore Deposits. Tucson, Arizona Geological Society, Digest 22, pp. 311–323.

Goldstein, R. H. and Reynolds, T. J. 1994. Systematics of fluid inclusions in diagenetic minerals. SEPM Short Course 31. p. 199.

Groves, D. I., Goldfarb, R. J., Gebre-Mariam, M., Hagemann, S. G., Robert, F. 1998. Orogenic gold deposits: A proposed classification in the context of their crustal distribution and relationship to other gold deposit types. Ore Geology Reviews 13. pp. 7-27.

Guillong, M., Meier, D. L., Allan, M. M., Heinrich, C. A., Yardley, B. W. D. 2008. SILLS: A MATLAB-based program for the reduction of laser ablation ICP-MS data of homogenous materials and inclusions. Mineralogical Association of Canada Short Course Series 40, 328-333.

Heilimo, E., Halla, J., Huhma, H. 2010. Single-grain zircon U-Pb age constraints of the western and eastern sanukitoid zones in the Finnish part of the Karelian Province. Lithos 121. pp. 87–99.

Heinrich, C. A., Ryan, C. G., Mernach, T. P., Eadington, P. J. 1992. Segregation of ore metals between magmatic brine and vapor: A fluid inclusion study using PIXE microanalysis. Economic Geology, v. 87, pp. 1566–1583.

Hicks, M. 2015. Mineralization and Hydrothermal Alteration of the Korvilansuo Prospect, Hattu Schist Belt, Ilomantsi, Eastern Finland. University of Helsinki, Master’s Thesis.

Hoshino, K., Nagatomi, A., Watanabe, M., Okudaira, T., Beppu, Y. 2006. Nahcolite in fluid inclusions from the Ryoke metamorphic rocks and its implication for fluid genesis. Journal of Mineralogical and Petrological Sciences, Volume 101, p. 254-259.

Hurai, V., Huraiová, M., Slobodnik, M., Thomas, R. 2015. Geofluids – Developments in Microthermometry, Spectroscopy, Thermodynamics, and Stable Isotopes. Elsevier.

JiaJun, L., GaungJian, M., XingHua, M., LiXing, L., YuGian, G., GuangZhi, L. 2008. Discovery of Cu-Ni-Zn-Sn-Fe intermetallic compounds and S-bearing alloys in the Zhaishang gold deposit, southern Gansu Province and its geological significance.

Kamenetsky, V. S., Achterbergh, E. A., Ryan, C. G., Naumov, V. B., Mernagh, T. P., Davidson, P. 2002. Extreme heterogeneity of granite-derived hydrothermal fluids: An example from inclusions in a single crystal of miarolitic quartz. Geology, v. 30, pp. 459–462.

Kerkhof Van Den, A. M. and Hein, U. F. 2001. Fluid inclusion petrography. Lithos 55, 27-47.

Kerrich, R. 1988. Source processes for Archean Au-Ag vein deposits: evidence from lithophile-element systematics of the Hollinger – McIntyre and Buffalo Ankerite deposits, Timmins. Can. J. Earth Sci. 26, 755–181.

Kesler, S. E. 2005. Ore-forming fluids. Elements, January 2005; 1.

Kojonen, K., Johanson, B., O’Brien, H., Pakkanen, I. 1993. Mineralogy of gold occurrences in the late Archean Hattu schist belt, Ilomantsi, eastern Finland. Geological Survey of Finland, Special paper 17, p. 233-271.

Lowenstern, J. B. 2001. Carbon dioxide in magmas and implications for hydrothermal systems. Mineralium Deposita, 36, 490-502.

McCaig, A. M., Tritlla, J., Banks, D. A. 2000. Fluid mixing and recycling during Pyrenean thrusting: Evidence from fluid inclusion halogen ratios. Geochimica et Cosmochimica Acta, v. 64, pp. 3395–3412.

Meere, P. A., Banks, D. A. 1997. Upper crustal fluid migration: An example from the Variscides of SW Ireland: Journal of the Geological Society of London, v. 154, pp. 975–985.

Mikucki, E. J. 1998. Hydrothermal transport and depositional process in Archean lode-gold systems: A review. Ore Geology Reviews 13, 307–321.

Miron, G. D., Wagner, T., Wälle, M., Heinrich, C. A. 2013. Major and trace-element composition and pressure-temperature evolution of rock-buffered fluids in low-grade accretionary-wedge metasediments, Central Alps. Contrib Mineral Petrol, 165, pp. 981–1008.

Molnár, F., O'Brien, H., Lahaye, Y., Käpyaho, A., Sorjonen-Ward, P., Hyodo, H., Sakellaris, G. 2016. Signatures of Multiple Mineralization Processes in the Archean Orogenic Gold Deposit of the Pampalo Mine, Hattu Schist Belt, Eastern Finland. Economic Geology, v. 111, pp. 1659-1703.

Molnár, F., Mänttäri, I., O'Brien, H., Lahaye, Y., Pakkanen, L., Johansson, B., Käpyaho, A., Sorjonen-Ward, P., Whitehouse, M., Sakellaris, G. 2016. Boron, Sulphur and copper isotope systematics in the orogenic gold deposits of the Archean Hattu schist belt, eastern Finland. Ore Geology Reviews. 77, p. 133-162.

Munz, I. A., Yardley, B. W. D., Banks, D. A., Wayne, D. 1995. Deep penetration of sedimentary fluids in basement rocks from southern Norway: Evidence from hydrocarbon and brine inclusions in quarz veins. Geochimica et Cosmochimica Acta, v. 59, pp. 239–254.

Nurmi, P. A. 1993. Genetic Aspects of Mesothermal Gold Mineralization and Implications for Exploration in the Late Archean Hattu Schist Belt, Ilomantsi, Eastern Finland. Geological Survey of Finland, Special Paper Vol. 17, pp. 373–386.

Nurmi, P. A., Sorjonen-Ward, P., Damstén, M. 1993. Geological setting, characteristics and exploration history of mesothermal gold occurrences in the late Archean Hattu schist belt, Ilomantsi, eastern Finland. Geological Survey of Finland, Special Paper 17, pp. 193–231.

O'Brien, H., Huhma, H. and Sorjonen-Ward, P. 1993. Petrogenesis of the late Archean Hattu schist belt, Ilomantsi, eastern Finland: Geochemistry and Sr, Nd isotopic composition. Geological Survey of Finland, Special Paper 17, 147–184.

Phillips, G. N. 1993. Metamorphic fluids and gold. Mineralogical Magazine, September, Vol. 57. p. 365–374.

Phillips, G. N., Powell, R. 1993. Link between Gold Provinces. Economic Geology, Vol. 88, pp. 1084-1098.

Phillips, G. N., Powell, R. 2010. Formation of gold deposits–a metamorphic devolatilization model. Journal of Metamorphic Geology 28, pp. 689–718.

Poutiainen, M. and Partamies, S. 2003. Fluid Inclusion Characteristics of Auriferous Quartz Veins in Archean and Paleoproterozoic Greenstone Belts of Eastern and Southern Finland. Economic Geology. Vol. 98. p. 1355-1369.

Poutiainen, M. and Partamies, S. 2003. Fluid evolution of the late Archean Rämepuro gold deposit in the Ilomantsi greenstone belt in eastern Finland. Mineralium Deposita. Vol. 38. p. 196-207.

Randive, K., Hari, K. R., Dora, M. L., Malpe, D. B. 2014. Study of Fluid Inclusions: Methods, Techniques and Applications. Gond. Geol. Mag., V. 29(1 and 2), June and December, 2014. pp. 19-28.

Rasilainen, K. 1996. Alteration geochemistry of gold occurrences in the late Archean Hattu schist belt, Ilomantsi, eastern Finland: Synopsis. Geological Survey of Finland, Special Publication, Vol. 21.

Ridley, J. R., Diamond, L. W. 2000. Fluid Chemistry of Orogenic Lode Gold Deposits and Implications for Genetic Models. Reviews in Economic Geology, Vol. 13.

Rittenhouse, G. 1967. Bromine in Oil-Field Waters and Its Use in Determining Possibilities of Origin of These Waters. American Association of Petroleum Geologist Bulletin, 51. pp. 2430–2440.

Robb, L. 2005. Introduction to Ore-Forming Processes. Blackwell science Ltd.

Roedder, E. 1972. Data of Geochemistry. Geological Survey Professional Paper 440-JJ. Sixth Ed.

Roedder, E. 1984. Volume 12: Fluid inclusions. REVIEWS in MINERALOGY, volume 12.

Rusk, B. G., Reed, M. H., Dilles, J. H., Klemm, L. M., Heinrich, C. A. 2004. Composition of magmatic hydrothermal fluids determined by LA-ICP-MS of fluid inclusions from the porphyry copper-molybdenum deposit at Butte, MT. Chemical Geology, Vol 210, pp. 173–199.

Smith, M.P., Banks, D. A., Yardley, B. W. D., Boyce, A. 1996. Fluid inclusion and stable isotope constraints on the genesis of the Cligga Head Sn-W deposit, S.W. England. European Journal of Mineralogy, v. 8, pp. 961–974.

Sorjonen-Ward, P. 1993. An overview of structural evolution and lithic units within and intruding the late Archean Hattu schist belt, Ilomantsi, eastern Finland. Geological Survey of Finland, Special paper 17, p. 9-102.

Sorjonen-Ward, P. B., Hartikainen, A., Nurmi, P. A., Rasilainen, K., Schaubs, P., Zhang, Y., Liikanen, J. 2015. Exploration Targeting and Geological Context of Gold Mineralization in the Neoarchean Ilomantsi Greenstone belt in Eastern Finland. In: Maier, W. D, Lahtinen, R., O'Brien, H. (Editors), Mineral deposits of Finland. Elsevier, Amsterdam, chapter 5.3, pp. 435-466.

Spandler, C., Pettke, T., Rubatto, D. 2011. Internal and external fluid sources for eclogite-facies veins in the Monviso meta-ophiolite, Western Alps: implications for fluid flow in subduction zones. J. Petrol, vol. 52, pp. 1207–1236.

Stein, H. J., Sundblad, K., Markey, R. J., Morgan, J. W., Motuza, G. 1998. Re-Os ages for Archean molybdenite and pyrite, Kuittila-Kivisuo, Finland and Proterozoic molybdenite, Kabeliai, Lithuania: testing the chronometer in a metamorphic and metasomatic setting. Mineralium Deposita. Vol. 33, p. 329-345.

Tarantola, A., Diamond, L. W., Stünitz, H. 2010. Modification of fluid inclusions in quartz by deviatoric stress I: Experimentally included changes in inclusion shapes and microstructures. Contributions to Mineralogy and Petrology, v. 160, p 825-843.

Tomkins, A. G. 2013. On the source of orogenic gold. Geology, volume 41, number 12. pp. 1255–1256.

Touret, J. L. R. 2001. Fluids in metamorphic rocks. Lithos 55. p. 1–25.

Vaasjoki, M., Korsman, K., Koistinen, T. 2005. Overview. In: Lehtinen, M., Nurmi, P. A., Rämö, O. T. (editors), Precambrian Geology of Finland – Key to the Evolution of the the Fennoscandian Shield. Elsevier B.V., Amsterdam. p. 1-18.

Wilkinson, J. J. 2001. Fluid inclusions in hydrothermal ore deposits. Lithos 229-272.

Winter, J. D. 2001. An Introduction to Igneous and Metamorphic Petrology. Prentice-Hall.

Worden, R. H. 1996. Controls on halogen concentrations in sedimentary formation waters. Mineralogical Magazine, April 1996, Vol. 60. pp. 259–274.

Yardley, B. W. D., Bodnar, R.J. 2014. Fluids in the Continental Crust. Geochemical Perspectives, vol. 3, number 1.

Yardley, B. W. D., Cleverley, J.S. 2013. The role of metamorphic fluids in the formation of ore deposits. Geological Society of London Special Publication 393.

Yardley, B. W. D. 2005. Metal Concentrations in Crustal Fluids and Their Relationship to Ore Formation. Economic Geology, v. 100, pp. 613–632.